NAME OF AUTHOR/NOM DE L'AUTEUR___Kirk H. MICHAELIAN

TITLE OF THESIS/TITRE DE LA THÈSE___Raman Resonance of Electron Donor/Acceptor Complexes of

Tetracyanoethylene

UNIVERSITY/UNIVERSITÉ___Simon Fraser University

DEGREE FOR WHICH THESIS WAS PRESENTED/
GRADE POUR LEQUEL CETTE THÈSE FUT PRÉSENTÉE___Doctor of Philosophy

YEAR THIS DEGREE CONFERRED/ANNÉE D'OBTENTION DE CE GRADE___1977

NAME OF SUPERVISOR/NOM DU DIRECTEUR DE THÈSE___Dr E.M. Voigt and Dr. K. Rieckhoff

DATED/DATÉ_15 August 1976___ SIGNED/SIGNÉ.

PERMANENT ADDRESS/RÉSIDENCE FIXÉ

NOTICE

AVIS

RAMAN RESONANCE

OF

ELECTRON DONOR/ACCEPTOR COMPLEXES

OF TETRACYANOETHYLENE

by

Kirk Haig Michaelian

B.Sc., California State University, Fresno

M.Sc., California State University, Fresno

A THESIS SUBMITTED IN PARTIAL FULFILLMENT

OF THE REQUIREMENTS FOR THE DEGREE OF

DOCTOR OF PHILOSOPHY

in the Department

of

Chemistry

© Kirk Haig Michaelian 1976

Simon Fraser University

August 1976

Name: Kirk Haig Michaelian

Degree: Doctor of Philosophy

Title of Thesis: Raman Resonance of Electron
Donor/Acceptor Complexes of
Tetracyanoethylene

Examining Committee:

    Chairman: F.W.B. Einstein

E.M. Voigt
Senior Supervisor

K.E. Rieckhoff
Senior Supervisor

S.K./Lower

A.C. Oehlschlager

J.C. Irwin

W.L. Peticolas
External Examiner
Professor
University of Oregon, Eugene, Oregon

Date Approved: 16 August 1976

Title of Thesis/Dissertation:

Raman Resonance of Electron Donor/Acceptor Complexes of

Tetracyanoethylene.

Author:

(signature)

Kirk H. Michaelian

(name)

18 August 1976

(date)

Abstract

The ground electronic state of a π-π electron donor/acceptor (EDA) complex, generally characterised by comparatively minor changes in the geometric and electronic structures of the components on complexation, can be studied by a variety of physical methods, including vibrational spectroscopy. Although the infrared spectra of a few π-π EDA complexes had been obtained prior to this research, no successful Raman experiments had been reported. This research is the first detailed Raman spectroscopic investigation of a series of π-π complexes.

In the present study, the Raman spectra of EDA complexes having tetracyanoethylene (TCNE) as electron acceptor and aromatic electron donors are examined in detail. The spectra studied are for room temperature solutions in either the (liquid) donor or an inert solvent. Because of the strong absorption of these complexes, the conventional geometry of the Raman experiment is inappropriate; instead, a new "backscattering" geometry had to be developed. The resulting Raman signals from these coloured solutions are very weak, requiring the use of sophisticated optical equipment and photon counting electronics.

The principal results obtained for the Raman spectra of the EDA complexes of TCNE are the following: (i) the totally symmetric bands of TCNE exhibit considerable intensity enhancements on complexation; (ii) both the intensities and the positions of the donor bands are not greatly affected by complexation; (iii) small yet systematic changes are observed in the positions of some of the TCNE bands with complexation. Because they exhibit the most

pronounced effects, the TCNE Raman bands were chosen as the subject for more detailed investigations. The intensity changes in the TCNE Raman spectrum on complexation are found to arise from the preresonance or resonance Raman effects, depending on the location of the excitation frequency with respect to the absorption band (or bands) of each complex.

The preresonance Raman spectra of EDA complexes of TCNE display intensity changes of about an order of magnitude in the TCNE C=C and C≡N stretching bands. The excitation frequency dependence of the intensities of both bands establishes the role of the first excited states of the complexes as intermediate states, and also shows that the higher excited states of the components or of the complex take part in the scattering. The depolarisation ratios of the C=C stretching bands at preresonance approach 1/3, which indicates that the first excited states of the complexes (with the possible exception of benzene/TCNE) are not degenerate.

The resonance Raman spectra of the complexes show intensity increases up to an order of magnitude greater than those in the preresonance Raman spectra. The resonance Raman excitation profiles of the C=C and C≡N bands of a number of complexes are shifted by about 1000 - 2000 cm^{-1} to the low energy side of the bands, and generally display the same characteristics whether the excitation falls within the first or the second absorption band of a complex. The resonance Raman excitation spectra were found to be red shifted with respect to the absorption profiles. This red shift is interpreted in terms of the vibronic theory of

resonance Raman scattering, and in terms of a model of the EDA complex in which the higher vibronic levels of the ground and/or excited states are nonradiatively damped by interactions with the environment. The independent resonance with either absorption band of a complex favours the argument that when there are two absorption bands these bands arise from different geometrical configurations of the complex.

A new method for the determination of equilibrium constants for the formation of EDA complexes was developed using the intensity changes in the TCNE C=C and C≡N bands. The results of this new method agree well with published data obtained by previously established methods, where comparative data are available, and thus confirm the usefulness of this method.

The low energy Raman spectra of the EDA complexes contain a resonance-enhanced acceptor band which leads to a revised vibrational assignment of TCNE in this region. These investigations resulted in a new assignment of the entire Raman spectrum of TCNE.

For Diane

Acknowledgments

TABLE OF CONTENTS

LIST OF TABLES

xv

1. INTRODUCTION

The theory of π-π electron donor/acceptor (EDA)[†] complexes,
given a number of years ago by Mulliken[††], has served as the basis
for the interpretation of a vast amount of spectroscopic data.
Many of these investigations have been carried out in an attempt
to elucidate the nature of the donor/acceptor interaction in the
ground and first excited electronic states of the complexes. The
majority of this work involves the study of electronic absorption
spectra for transitions between the ground and excited charge
transfer (CT) states; this preponderance of absorption spectra is
at least partly due to the ready accessibility of absorption
spectra in the visible and the ultraviolet regions, where the CT
transitions usually occur.

In contrast to electronic spectra, <u>vibrational</u> spectra have
been studied for only a rather limited number of EDA complexes.
In spite of this, vibrational spectroscopy is certainly a suitable
method with which the ground states of EDA complexes can be probed,
since the vibrational transitions occur within this lowest
electronic state. Both infrared and Raman spectra can thus be
considered as possible means to provide information on the nature
of the complexes.

Because of the role of virtual (intermediate) states in Raman
scattering, vibrational Raman spectroscopy also yields information

---

[†] A summary of abbreviations is given in Appendix A.
[††] The important early papers by Mulliken on EDA complexes are
reprinted in ref. 1.

on the excited electronic states when the excitation (laser) frequency is near an electronic transition of the scattering species. Thus, Raman spectra can furnish information not available from infrared absorption spectra, and in appropriate cases allow examination of both the ground and the excited electronic states 'of EDA complexes.

The suitability of Raman spectroscopy for the study of EDA complexes also arises from the fact that vibrational frequencies range from about 10^{14} s^{-1} to $10^{13}s^{-1}$, whereas the lifetimes of complexes in solutions at room temperature are variously estimated[2] to be between 10^{-3} s and 10^{-12} s. This means that many vibrations can take place before the complex, which is present in equilibrium with its components, can dissociate. The Raman spectra of both free and associated species can thus be obtained[3,4]; in this case, the complex is said to be spectroscopic[5], i.e. to have a mean lifetime longer than the measurement time of the spectroscopic method. Although the effects of weak complex formation on the component spectra are in general not very great, the optical and electronic equipment which are used to obtain Raman spectra make the identification of bands of both complexed and uncomplexed species possible.

The study of the Raman spectra of an EDA complex logically includes the following aspects[6]:

(a) the comparison of the positions of the bands in the spectra of the free components with those in the spectrum of the complex;

(b) the comparison of band intensities in the spectra of the

free donor and the free acceptor with the intensities in the spectrum of the complex;

(c) the examination of the spectrum of the complex for the appearance of new or activated bands which do not appear in the spectra of either of the uncomplexed components.

Frequency shifts on complexation, which may be revealed by the first kind of investigation, can often give an indication of changes in the geometric structures of the components arising from the donor/acceptor interaction. On the other hand, activation or intensification of the bands as a consequence of complex formation are generally due to changes in molecular symmetry or to differences in the electronic structures of the complexed components as compared to the free components. Finally, the most dramatic feature of the Raman spectrum of a complex is the appearance of a new band (or bands) which arise from stretching or bending of the intermolecular bond. Identification of the vibrations of the complex molecule comprises one main area of interest for the Raman spectra of EDA complexes.

The complexes studied in this research have tetracyanoethylene (TCNE) as the electron acceptor, and aromatic organic compounds as electron donors; the complexes investigated most thoroughly are those with methyl or methoxy substituted benzenes as donors. The Raman spectra of TCNE complexes are of interest partly because many of their other properties have already been reported, including absorption spectra[7-9], fluorescence spectra[10-13], equilibrium constants for complex formation[14-18], and others[19]. A particularly interesting question for some of these TCNE EDA complexes is that

of the possible existence of more than one geometric isomer for a complex[7]; as shown in Chapter 5, the Raman spectra help to clarify this matter.

· In order that the intermolecular interactions of the EDA · complexes are not subject to the additional forces present in a crystal lattice, the present investigation of the Raman spectra is confined to solution studies at ordinary temperatures. This proves to be advantageous, because the strong visible absorption of the TCNE complexes means that Raman spectra are more easily obtained for solutions than for crystalline complexes. Furthermore, since most of the published data for these complexes (see above) has been obtained for solutions, the results of the present study can be directly compared to the relevant literature results.

The Raman spectra of a limited number of EDA complexes had been obtained prior to the time at which the research described here was undertaken, although no successful studies of $\pi-\pi$ complexes had been reported. Some data were available for complexes between σ acceptors and π donors such as I_2 complexes with benzene or methylbenzenes[4], and for complexes between σ acceptors and n donors, especially halogen and interhalogen complexes with pyridine and related donors[3]. These spectra show generally that the effect of complexation on the component bands increases with the strength of the complex formed. A much more significant result was found for the strong pyridine-iodine system, where a band at 163 cm^{-1} was interpreted as the N-I intermolecular stretching mode[3]. This suggested the investigation of the Raman spectra of $\pi-\pi$ complexes with the goal of identification of the intermolecular vibration,

which however is expected to occur at considerably lower energy than the 163 cm^{-1} quoted above because of the weaker nature of π-π complexes.

The older Raman spectra of EDA complexes mentioned above were obtained, of course, using an excitation source then in common use, in particular the Helium-Neon laser. Many of the complexes whose spectra were obtained with this laser do not absorb significantly at 632.8 nm, hence resonance Raman scattering was usually not observed. In contrast, when the excitation light is absorbed by the complexes, the resonance effects which occur provide much new information, as is shown by the Raman spectra of TCNE EDA complexes described in this thesis.

The infrared absorption spectra of several TCNE EDA complexes have been reported[20-24]. Since virtually all of these spectra were obtained for solid complexes, where the charge transfer interaction is weaker than in solution, the IR spectra are generally not very useful in the interpretation of the Raman solution data. The totally symmetric TCNE C=C and C≡N stretching vibrations, $\nu_{C=C}$ and $\nu_{C\equiv N}$ - active only in the Raman spectrum of uncomplexed TCNE - appear in the infrared spectra of the crystalline complexes and are shifted with respect to the $\nu_{C=C}$ and $\nu_{C\equiv N}$ bands for uncomplexed TCNE, a fact which can be related to the degree of charge transfer in the ground electronic states of the complexes. Similar shifts in these bands occur in the Raman spectra of a number of TCNE complexes as is shown by the results of the present investigation.

Among the published infrared absorption spectra of TCNE EDA

complexes, the far infrared data of Larkindale and Simkin[25] are of particular interest. These authors reported a band at 115 cm^{-1} in the spectrum of mesitylene/TCNE which they asserted was not present in the spectra of either of the uncomplexed compounds, and they assigned this band to the intermolecular stretching vibration of this complex, which made this the first published assignment of such a vibration for a $\pi-\pi$ complex. Even though some doubt as to the validity of this assignment exists because of the published IR data for uncomplexed TCNE[26], the possiblity of the occurrence of an intermolecular vibration in this frequency region is an important reason for investigating the low frequency Raman spectra of this and related TCNE complexes.

While the research described in this thesis was under way, the Raman spectra of the complexes benzene/TCNE[27,28], toluene/TCNE[28], m-xylene/TCNE[28] and anisole/TCNE[29] were reported. Although the investigations described in these papers are not nearly as extensive as those described here, the data in them on intensity changes and frequency shifts of some TCNE bands on complexation confirm the results of the present research. The conclusions in these publications are discussed in appropriate detail in Chapter 5.

1.1 Organisation of the Thesis

The main part of this thesis is arranged as described in the following paragraph. In Chapter 2, a brief summary of Raman intensity theory is given; this review is not comprehensive, but rather is intended to provide the reader with sufficient background for the subsequent interpretation of results. Chapter 3 reviews

the theory of $\pi-\pi$ EDA complexes; like Chapter 2, it includes topics chosen from a large field and is therefore selective in subject matter. The apparatus and methods used to obtain the Raman spectra of TCNE EDA complexes are described in Chapter 4. These spectra are presented in Chapter 5 and discussed in detail; this chapter constitutes the main part of the thesis. The preresonance Raman and resonance Raman effects in the TCNE bands in the spectra of the complexes are described in the first two sections of Chapter 5 and are then used to determine equilibrium constants of the complexes, which is a new method. Also discussed in this chapter are the low energy bands and the remaining bands in the spectra. The intensities in the Raman spectra of the complexes lead to an improved vibrational assignment of TCNE, which is the subject of Chapter 6. Finally in Chapter 7, conclusions based on the results in Chapter 5 are given, as are some suggestions for further work.

Several appendices follow the main text of the thesis. In the first one, all abbreviations used are defined. The Raman spectra of the compounds used as electron donors are not essential to the main investigation, and are therefore given as Appendix B. Calculations of resonance Raman excitation profiles, absorption spectra and fluorescence spectra which are based on a model of resonance Raman scattering proposed in Chapter 5 are described in Appendix C. In the last appendix the results of a photoconductivity experiment which can detect the ionic dissociation of the complexes in their first excited states, and thereby confirm further the model of resonance Raman scattering mentioned above, are presented.

REFERENCES

1. R.S. Mulliken and W.B. Person, Molecular Complexes, A Lecture and Reprint Volume, (Wiley-Interscience, New York, 1969).

2. J. Yarwood, in Spectroscopy and Structure of Molecular Complexes, J. Yarwood, ed. (Plenum Press, London, 1973).

3. P. Klaboe, J. Am. Chem. Soc. 89, 3667 (1967).

4. H. Rosen, Y.R. Shen and F. Stenman, Mol. Phys. 22, 33 (1971).

5. R. Mierzecki, Adv. Mol. Rel. Proc. 5, 129 (1973).

6. G. Briegleb, Elektronen-Donator-Acceptor-Komplexe, (Springer-Verlag, Berlin, 1961).

7. E.M. Voigt, J. Am. Chem. Soc. 86, 3611 (1964).

8. E.M. Voigt and C. Reid, J. Am. Chem. Soc. 86, 3930 (1964).

9. A. Zweig, J. Phys. Chem. 67, 506 (1963).

10. J. Prochorow, Bull. Acad. Polon. Sci., Ser. Sci. Math. Astr. Phys. 15, 37 (1967).

11. J. Prochorow and A. Tramer, J. Chem. Phys. 47, 775 (1967).

12. J. Prochorow, J. Luminescence 9, 131 (1974).

13. J. Prochorow, Bull. Acad. Polon. Sci., Ser. Sci. Math. Astr. Phys. 22, 1283 (1974).

14. R.E. Merrifield and W.D. Phillips, J. Am. Chem. Soc. 80, 2778 (1958).

15. M.J.S. Dewar and C.C. Thompson, Tetrahedron, Suppl. 7, 97 (1966).

16. R. Foster and I.B.C. Matheson, Spectrochim. Acta 23A, 2037 (1967).

17. S.C. Liao and R.K. Chan, Can. J. Chem. 49, 2700 (1971).

18. B.B. Bhowmik and P.K. Srimani, Spectrochim. Acta 29A, 935 (1973).

19. A.H. Rice, in Spectroscopy and Structure of Molecular Complexes, J. Yarwood, ed. (Plenum Press, London, 1973).

20. J. Stanley, D. Smith, B. Latimer and J.P. Devlin, J. Phys. Chem. 70, 2011 (1966).

21. B. Moszynska and A. Tramer, J. Chem. Phys. 46, 820 (1967).

22. B. Moszynska, Acta Phys. Polon. 33, 959 (1968).

23. B. Boszynska, Bull. Acad. Polon. Sci., Ser. Sci. Math. Astr. Phys. 17, 99 (1969).

24. J.C. Moore, D. Smith, Y. Youhne and J.P. Devlin, J. Phys. Chem. 75, 325 (1971).

25. J.P. Larkindale and D.J. Simkin, J.Chem. Phys. 56, 3730 (1972).

26. F.A. Miller, O. Sala, P. Devlin, J. Overend, E. Lippert, W. Luder, H. Moser and J. Varchmin, Spectrochim. Acta 20, 1233 (1964).

27. L.M. Fraas, J.E. Moore and R.E. Bruns, Chem. Phys. Lett. 21, 357 (1973).

28. K. Kaya, A. Nakatsuka, N. Kubota and M. Ito, J. Raman Spectrosc. 1, 595 (1973).

29. P.W. Jensen, Chem. Phys. Lett. 39, 138 (1976).

2. SUMMARY OF RAMAN INTENSITY THEORY

Before the results of the Raman intensity studies of the
TCNE EDA complexes are discussed, it is necessary to review some
of the principles of the theories of Raman scattering. Therefore,
this chapter is intended to provide sufficient theoretical
background for the interpretation of the Raman spectra presented
in Chapter 5. For a more comprehensive survey of the theories
of Raman intensity, the recent review of Hester[1] can be consulted.

As shown in Chapter 5, the preresonance Raman effect and the
resonance Raman (RR) effect are very important in the spectra of
the TCNE EDA complexes. These two particular types of Raman
scattering account for the appearance of the TCNE bands in the
spectra of the complexes; accordingly, each one is discussed in
the present chapter. Other bands in the spectra are due to
nonresonance scattering, so a section of this chapter is also
devoted to this process. In the discussions of each type of
scattering, particular attention is paid to the excitation
frequency dependence of the Raman intensity, since this dependence
can be used to identify the type of scattering observed, and to
provide a convenient check on the theories.

2.1 Nonresonance Raman Intensities

Ordinary Raman scattering occurs when the frequency of the
exciting light is far from any electronic absorption associated
with the scattering molecule (Fig. 1). This scattering occurs
when the separation between the excitation frequency and the
absorption band is about 10,000 cm^{-1} or more. The intensities of
Raman bands far from resonance can be discussed in terms of
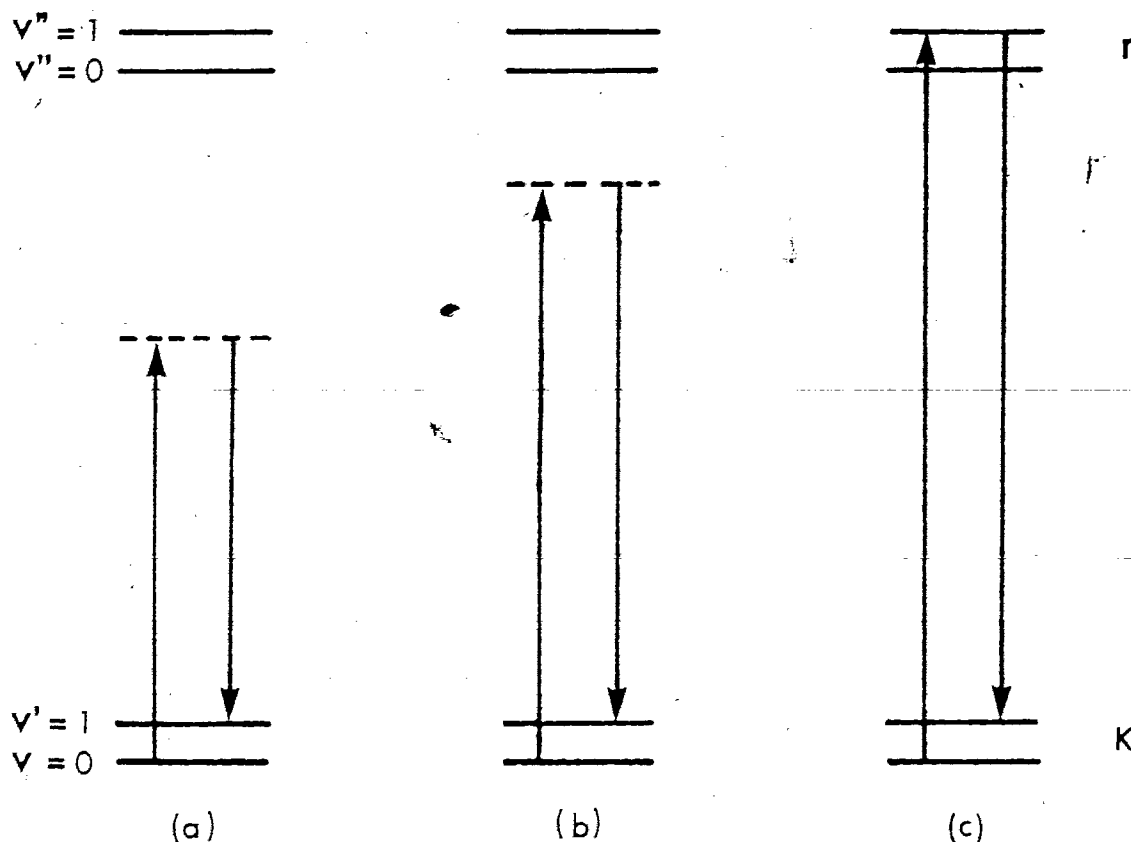
Fig. 1 Schematic representation of three
types of Raman scattering. (a), nonresonance
Raman; (b), preresonance Raman; (c), resonance
Raman. k is the ground electronic state
and r is an excited electronic state; v, v'
and v" are vibrational quantum numbers.

either the classical[2] or the quantum mechanical theories; the

quantum theory is outlined below.

2.1.1 Quantum Theory

   In the quantum mechanical picture of light scattering, the

electric field of the incident light, acting on the charges of

the molecule, perturbs its wavefunction. This approach to

scattering, which involves the summation over states problem of

second order perturbation theory, was first developed in 1925

by Kramers and Heisenberg[3] by analogy to the classical theory of

dispersion. Based on their results, the quantum mechanical expression for the scattering tensor is[4]

$$(\alpha_{\rho\sigma})_{vv'} = \frac{1}{h} \sum_r \left(\frac{(M_\rho^0)_{rk}^{v''v'} (M_\sigma^0)_{kr}^{vv''}}{\nu_{r,v'';k,v} - \nu_0} + \frac{(M_\rho^0)_{kr}^{vv''} (M_\sigma^0)_{rk}^{v''v'}}{\nu_{r,v'';k,v'} + \nu_0} \right) \qquad (2.1)$$

where h is Planck's constant; ρ and σ are the Cartesian axes x, y and z; $(M_\rho^0)_{rk}^{v''v'}$ is the ρth component of the vibronic matrix element $M_{rk}^{v''v'} = \langle k,v' | M | r,v'' \rangle$ with M the electric dipole operator; the v" are the vibrational levels of the intermediate states r; k denotes the ground electronic state; v and v' are the initial and the final vibrational levels involved in the transition, respectively. The summation in equation (2.1) can be evaluated either by means of a vibronic expansion or else in terms of the ground state polarisability; the various procedures for the simplification of this sum have been reviewed by Tang and Albrecht[5].

The total intensity of the Stokes Raman light of frequency $\nu_0 - \nu_m$ scattered into the solid angle 4π is[5]

$$I_{vv'} = \frac{2^7 \pi^5}{3^2 c^4} I_0 (\nu_0 - \nu_m)^4 \sum_{\rho,\sigma} |(\alpha_{\rho\sigma})_{vv'}|^2 \qquad (2.2)$$

Because of the denominators in equation (2.1), $(\alpha_{\rho\sigma})_{vv'}$ depends on the excitation frequency. However, far from resonance, the frequency denominators in equation (2.1) vary slowly with ν_0, and the scattered intensity hardly deviates from the $I_{vv'} \sim (\nu_0 - \nu_m)^4$ relation. This ν^4 dependence of the scattered intensity is commonly observed in the spectra of a wide variety of molecules.

2.2 Preresonance Raman Effect

According to equations (2.1) and (2.2), when the excitation frequency approaches an absorption band, the intensities of the Raman bands of the absorbing compound can no longer be expected to follow the ν^4 law. The first term in equation (2.1) begins to outweigh the second, and the scattered intensity increases with ν_0 faster than ν^4 increases. The excitation frequency is said to be in the preresonance region; the preresonance Raman intensities are generally about one order of magnitude greater than the non-resonance Raman intensities. Preresonance scattering occurs when the excitation frequency is approximately 3,000 cm^{-1} to 10,000 cm^{-1} away from the absorption maximum[6]; the onset of preresonance for a compound is not well defined, since its various Raman bands may first show deviations from the ν^4 law at different excitation frequencies.

Besides having a stronger ν_0 dependence than the ordinary Raman effect, preresonance Raman scattering is also distinguished by changes in the depolarisation ratios of the intensified bands with respect to their nonresonance values. The explanation for these changes is given in Sec. 2.2.2.

2.2.1 Sources of Preresonance Raman Intensity

When the excitation frequency is in the preresonance region, there are two important sources of Raman intensity[7]. The first is based on a shift of the equilibrium nuclear position along the Raman active vibrational coordinate upon excitation of the molecule; such a Raman band is Condon allowed[8], and derives its intensity from the difference between the geometries of the two

electronic states[9]. The other origin of preresonance Raman intensity involves a vibronic coupling of the first excited electronic state with one or more higher excited electronic states; this mechanism is closely connected with the activity of the vibrations in the vibronic spectra of the molecules[10].

These two types of scattering can be distinguished experimentally by means of their different excitation frequency dependences. Expressions for these ν_0 dependences were derived by Albrecht and Hutley[7] through a modification of the vibronic expansion[5] of equation (2.1). The results of their analysis are the frequency factors

$$F_A = \nu^2 \; \frac{\nu_{rk}^2 + \nu_0^2}{(\nu_{rk}^2 - \nu_0^2)^2} \qquad F_B = 2\nu^2 \; \frac{\nu_{tk}\nu_{rk} + \nu_0^2}{(\nu_{rk}^2 - \nu_0^2)(\nu_{tk}^2 - \nu_0^2)} \qquad (2.3)$$

where ν_{rk} and ν_{tk} are the transition frequencies to the first excited electronic state r and to a higher excited state (or average of states) t, respectively; ν is the frequency of the scattered light. If the preresonance Raman band derives its intensity from the Condon mechanism, its intensity is predicted to be proportional to F_A^2; if vibronic coupling is important, then the intensity should vary as F_B^2. These results were derived for a totally symmetric vibration by assuming that only one component of the scattering tensor is enhanced under the preresonance condition (cf. Sec. 2.2.2). Examples of F_A^2 dependence[11] and of F_B^2 dependence[12] of preresonance Raman intensities can be found in the literature.

An essential feature of the F_B term is that the Raman

intensity depends on the vibronic coupling matrix element which connects states r and t, and in order that these states may be coupled, the transitions to them must have the same polarisation[7]. In the theory of vibronic coupling[10], the vibrations which couple states r and t are predicted to give preresonance enhanced bands. The activity in the preresonance Raman spectra of vibrations known to mix the first excited state with higher excited states supports this vibronic theory[12,13].

2.2.2 Depolarisation Ratios

One essential aspect of the preresonance Raman spectra is the depolarisation data for the bands which are enhanced in intensity. In this section, the tendency of these depolarisation ratios to approach certain limiting values is explained, and shown to depend on the degeneracy of the excited state r which is near the Raman excitation frequency. Finally, the analysis is extended to include resonance Raman scattering, and a selection rule for the enhanced Raman bands is given.

The depolarisation ratio of a Raman band when excited with plane polarised light is[3]

$$\rho_i = \frac{3\beta^2}{45\alpha^2 + 4\beta^2} \tag{2.4}$$

where the spherical part of the polarisability derivative is

$$\alpha = \frac{1}{3}(\alpha'_{xx} + \alpha'_{yy} + \alpha'_{zz})$$

and its anisotropy is

$$\varepsilon^2 = \frac{1}{2}\left\{ (\alpha'_{xx} - \alpha'_{yy})^2 + (\alpha'_{yy} - \alpha'_{zz})^2 + (\alpha'_{zz} - \alpha'_{xx})^2 + 6(\alpha'^2_{xy} + \alpha'^2_{xz} + \alpha'^2_{yz}) \right\}$$

where the α'_{ij} are the components of the polarisability derivative with respect to the vibrational coordinate.

When a single electronic state is the dominant source of the preresonance Raman intensity, and the transition to this state is in a specific direction, e.g. x, all α'_{ij} except α'_{xx} vanish[14]. In this case, $\alpha = \frac{1}{3}(\alpha'_{xx})$, $\varepsilon^2 = \alpha'^2_{xx}$ and equation (2.4) becomes

$$\rho_\ell = \frac{3\alpha'^2_{xx}}{45\left(\frac{1}{9}\alpha'^2_{xx}\right) + 4\alpha'^2_{xx}} = \frac{1}{3} \tag{2.4a}$$

The limiting value $\rho_\ell = 0.33$ occurs in the preresonance Raman enhanced bands of many different compounds[15].

If the preresonant excited state is doubly degenerate, then the dipole transition can be in either of two directions with respect to the molecule. Thus e.g. $\alpha'_{xx} = \alpha'_{yy} \neq 0$, with all other $\alpha'_{ij} = 0$; in this case equation (2.4) reduces to $\rho_\ell = 1/8$. If the degeneracy is any higher, $\rho_\ell = 0$. Observed depolarisation ratios equal to 1/8 for resonance Raman bands have been cited as evidence of the degeneracy of the resonant excited state[11,16].

In the case of resonance Raman scattering (Sec. 2.3), α and β take on new meanings, and then correspond to the absolute squares of the transition moments along or across the bond axis, respectively[17,18]. However, the limiting values of the depolarisation ratios are the same as those given above for preresonance Raman scattering[17].

Equation (2.4a) permits a conclusion regarding the activity of vibrations in the preresonance or resonance Raman spectra.

Because ρ_ℓ is less than 0.75 only for totally symmetric vibra-
tions[4], the above analysis implies that only totally symmetric
vibrations are allowed in the preresonance or resonance Raman
effects. A somewhat different approach for the case of resonance
Raman scattering leads to the same conclusion regarding the
symmetry of the allowed vibrations, provided that the symmetry of
the molecule in the excited state is the same as that in the
ground-state[19].

2.3 Resonance Raman Intensities

When the wavelength of the excitation light falls within an
absorption band of the sample, the resonance Raman effect may be
observed. The most obvious characteristic of this effect is an
increase of up to several orders of magnitude in the intensities of
the affected bands. RR scattering, like preresonance Raman
scattering, is characterised by changes in depolarisation ratios
of the intensity enhanced bands with respect to their nonresonance
values (Sec. 2.2.2).

At resonance, equation (2.1) is not valid, and must be
modified by the introduction of a damping term into the frequency
denominator. When this is done, the denominators account for many
of the features of RR scattering, including the RR intensity
enhancements and the dominance of the first term under the summation.
Because of the proximity of ν_0 to the molecular vibronic frequency
$\nu_{r,v'';k,v}$ very few states r contribute to the scattering tensor;
since $\nu_{r,v'';k,v} - \nu_0$ is of the order of ν_m, the summation must be
extended over v''. Consistent with the above discussion of
preresonance Raman scattering, the RR scattering region can be

defined to include excitation frequencies within about 3000 cm^{-1}, on either side of the absorption maximum.

Because of the considerable amount of material on the subject of RR scattering published in recent years, a detailed review is clearly beyond the scope of this section. Instead, an outline of the theories of RR scattering which are used in the interpretation of the spectra of the TCNE complexes is presented here. For comprehensive reviews of theoretical[17] and experimental[14] aspects of RR scattering, the publications of Behringer should be consulted.

2.3.1 Theory of Behringer

The simplification of the RR scattering tensor considered first is the one proposed a number of years ago by Behringer[20]. In this approach, the tensor is decomposed into real and imaginary parts, and the behaviour of each part is investigated as the excitation frequency varies across the absorption band. This method is discussed here because of its similarity to the approach used for the calculation of RR excitation profiles in Appendix C.

Beginning with equation (2.1), the damping factor $\gamma_{r,v''}$ is introduced into the scattering tensor, and the second term under the summation is neglected. Reexpressing the vibronic transition moments as products of pure electronic transition moments and vibrational overlap integrals then gives

$$(\alpha_{\rho\sigma})_{vv'} = \frac{1}{\hbar} \sum_{v''} \frac{(M_\sigma^0)_{kr} (M_\rho^0)_{rk} \langle v|v''\rangle\langle v''|v'\rangle}{\nu_{r,v'';k,v} - \nu_0 + i\gamma_{r,v''}} \tag{2.5}$$

wherein the summation over all the states r,v'' is reduced to a
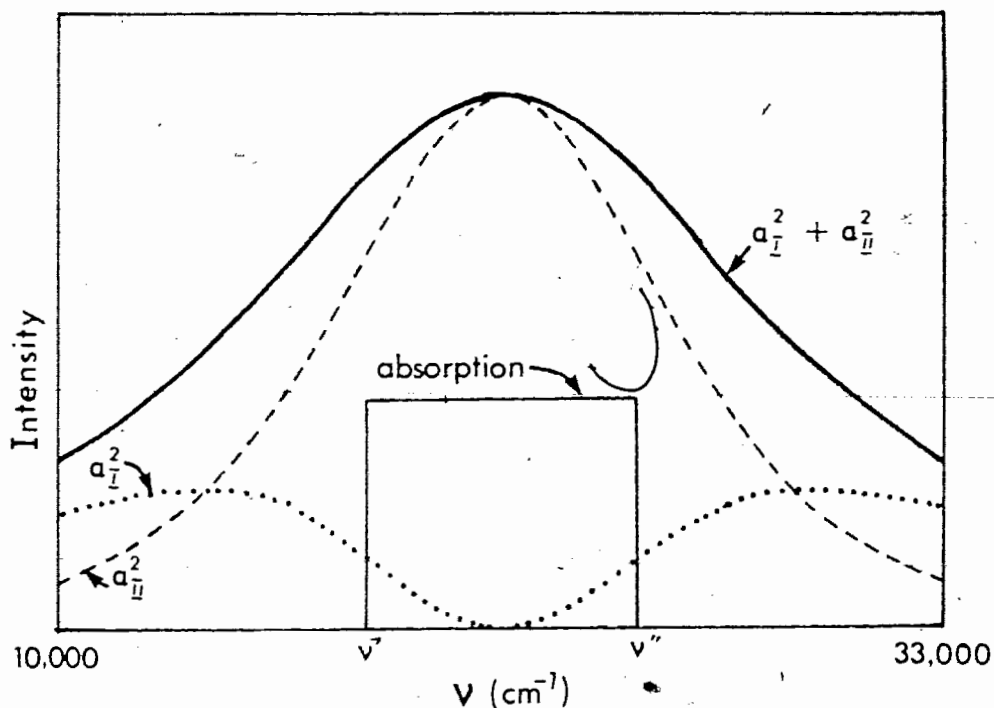
Fig. 2 Frequency dependence of the resonance
Raman intensity according to the theory of
Behringer.

summation over the vibrational levels v" of the single resonating
state r; equation (2.5) is equivalent to the retention of only
the first term in the vibronic expansion of the scattering tensor
(Sec. 2.3.2). Behringer[20] restricted his analysis to the case
v = v' = 0, i.e. to resonance Rayleigh scattering, but the results
can be generalised to include resonance Raman scattering if the
potential energy surfaces of states k and r are different[4].

Assuming that the absorption probability is constant between
frequencies v' and v'', and vanishes elsewhere, a rectangular
absorption band is introduced. Approximation of the summation by
an integral over the extent of this absorption band then gives

$$(\alpha_{\rho\sigma})_{vv'} = \frac{1}{h} \int_{v'}^{v''} \frac{dv}{v - v_0 + i\gamma_{r,v''}} = \alpha_I + i\alpha_{II} \tag{2.6}$$

where

$$\alpha_I = \frac{1}{h} \int_{\nu'}^{\nu''} \frac{(\nu - \nu_0)d\nu}{(\nu - \nu_0)^2 + \gamma_{r,v''}^2} \qquad \alpha_{II} = -\frac{1}{h} \int_{\nu'}^{\nu''} \frac{\gamma_{r,v''}d\nu}{(\nu - \nu_0)^2 + \gamma_{r,v''}^2}$$

where ν' and ν'' are the lower and the upper limits of the absorption (Fig. 2). As shown in equation (2.6), the RR scattering tensor contains both real and imaginary components.

According to equation (2.2), the Raman intensity is proportional to the squared modulus of the scattering tensor; thus the RR excitation profile varies as $\alpha_I^2 + \alpha_{II}^2$. In Fig. 2, this sum and its components are plotted in the vicinity of the rectangular absorption band. As shown in the Figure, far from resonance the contribution of α_{II} is comparatively unimportant; on the other hand, in the centre of the absorption band the scattering tensor is imaginary, i.e. only the α_{II} component determines the Raman intensity. The inclusion of the damping term $i\gamma_{r,v''}$ in the expression for the RR scattering tensor, which mathematically leads to the existence of α_{II}, is therefore most essential. In the context of this theory, the excitation frequency dependence of the sum $\alpha_I^2 + \alpha_{II}^2$ is responsible for the deviation of the scattered intensity from the ν^4 law.

2.3.2 Vibronic Expansion of the Scattering Tensor

There has been a considerable amount of research into the vibronic expansion theories of RR intensity recently[5,6,10,21-24]. Of special interest here is the theory of Albrecht[10] and some of its refinements, which are amenable to experimental verification.

According to Koningstein and co-workers[3,22], based on the vibronic coupling model of Albrecht[10] the RR scattering tensor is given by the expression

$$(\alpha_{\rho\sigma})_{vv'} = \frac{1}{h(\nu_{r,v'';k,v} - \nu_0 + i\gamma_{r,v''})}\left(\sum_{r,v''}(M^0_\rho)_{rk}(M^0_\sigma)_{kr}<v|v''><v''|v'> + \right.$$

$$+\sum_{r,t,v''} h^Q_{tr}\left[(M^0_\sigma)_{kt}(M^0_\rho)_{rk}<v'|v''><v''|Q|v> + \right.$$

$$\left. + (M^0_\rho)_{tk}(M^0_\sigma)_{kr}<v|v''><v''|Q|v'>\right] +$$

$$+\sum_{\substack{r,t\neq k, \\ v''}} h^Q_{tk}\left[(M^0_\rho)_{rk}(M^0_\sigma)_{tr}<v'|v''><v''|Q|v> + \right.$$

$$\left.\left. + (M^0_\sigma)_{kr}(M^0_\rho)_{tr}<v|v''><v''|Q|v'>\right]\right)$$

(2.7)

where $h^Q_{tr} = <t|\frac{\partial H}{\partial Q}|r> / (E^0_r - E^0_t)$ is the vibronic coupling operator in which the Hamiltonian H is differentiated with respect to the coordinate Q at the equilibrium position of the nuclei, and all of the other symbols have the same meanings as previously stated. As can be seen from the frequency denominator, equation (2.7) comes from the expansion of the first term only in equation (2.1).

In the vibronic theory of RR intensity, the selection rules are based on the conditions for the nonvanishing of the vibrational overlap integrals $<v|v''>$ and $<v''|v'>$ and of the matrix elements $<v|Q|v''>$, etc. These selection rules depend upon the location of the resonance frequency with respect to the pure electronic transition frequency of the molecule, and on the differences which may exist between the potential energy surfaces of the ground

and excited states. In the event that these potential energy surfaces are not equal, all of the terms in equation (2.7) can contribute to the scattering tensor.

Since resonance can occur with a pure electronic transition $(\nu_{r,v";k,v} = \nu_{r,0;k,0})$ or with a vibronic transition (e.g. $\nu_{r,v";k,v} = \nu_{r,1;k,0}$), the restrictions on $v"$ which determine the selection rules also locate the position of the resonance $\nu_{r,v";k,v} - \nu_0 \approx 0$. Thus, it is possible that the terms in equation (2.7) may resonate at different frequencies, according to the value of $v"$ in the numerator of each term[22]. This principle is utilized in Chapter 5 for the simplification of the RR scattering tensor for the EDA complexes.

REFERENCES

1. P.E. Hester, in Molecular Spectroscopy, Vol. 2, (The Chemical Society, London, 1974).

2. L.A. Woodward, Introduction to the Theory of Molecular Vibrations and Vibrational Spectroscopy, (Oxford University Press, London, 1972).

3. H.A. Kramers and W. Heisenberg, Z. Physik 31, 681 (1925).

4. J.A. Koningstein, Introduction to the Theory of the Raman Effect, (D. Reidel, Dordrecht, Holland, 1972).

5. J. Tang and A.C. Albrecht, in Raman Spectroscopy, Vol. 2, H.A. Szymanski, ed. (Plenum Press, New York, 1970).

6. G.J. Small and E.S. Yeung, Chem. Phys. 9, 379 (1975).

7. A.C. Albrecht and M.C. Hutley, J. Chem. Phys. 55, 4438 (1971).

8. E.S. Yeung, M. Heiling and G.J. Small, Spectrochim. Acta 31A, 1921 (1975).

9. A.Y. Hirakawa and M. Tsuboi, Science 188, 359 (1975).

10. A.C. Albrecht, J. Chem. Phys. 34, 1476 (1961).

11. T.C. Strekas, A.J. Packer and T.G. Spiro, J. Raman Spectrosc. 1, 197 (1973).

12. T.C. Strekas and T.G. Spiro, J. Raman Spectrosc. 1, 387 (1973).

13. A.H. Kalantar, E.S. Franzosa and K.K. Innes, Chem. Phys. Lett. 17, 335 (1972).

14. J. Behringer, in Raman Spectroscopy, Vol. 1, H.A. Szymanski, ed. (Plenum Press, New York, 1967).

15. Y. Udagawa, M. Iijima and M. Ito, J. Raman Spectrosc. 2, 313 (1974).

16. Y.S. Bobovich, I.V. Aleksandrov, V.G. Maslov and A.N. Sidorov, JETP Lett. 18, 102 (1973).

17. J. Behringer, in Molecular Spectroscopy, Vol. 2, (The Chemical Society, London, 1974).

18. C. Manneback, Z. Physik 62, 224 (1930).

19. D. Van Labeke, M. Jacon and L. Bernard, Chem. Phys. Lett. 27, 123 (1974).

20. J. Behringer, Z. Elektrochem. 62, 906 (1958).

21. M. Mingardi and W. Siebrand, J. Chem. Phys. 62, 1074 (1975).

22. J.A. Koningstein and B.G. Jakubinek, J. Raman Spectrosc. 2, 317 (1974).

23. M.Z. Zgierski, Chem. Phys. Lett. 36, 390 (1975).

24. O. Sonnich Mortensen, Chem. Phys. Lett. 30, 406 (1975).

3.   THEORY OF $\pi-\pi$ ELECTRON DONOR/ACCEPTOR COMPLEXES

A brief theoretical background to the electronic and the vibrational spectra of $\pi-\pi$ EDA complexes is given in this chapter. This discussion is not intended to be comprehensive, but rather to describe certain aspects of the nature of EDA complexes. For more detailed theoretical descriptions of these complexes, other references can be consulted[1,2]. The goal of this chapter is to outline the most important theories of the electronic spectra, and to present some predictions regarding the vibrational spectra of $\pi-\pi$ EDA complexes, so that the experimental results described in Chapter 5 can be more fully understood.

3.1   Electronic Spectra

In this section, the electronic absorption spectrum characteristic of the EDA complex is explained in terms of its electronic states. The valence-bond treatment of Mulliken and the molecular orbital description of EDA complexes are discussed here; alternative descriptions of weak donor/acceptor interactions are given elsewhere[2].

3.1.1   Valence-Bond Model[3]

According to the valence-bond model of EDA complexes, the ground state ("normal state") wavefunction for a weak complex is written

$$\Psi_N(DA) = a\Psi_0(D\cdots A) + b\Psi_1(D^+\cdots A^-) \qquad (3.1)$$

where $\Psi_0(D\cdots A)$ is the so-called "no-bond" wavefunction, and corresponds to the structure of the complex in which the bonding occurs as a result of dipole-dipole forces, London dispersion

forces, etc. $\Psi_1(D^+\cdots A^-)$ represents the dative, or charge transfer, wavefunction, and characterises the complex in which an electron has been transferred from the donor to the acceptor. For weak complexes, such as the $\pi-\pi$ complexes studied in the present research, $a \gg b$.

The coefficients a and b determine the relative contributions of the normalised no-bond and dative wavefunctions. These coefficients satisfy the normalisation condition

$$(a^2 + abS) + (b^2 + abS) = 1 \qquad (3.2)$$

where the overlap integral S is defined by

$$S = \int \Psi_0^*(D\cdots A) \Psi_1(D^+\cdots A^-) d\tau \qquad (3.3)$$

and is proportional to the overlap integral between the highest filled molecular orbital of the donor and the lowest unfilled molecular orbital of the acceptor. According to the overlap and orientation principle, the donor and the acceptor molecules tend to orient themselves so as to make S a maximum. The quantity $(b^2 + abS)$ is a measure of the extent of charge transfer in the ground electronic state.[†]

The excited state of the complex has as its wavefunction

$$\Psi_E(DA) = a^*\Psi_1(D^+\cdots A^-) - b^*\Psi_0(D\cdots A) \qquad (3.4)$$

[†] Alternatively, the ratio $b^2/(a^2 + b^2)$ is sometimes referred to as the degree of charge transfer in the ground state. These two quantities are not necessarily equal; e.g. for $a = .95$, $b = .23$ and $S = .1$, the normalisation condition in equation (3.2) is satisfied, $b^2 + abS = .075$, and $b^2/(a^2 + b^2) = .056$.

where the coefficients a^* and b^* satisfy a normalisation relation

analogous to equation (3.2). In the excited state, the complex

has a high degree of ionic character, i.e. $a^* >> b^*$.

The wavefunctions in equations (3.1) and (3.4) may also

contain contributions from locally excited donor or acceptor

states [e.g. $\Psi(D^*A)$]; such contributions are ordinarily insig-

nificant for Ψ_N, but can be important in the case of Ψ_E, especially

when the energy of the locally excited state is comparable to that

of Ψ_1.

The energy levels of the EDA complex which emerge from this

resonance structure theory[4] are shown in Fig. 3. The intermolec-

ular charge transfer transition energy $h\nu_{CT}$ is given by the

equation[5]

$$h\nu_{CT} = I_D - (E_A + G_1 + G_0') + X_1 - X_0 \qquad (3.5)$$

where I_D is the vertical ionisation potential (ionisation energy);

E_A is the vertical electron affinity of the acceptor; G_0 is the

sum of ground state no-bond terms including electrostatic energy

and van der Waals energy; G_1 is the sum of dative state terms

including the Coulomb interaction; X_0 and X_1 are the resonance

energies between the no-bond and the dative structures in the

ground and excited states, respectively. Because of these

resonance energies, $h\nu_{CT}$ is not simply equal to the energy required

to transfer an electron from the donor to the acceptor (i.e. the

energy difference between the no-bond and the dative states);

instead, it is the energy of the transition between the states

whose wavefunctions are Ψ_N and Ψ_E. The sum $G_0 + X_0$ equals the

$$D^+ + A + e^-$$
$$D^+ + A^-$$
$$\underline{D^+ \cdots A^-} \longleftrightarrow D^* \cdots A$$
$$D^+ \cdots A^-$$

$$h\nu_{CT}$$

$$D + A$$

$$D \cdots A$$
$$\underline{D \cdots A} \longleftrightarrow D^+ \cdots A^-$$
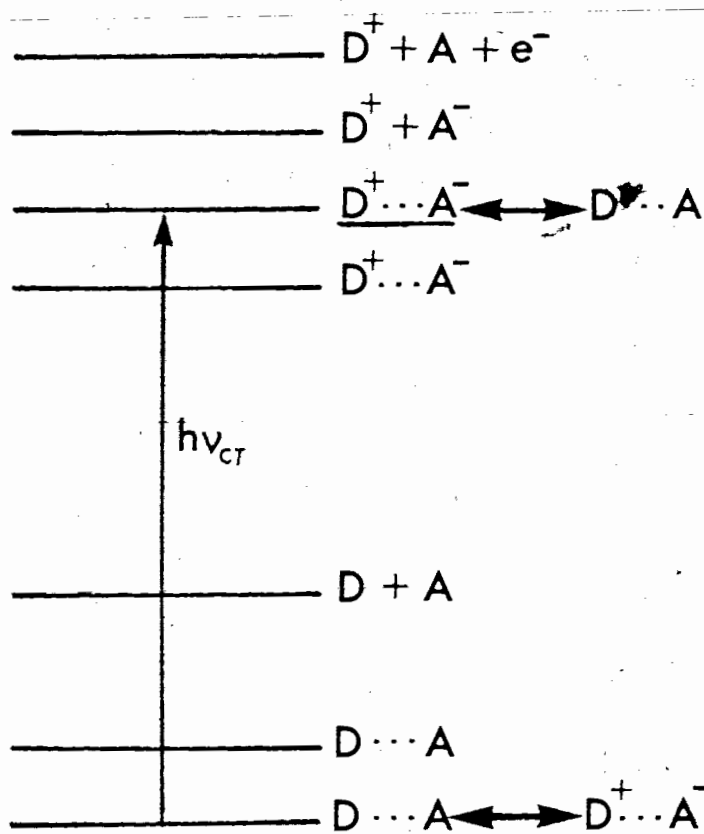
Fig. 3 Energy level diagram of an EDA complex.
The underlined structures are the dominant ones
for the ground and the excited electronic states.

binding energy, i.e. the energy given up when two molecules

interact and form a complex in the ground electronic state. This

intermolecular binding energy is the thermodynamic quantity ΔH.

For π-π complexes such as those studied here, I_D is the

dominant term in equation (3.5); because of this, for a series of

complexes having the same acceptor, $h\nu_{CT}$ has an almost linear

relationship with the ionisation potentials of the donors. The

dependence of the energy of the CT band on the donor ionisation

potential has been discussed extensively elsewhere[2,4].

It should be pointed out that this analysis strictly applies

only to EDA complexes in the vapour phase, and that the energetics

of these complexes are somewhat changed in solution. However, most experimental data are obtained for solutions and often must be interpreted without specific consideration of solvation effects, the extent of which are known for only a limited number of cases.

3.1.2 Molecular Orbital Treatment

A simple molecular orbital picture of the EDA complex[6,7] can be used to discuss its electronic transitions without recourse to the valence-bond model described above. In this molecular orbital approach, the CT band of the complex, or the lowest energy CT band of a complex which has multiple CT bands, is attributed to the transfer of an electron from the highest occupied molecular orbital of the donor to the lowest vacant molecular orbital of the acceptor.

Some comments on the molecular orbital interpretation of the CT transitions in the complexes where substituted benzenes are the electron donors are appropriate here, since these donors are used extensively in this work. In benzene, the highest occupied electronic state is of E_{1g} symmetry, and is thus doubly degenerate. Substitution on the benzene ring removes this degeneracy, and produces two occupied orbitals whose energy difference depends on the number of substituents, their nature, and their positions on the ring[8]. As a consequence, two CT bands are usually observed for EDA complexes having substituted benzenes as electron donors (except when the substitution does not remove the degeneracy, e.g. in hexamethylbenzene). For TCNE complexes, a correlation has been observed between the difference in the energies of the two highest occupied donor orbitals and the spacing of the CT absorption bands[8,9], which is consistent with this analysis.

In the complexes where the degeneracy of the highest filled benzene orbital has been removed by substitution, the overlap and orientation principle (Sec. 3.1.1) predicts two definite configurations of the complex; in favourable cases, these geometric isomers can be correlated with the two CT bands, although it should be remembered that for room temperature solutions, the barrier to the rotation between these configurations is small enough that the distinction between them may be lost[2]. The question of the correlation of the two distinct geometric structures of a complex with its multiple CT bands is considered from the standpoint of the experimental results for the TCNE EDA complexes in Chapter 5.

3.2 Vibrational Spectra

The theory of the vibrational spectra of EDA complexes, in contrast to that of the electronic spectra, has not been developed very extensively. Because of this, only a brief discussion can be presented in this section. For an extensive review of the theoretical aspects of these vibrational spectra, the recent publication of Person[10] should be consulted, especially with regard to the infrared absorption spectra of EDA complexes.

One area of the vibrational spectra for which some theoretical predictions can be made concerns the frequency shifts in the donor and acceptor bands which accompany complexation. These frequency shifts in general can be caused by the coupling of the affected vibrations with other donor or acceptor vibrations, by geometric structure changes of the component molecules on complexation, or by changes in the vibrations which are due to electrostatic or

dispersion effects[10]. Any theory which accounts for these effects must predict changes in the force constants of the bonds which are affected by the complexation.

According to the valence-bond theory described in Sec. 3.1.1, the changes in the force constants which accompany the formation of $\pi-\pi$ EDA complexes are expected to be very small. If several C=C bonds are involved in the donor vibration (e.g. in a ring mode of benzene or a substituted benzene), although a slight weakening of the stretching force constants is expected because of the sacrificial character of the donor, when this effect is delocalised over a number of bonds, it may be too weak to be observed. The C=C stretching frequency in a π acceptor such as TCNE should be lowered by complexation, since the electron accepted by the molecule goes into an antibonding orbital, weakening the C=C bond; since the delocalisation is much less extensive in a small molecule such as TCNE, the chance of observing such a decrease in frequency is much greater than in the case of a molecule such as benzene.

The "classical" electrostatic and dispersion interactions mentioned above can also affect the positions of the component vibrational bands; in the case of $\pi-\pi$ complexes, the resulting frequency shifts can be as great as those which are due to complexation. Because of this, the solvent effect of liquid electron donors such as benzene and some of the substituted benzenes on the band positions must be taken into consideration when the donor serves as the solvent.

The subject of Raman intensity effects in the spectra of $\pi-\pi$

EDA complexes, which is the central theme of this thesis, is a

new one; consequently, no references to this topic can be cited

here.   Instead, Raman intensity theory is discussed from a some-

what more general viewpoint in Chapter 2.

- REFERENCES

1. R.S. Mulliken and W.B. Person, <u>Molecular Complexes, A Lecture and Reprint Volume</u>, (Wiley-Interscience, New York, 1969).

2. R. Foster, <u>Organic Charge Transfer Complexes</u>, (Academic Press, London, 1969).

3. R.S. Mulliken, <u>J. Am. Chem. Soc.</u> <u>74</u>, 811 (1952).

4. G. Briegleb, <u>Elektronen-Donator-Acceptor-Komplexe</u>, (Springer-Verlag, Berlin, 1961).

5. R.S. Mulliken and W.B. Person, in <u>Annual Review of Physical Chemistry</u>, H. Eyring, ed. (Annual Reviews, Palo Alto, U.S.A., 1962).

6. M.J.S. Dewar and A.R. Lepley, <u>J. Am. Chem. Soc.</u> <u>83</u>, 4560 (1961).

7. A.R. Lepley and C.C. Thompson, <u>J. Am. Chem. Soc.</u> <u>89</u>, 5523 (1967).

8. E.M. Voigt, <u>J. Am. Chem. Soc.</u> <u>86</u>, 3611 (1964).

9. S. Pignataro and G. Aloisi, <u>Z. Naturforsch.</u> <u>27A</u>, 1165 (1972).

10. W.B. Person, in <u>Spectroscopy and Structure of Molecular Complexes</u>, J. Yarwood, ed. (Plenum Press, London, 1973).

4. EXPERIMENTAL

4.1 Excitation and Detection

Most of the Raman spectra reported in this thesis were obtained with a Coherent Radiation Model 52G Argon Ion laser as the excitation source. The eight visible lines of this laser ranging from 514.5 nm (19,430 cm^{-1}) to 457.9 nm (21,831 cm^{-1}) are each of sufficient power to produce satisfactory spectra of the EDA complexes of TCNE; another line at 454.5 nm is too weak for the study of the complexes.

Spectra excited with the Argon laser are complicated in some cases by plasma emission lines[1], which are of comparable intensity to the weak Raman bands of the EDA complexes. The appearance of these plasma lines in the spectra may be conveniently kept to a minimum through careful choice of the appropriate experimental geometry; various checks were made to ensure that none of the observed bands in the spectra are attributable to the plasma lines.

A few Raman spectra of the EDA complexes were excited with a Spectra-Physics Model 125 Helium-Neon laser, which has an output wavelength of 632.8 nm (15,798 cm^{-1}). Because of the comparatively low (about 50 mw) power of this laser, it can be used for the spectra of the complexes only when the absorptions of the samples at the laser wavelength are small. Raman spectra excited with a Helium-Neon laser can be interfered with by Neon emission lines[1]; as in the case of Argon laser excitation, experimental safeguards prevent these lines from being interpreted as Raman bands of the samples.

A small number of the Raman spectra were excited with a

Coherent Radiation Model 590 Dye Laser; the dye laser was pumped with the Argon laser. The lasing dye was Rhodamine 6G dissolved in ethylene glycol, and the wavelength of the dye laser radiation was in the vicinity of 600 nm.

Because of the strong absorption of the laser light by most of the EDA complexes, the laser power had to be kept below about 250 mw to avoid significant heating of the samples. The use of higher laser power for strongly absorbing solutions produces spurious heating effects in the spectra (relative intensities dependent upon power used)[2]. This heating effect is first noticeable when the laser power is about 400 mw; with the power at 250 mw or less, no measurable temperature rise occurs within the time required to record a spectrum. The measurement of the Stokes/antiStokes intensity ratio for the bands of a strongly absorbing EDA complex solution when excited with about 200 mw laser power confirmed that no detectable temperature rise occurs within such a solution.

The solutions to be studied were contained in ordinary 1 cm^2 quartz cells. Raman spectra of strongly absorbing solutions within these cuvettes sometimes contain the interfering broad quartz Raman bands at about 450 cm^{-1}, 800 cm^{-1} and 1050 cm^{-1}; these quartz bands tend to mask medium or weak bands arising from the solutions.

Several authors have successfully recorded Raman spectra of coloured solutions or solids through the use of the rotating sample technique[3-6]. The good results obtainable by that method suggested that a similar technique should be used with the TCNE EDA complexes.

Therefore, a rotating Raman solution cell with two compartments (suitable for ordinary spectra or difference spectra), of a design similar to that described by Kiefer[6], was constructed.† This rotating cell gave satisfactory spectra of the EDA complexes; however, the spectra thus obtained had a lower signal-to-noise ratio than that found with the 1 cm^2 cell. Because of this, the quartz cells were used almost exclusively.

The scattered light was collected with an f/0.9 lens and focused onto the entrance slit of the spectrometer. The perpendicular and the parallel polarised components of the scattered light were selected with an analyser, located in front of the entrance slit.

In the spectra recorded prior to December 1974, the scattered light was dispersed with a 3/4 metre Spex monochromator. In order to reduce background light to an acceptable level, the output of this spectrometer was passed through a second monochromator, a Spex Minimate Model 1650. In this tandem arrangement, the 3/4 metre spectrometer was scanned across the wavelength range (i.e. bandpass) for the particular Minimate settings. The accuracy of the band positions thus obtained[7] was within ±3 cm^{-1}; however, the relative intensities observed with this apparatus are not very accurate, because the efficiency of the transmission of light by the Minimate depends on the location of its wavelength with regard to the centre of the spectral bandpass for the Minimate setting.

For the more recently recorded spectra, the scattered light was analysed with a Spex Model 1301 ½ metre double spectrometer. The performance of this double spectrometer was far superior to that of the arrangement described above, so that a number of spectra obtained using the two monochromators in series could be improved with the double spectrometer. The accuracy of the band positions obtained with the Spex 1301 was also within ± 3 cm^{-1}.

The scattered light was detected with an ITT FW-130 photomultiplier tube (S-20 response), contained in a Products For Research Model TE-200 shielded housing. The generally weak Raman spectra of the complexes necessitate low background count rates, and these are achieved by cooling the PMT with a dry ice-methanol mixture.

The signals from the photomultiplier were detected with photon counting electronics; the latter consisted of an SSR Model 1120 Amplifier/Discriminator followed by either an SSR Model 1105 Data Converter or an SSR Model 1110 Digital Synchronous Computer (DSC). The DSC, which has two channels for accumulating data, was arranged to yield source-compensated spectra by using a second PMT to detect a small fixed fraction of the laser beam, and comparing the counts in the signal and the reference channels. The limiting sample count rates for an S/N ratio of one with the photon counting equipment were about 5 photons/s, while the signals for the strongly absorbing solutions usually were between 50 and 1000 photons/s. The spectra were recorded on a Riken Denshi SP-H4 Chart Recorder.

The spectral sensitivity and the relative polarisation

response of the system (photomultiplier + spectrometer) were determined using an Electron Optics Associates L-101 Standard Lamp. The results of this calibration were in turn used to correct the relative intensities and the observed depolarisation ratios.

4.2 Raman Spectra of Colourless Samples

Spectra of each of the solid electron donors and of solid TCNE were obtained by allowing the laser beam to strike a few lumps of each polycrystalline sample, and viewing the scattered light at an angle of 90° with respect to the incident beam. Raman spectra of non-absorbing liquids (including solutions of TCNE in noncomplexing solvents) were recorded in a similar manner. For both solids and liquids, slight impurities in the samples occasionally caused fluorescence, especially with 488.0 nm excitation; this interference could be eliminated (in most cases) by using 514.5 nm or 632.8 nm excitation.

4.3 Raman Spectra of EDA Complexes of TCNE

Because of the strong absorption of the laser light by most of the EDA complexes, attempts to obtain their Raman spectra meet with several problems. For a few complexes, e.g. benzene/TCNE, a conventional 90° sample geometry can be used successfully; however, for most complexes this arrangement is not suitable.

For the solutions which significantly absorb the laser beam, a "backscattering" geometry[2] was found to be the most suitable (see Fig. 4). In this arrangement, the laser beam is incident on the cuvette wall at an angle of approximately -30° with respect to the normal, and the scattered light is collected in the direction
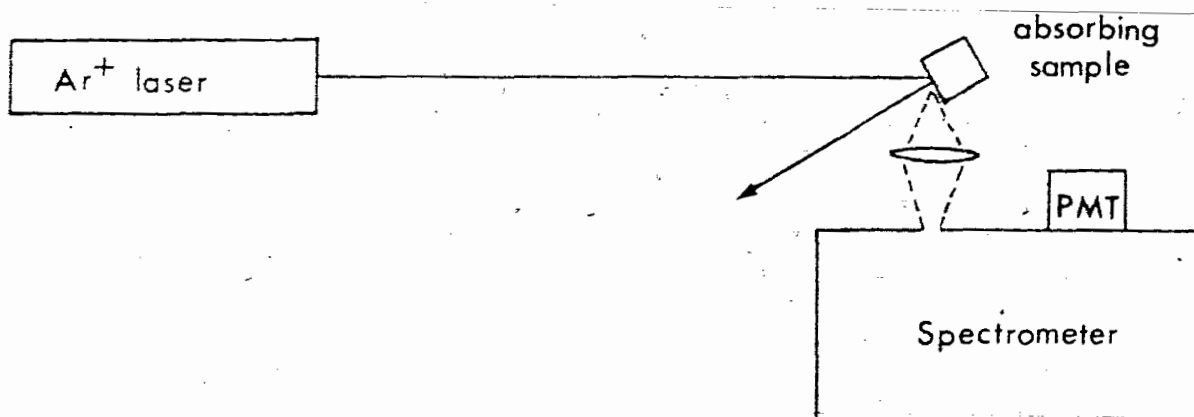
Fig. 4 Backscattering geometry used to obtain
Raman spectra of strongly absorbing EDA complex
solutions.

of approximately +60° with respect to the normal. Thus, the

direction of observation is still at right angles with respect to

the incident light, and the depolarisation ratios obtained with

this backscattering geometry can be compared with those observed

for transparent solutions with conventional 90° geometry. When

the concentration of the complex is about 10^{-2} M (Molar) or less, no

significant reabsorption problems are encountered with the

backscattering geometry, since the scattered light is collected

only from the surface layers of the sample. At higher concentra-

tions, a reabsorption effect sometimes occurs when this geometry

is used (Sec. 5.2.5).

The internal intensity standards for the preresonance Raman

and resonance Raman investigations were either the CH_2Cl_2 283 cm^{-1}

and/or 704 cm^{-1} bands, or the donor bands at about 1600 cm^{-1}

(when they were of sufficient strength). The latter reference is

especially advantageous for the study of the excitation wavelength

dependence of the TCNE $\nu_{C=C}$ band, due to their proximity and

consequent similar reabsorption intensity losses. The TCNE $\nu_{C\equiv N}$

band (about 2230 cm^{-1}) also can be studied successfully with this internal standard, except at relatively high concentrations.

The intensities of the bands used as internal standards were corrected for the (nonresonance) ν^4 excitation frequency dependence. For the case of benzene/TCNE, the 1585/1604 cm^{-1} benzene doublet, which is used as the internal standard, has been shown to follow the ν^4 law over the wavelength range covered by the Argon laser[8].

4.4 Absorption and Fluorescence Spectra

The absorption spectra of the TCNE EDA complexes were taken on a Cary Model 14 or a Cary Model 17 spectrophotometer. The measurements were made at room temperature; in most cases the solvent was used as the reference.

Fluorescence spectra of the EDA complexes in solution were measured at 77 K and, when they were observable, at 300 K. The 77 K spectra were obtained by placing the samples in capillaries, which were then immersed in a dewar containing liquid nitrogen, and viewing the light from the sample at an angle of 90°. The room temperature fluorescence spectra were recorded in a manner similar to that in which the Raman spectra of the complexes were observed.

4.5 Chemicals

TCNE and the various compounds used as electron donors were obtained in either reagent, spectroquality or chromatoquality grades from the following suppliers: Eastman Kodak Company; K & K Laboratories; Matheson Coleman & Bell; Fluka A G; Fisher Scientific Company; Aldrich Chemical Company; and J.T. Baker

Chemical Company. When necessary, solids were purified by recrystallisation or sublimation and liquids were purified by distillations.

Because of its high reactivity, the purification and storage of TCNE were given more attention than that for most of the other chemicals. In particular, the TCNE used for the preparation of the complexes was sublimed two or more times, and stored in the dark in a dry atmosphere. When TCNE is treated in this manner, it remains pure for several months.

REFERENCES

1. J. Loader, Basic Laser Raman Spectroscopy, (Heyden & Son Ltd., London, 1970).

2. K.H. Michaelian, K.E. Rieckhoff and E.M. Voigt, Proc. Natl. Acad. Sci. USA 72, 4196 (1975).

3. W. Kiefer and H.J. Bernstein, Appl. Spectrosc. 25, 500 (1971).

4. W. Kiefer and H.J. Bernstein, Appl. Spectrosc. 25, 609 (1971).

5. H.J. Sloane and R.B. Cook, Appl. Spectrosc. 26, 589 (1972).

6. W. Kiefer, Appl. Spectrosc. 27, 253 (1973).

7. K.H. Michaelian, K.E. Rieckhoff and E.M. Voigt, Chem. Phys. Lett. 23, 5 (1973).

8. H. Buyken, K. Klauss and H. Moser, Ber. Bunsengesell. Phys. Chem. 71, 578 (1967).

5. <u>RESULTS AND DISCUSSION</u>

The Raman spectra of EDA complexes of TCNE are discussed in detail in this chapter. The main topics of interest in these spectra are the intensity effects and their applications, the low energy spectra, and the band positions. The organisation of the chapter is therefore as follows: the preresonance Raman effect and the resonance Raman effect deal with the intensities of bands, and are the subjects of the first two sections; the resonance Raman intensities are used for the determination of equilibrium constants in the next section; the low energy Raman spectra are discussed in a separate section because of their special interest; and finally, the comparison of the band positions in the spectra of the complexes with those in the spectra of the uncomplexed components is the topic of the last section.

The CT absorption band (or bands) of the TCNE complexes discussed in this chapter occur between about 350 nm and 700 nm. Thus when the Argon laser is used for excitation, both incident and scattered light are absorbed to some degree, and the resulting Raman spectra are comparatively weak; part of a typical spectrum is shown in Fig. 12. Because the spectra are generally weak, only a limited number of Raman bands are observed, and the measured intensities and positions of these bands carry greater uncertainties than Raman spectra of nonabsorbing samples do.

5.1 Preresonance Raman Effect in EDA Complexes of TCNE[1,2]

In this section, the preresonance Raman effect in suitable TCNE complexes is discussed. Specific information on the intermediate states in the preresonance scattering process is obtained

by studying the excitation frequency dependence of the intensities of the totally symmetric[†] C=C and C≡N TCNE Raman bands, and by measuring the depolarisation ratios of these bands. The stronger preresonance effect in the $\nu_{C=C}$ band is also shown to cause the excitation wavelength dependence of the $I(\nu_{C=C})/I(\nu_{C\equiv N})$ intensity. ratio.

As discussed in Sec. 2.2, the preresonance Raman effect is important when the wavelength of the excitation source is near the long wavelength absorption edge of the sample. In the present study this condition occurs when electron donors are chosen such that the CT absorption bands of their TCNE complexes have their maxima near 400 nm (the shortest useful wavelength available from the Argon laser is 457.9 nm), which is the case for toluene and fluorobenzene as donors. The CT absorption maxima of the TCNE complexes with these donors are given in Table I, and the long wavelength absorption edges for these complexes are shown in Fig. 5, along with the positions of the Argon laser lines.

5.1.1 Preresonance in TCNE Vibrations

As the excitation wavelength approaches the absorption maxima of a complex, the intensities of the bands assigned to totally symmetric vibrations in the spectrum of uncomplexed TCNE increase relative to the intensities of the nontotally symmetric bands. The bands which show this preresonance intensity enhancement are listed in Table II, together with their assignments. Since the symmetry of a TCNE EDA complex is lower than that of TCNE,

---

[†]This refers to the symmetry of an uncomplexed TCNE molecule (Chapter 6).
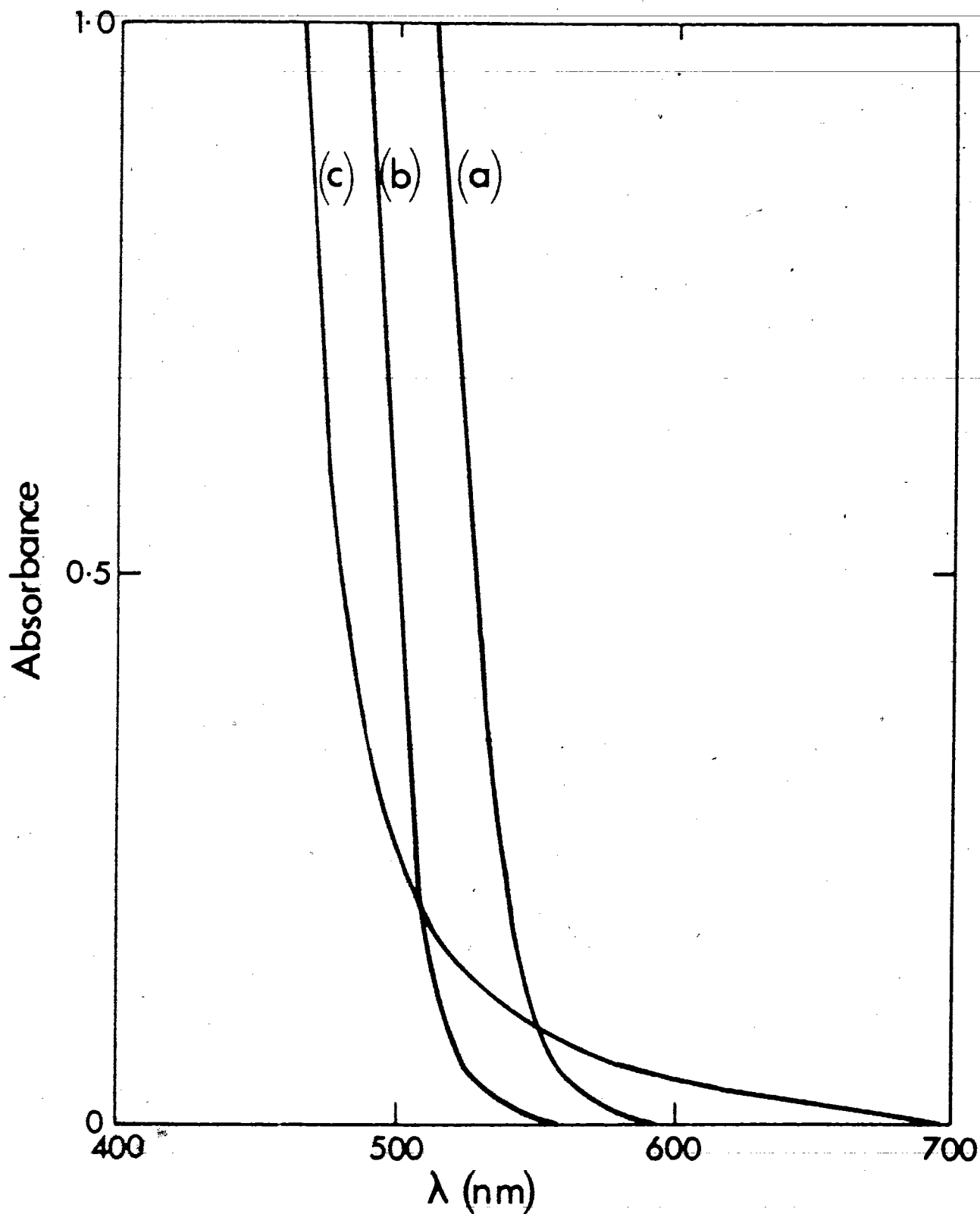
Fig. 5 Long wavelength absorption edges of TCNE EDA complexes which yield preresonance Raman spectra. (a) toluene/TCNE in CH_2Cl_2; (b) benzene/TCNE in CH_2Cl_2; (c) fluorobenzene/TCNE.

Table I.   Absorption maxima of the TCNE EDA complexes whose Raman
spectra show preresonance intensity effects

Complex	Solvent	λ_{rk} (nm)	ν_{rk} (cm^{-1})
fluorobenzene/TCNE	fluorobenzene	358	27,900
benzene/TCNE	CH_2Cl_2	389	25,700
toluene/TCNE	CH_2Cl_2	407	24,600

Table II.   TCNE vibrations increased in intensity in the
preresonance Raman spectra of TCNE EDA complexes

ν (cm^{-1})[a]	Description[b,c]
490	combination band
532	C–C≡N bend
1526	combination band
1567	C=C stretch
2236	C≡N stretch

[a]Band positions are for solid (uncomplexed) TCNE.
[b]All bands are of a_g symmetry in uncomplexed TCNE.
[c]Assignments are discussed in Chapter 6.

vibrations which are totally symmetric in uncomplexed TCNE, which belongs to the D_{2h} point group, are also totally symmetric in the EDA complex. The preresonance intensity behaviour is therefore consistent with the predicted activity of the bands in the preresonance Raman spectra, as discussed in Sec. 2.2.2.

Even when only totally symmetric bands are considered, their relative intensities in the preresonance region vary with excitation wavelength. (This is shown below to be the result of the different positions of the principal intermediate states for the vibrations involved.) The change which is most noticeable in the preresonance Raman spectra is the increase in intensity of the $\nu_{C=C}$ band with respect to the $\nu_{C\equiv N}$ band; the $I(\nu_{C=C})/I(\nu_{C\equiv N})$ intensity ratio in the benzene/TCNE spectrum increases from 1.2 for 514.5 nm excitation to 1.8 for 457.9 nm excitation. Both of these intensity ratios are well above that observed for uncomplexed TCNE, about 0.5 (Table III).

TCNE has two Raman active $C\equiv N$ stretching modes, one of a_g symmetry and one of b_{3g} symmetry. In the preresonance Raman spectra of TCNE complexes, the intensity of the $a_g \nu_{C\equiv N}$ band is considerably increased relative to that of the $b_{3g} \nu_{C\equiv N}$ band. For the preresonance intensity studies, the a_g/b_{3g} intensity ratio was further increased by viewing only the parallel component of the scattered light. Thus to a very good approximation, the intensity observed at preresonance is that of the a_g vibration; the following discussion is based on this premise.

The excitation wavelength dependence of the Raman intensities of the totally symmetric TCNE bands has also been observed by

Table III. Intensity changes in TCNE bands on complexation
(excitation wavelength 514.5 nm)

Sample	Solvent	$I(\nu_{C=C})/I(\nu_{C\equiv N})$ [a,b]
TCNE (solid)	---	.5
TCNE	CH_2Cl_2	.5
fluorobenzene/TCNE	fluorobenzene	.8
benzene/TCNE	CH_2Cl_2	1.2
toluene/TCNE	CH_2Cl_2	2.5

[a] Uncertainties in intensity ratios are ± .2 or less.
[b] The two close-lying C≡N stretching bands are not resolved.

others[3,4]. Although neither of these studies included all of the
bands in Table II, they do confirm the results of the present
investigation for the $\nu_{C=C}$ and $\nu_{C\equiv N}$ bands.

5.1.2 Intermediate States

According to the theory of Albrecht and Hutley[5] (Chapter 2),
the preresonance Raman intensity is proportional to one of the
frequency factors F_A^2 or F_B^2, with F_A and F_B given by equation (2.3).
The EDA complexes have a large number of excited electronic states
(donor, acceptor or charge transfer origin) which can be considered
as candidates for ν_{rk} and ν_{tk}; however, certain restrictions on
the intermediate states must be taken into account. According to
the preresonance theory[5], ν_{rk} and ν_{tk} must satisfy the following
criteria:

(1) electronic state r is the major active virtual electronic

state in the near resonance condition;

(2) the particular ν_{rk} and ν_{tk} guarantee that only one component of the scattering tensor is enhanced;

(3) the active virtual states t lie at energies sufficiently high to permit the use of some average ν_{tk};

(4) the transitions ν_{rk} and ν_{tk} must have the same polarisation.

For the analysis of the preresonance Raman spectra of the TCNE EDA complexes in terms of this theory, ν_{rk} is taken as the frequency of the CT absorption maximum (Table I). Two different frequencies were used for ν_{tk}. The first one, 36,170 cm^{-1}, is the frequency of the TCNE absorption band for TCNE in CH_2Cl_2, which by analogy with the TCNE absorption spectrum in ethanol solution[6] is assigned to an $n \rightarrow \pi^*$ TCNE transition. This is the lowest energy singlet transition of TCNE which is polarised perpendicular to the molecular plane. The second ν_{tk}, 55,560 cm^{-1}, represents an average far UV (180 nm) transition; when ν_{tk} is in the far UV, the exact frequency used hardly affects the F_B^2 values.

These choices for ν_{rk} and ν_{tk} are consistent with the above requirements of the preresonance theory, as will now be shown.

(1') The first excited electronic states of the EDA complexes in Table I (27,900 cm^{-1} to 24,600 cm^{-1}) are comparatively close to the Argon laser lines, which lie between 19,430 cm^{-1} and 21,831 cm^{-1}. These states are the only ones in this region and thus if preresonance occurs, it is likely that they are the major active virtual states. The importance of the first excited CT states as intermediate states is suggested by the intensity

changes in the TCNE Raman spectrum on complexation (Table III). Uncomplexed TCNE lacks such an electronic state, and yields $\nu_{C=C}$ and $\nu_{C\equiv N}$ intensities whose excitation frequency dependence does not vary significantly from the (nonresonance) ν^4 law.

(2') As described below, the $\nu_{C=C}$ band depolarisation ratios approach $\rho_\lambda = 1/3$ as the excitation wavelength nears the CT absorption maximum. This indicates that only one component of the scattering tensor is enhanced (Sec. 2.2.2).

(3') The frequency $\nu_{tk} = 36,170$ cm^{-1}, though not an average frequency, is still compatible with the theory, since it is close to the second excited singlet state of TCNE (band position in CHCl$_3$ about 38,000 cm^{-1})[7]. These two states are close enough that the use of either frequency as an average does not introduce significant error into the interpretation of the data.

The second value used for ν_{tk}, 55,560 cm^{-1}, is correctly considered as an average frequency, since there are numerous states in the UV associated with these polyatomic molecules, or with the EDA complexes, which might act as intermediate states.

(4') By analogy with the results for a number of EDA complexes[8], including one TCNE $\pi-\pi$ complex[9], the CT transitions for the complexes being discussed here can be assumed to be polarised along the intermolecular axis. Since the planes of the acceptor and of the donor molecules in TCNE $\pi-\pi$ complexes are approximately parallel[10], the CT transitions are thus assumed to be parallel to out-of-plane polarised donor or acceptor transitions. This is equivalent to the statement that the TCNE $n\rightarrow\pi^*$ transition at 36,170 cm^{-1} is polarised parallel to the CT transition, and

therefore the requirement that ν_{tk} and ν_{rk} be of the same polarisation is satisfied. Furthermore, the second excited singlet transition of TCNE has also been identified as an out-of-plane polarised transition[7]; thus it too is parallel to the CT transition. Since the 55,560 cm^{-1} value for ν_{tk} is an average frequency, no information is available which can tell whether it meets this polarisation requirement.

5.1.3 Comparison of Theory and Experiment

The frequency factors F_A^2 and F_B^2 calculated for the EDA complexes of TCNE are given in Tables IV - VI. Consistent with the form of F_A and F_B, the frequency dependence of the Raman intensity is stronger when the absorption maximum is nearer the excitation lines (toluene/TCNE) than when the absorption is farther from the excitation (fluorobenzene/TCNE). The choice of ν_{tk} considerably affects the magnitude of F_B^2, although the frequency dependence of F_B^2 is not greatly different for either ν_{tk}. The frequency factors for $\nu_{C=C}$ are only slightly larger than those for $\nu_{C\equiv N}$ and by themselves do not account for the increase in the $I(\nu_{C=C})/I(\nu_{C\equiv N})$ ratio on complexation; this increase also involves the cross sections for the electronic transitions and the vibronic energies[5].

In Figures 6 to 11 the frequency factors are compared with the experimental data. These figures show that in all three complexes, the $\nu_{C=C}$ intensities follow the upper F_B^2 curves (those having $\nu_{tk} = 36,170$ cm^{-1}); the $\nu_{C\equiv N}$ intensities tend to agree with the lower F_B^2 curves ($\nu_{tk} = 55,560$ cm^{-1}). The F_B^2 frequency dependences of these Raman bands confirm that the Argon laser

Table IV. Calculated preresonance Raman frequency factors for benzene/TCNE in CH_2Cl_2[a]

ν_0	$F_A^2(\nu_{rk}=25,700)$		$F_B^2(\nu_{tk}=36,170)$		$F_B^2(\nu_{tk}=55,560)$	
	$\nu_m=1560$	$\nu_m=2230$	$\nu_m=1560$	$\nu_m=2230$	$\nu_m=1560$	$\nu_m=2230$
19,430	17.137	14.708	10.046	8.6224	2.2620	1.9415
19,926	26.418	22.768	13.898	11.977	3.0186	2.6013
20,135	31.953	27.587	16.002	13.816	3.4210	2.9537
20,487	44.558	38.577	20.418	17.678	4.2490	3.6788
20,981	73.190	63.599	29.198	25.370	5.8419	5.0759
21,150	87.533	76.159	33.157	28.847	6.5429	5.6924
21,463	123.70	107.87	42.281	36.869	8.1288	7.0882
21,831	190.88	166.87	57.087	49.910	10.631	9.2945

[a]All frequencies are in cm^{-1}.

Table V. Calculated Preresonance Raman frequency factors for toluene/TCNE in CH_2Cl_2 [a]

ν_0	$F_A^2 (\nu_{rk}=24,600)$		$F_B^2 (\nu_{tk}=36,170)$		$F_B^2 (\nu_{tk}=55,560)$	
	$\nu_m=1560$	$\nu_m=2230$	$\nu_m=1560$	$\nu_m=2230$	$\nu_m=1560$	$\nu_m=2230$
19,430	36.673	31.473	14.592	12.524	3.2627	2.7999
19,926	60.924	52.509	20.954	18.060	4.5186	3.8947
20,135	76.386	65.947	24.562	21.205	5.2135	4.5008
20,487	114.00	98.690	32.418	28.067	6.6967	5.7980
20,981	209.96	182.44	49.087	42.654	9.7475	8.4704
21,150	262.86	228.71	57.031	49.621	11.169	9.7176
21,463	408.85	356.53	76.297	66.530	14.557	12.694
21,831	723.18	632.22	110.27	96.407	20.376	17.813

[a] All frequencies are in cm^{-1}.

Table VI. Calculated Preresonance Raman frequency factors for fluorobenzene/TCNE [a]

ν_0	$F_A^2 (\nu_{rk}=27,930)$		$F_B^2 (\nu_{tk}=36,170)$		$F_B^2 (\nu_{tk}=55,560)$	
	$\nu_m=1560$	$\nu_m=2230$	$\nu_m=1560$	$\nu_m=2230$	$\nu_m=1560$	$\nu_m=2230$
19,430	5.2039	4.4660	5.5951	4.8018	1.2762	1.0954
19,926	7.3241	6.3127	7.3984	6.3766	1.6284	1.4035
20,135	8.4914	7.3311	8.3394	7.1996	1.8071	1.5603
20,487	10.955	9.4839	10.236	8.8619	2.1597	1.8698
20,981	15.875	13.795	13.751	11.949	2.7906	2.4249
21,150	18.096	15.745	15.247	13.266	3.0517	2.6553
21,463	23.203	20.234	18.525	16.154	3.6127	3.1503
21,831	31.433	27.479	23.433	20.486	4.4277	3.8711

[a] All frequencies are in cm^{-1}.
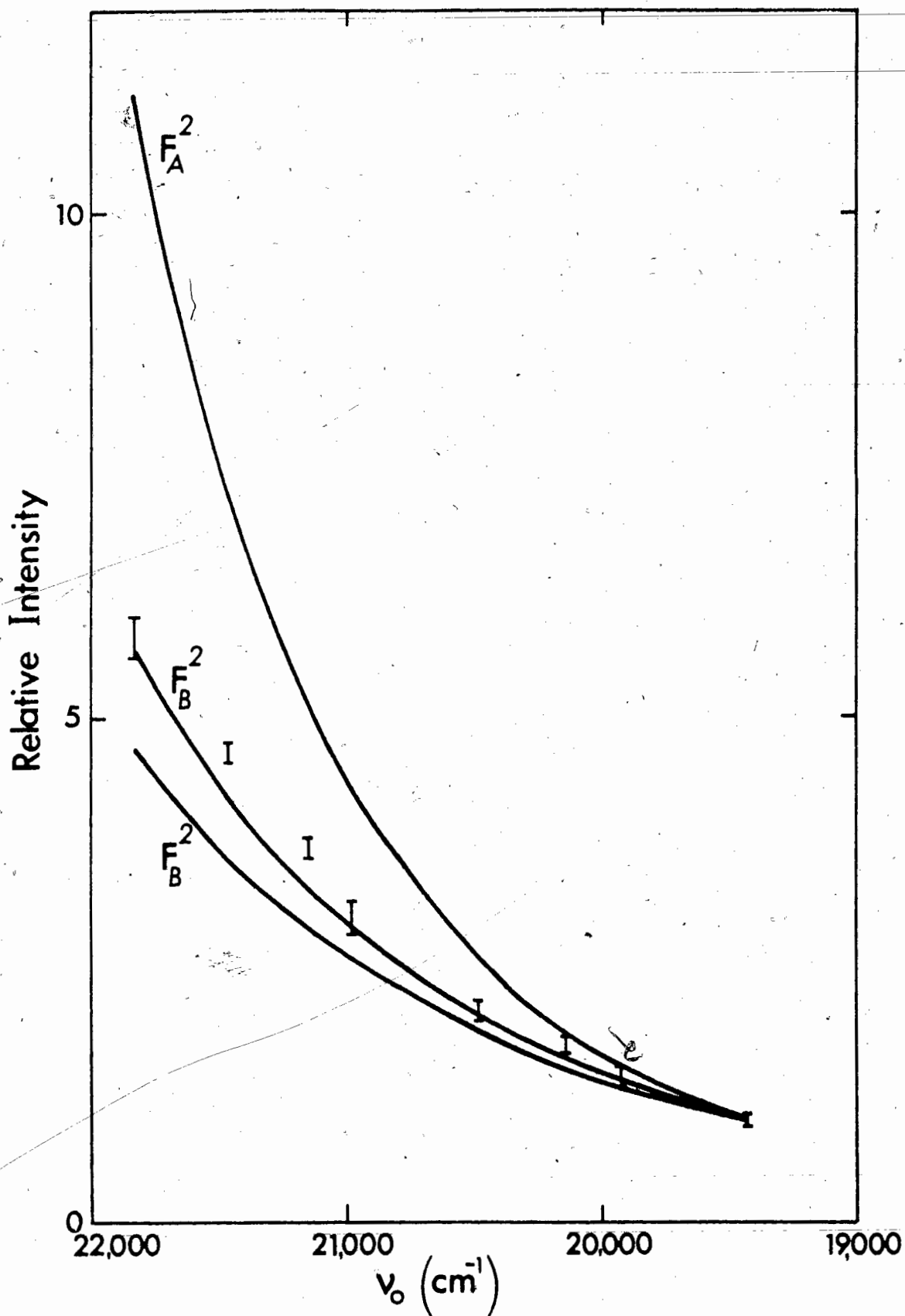
Fig. 6 Intensity of $\nu_{C=C}$ as a function of excitation frequency for benzene/TCNE in CH_2Cl_2. Upper F_B^2 curve: $\nu_{tk} = 36,170$ cm^{-1}; lower F_B^2 curve: $\nu_{tk} = 55,560$ cm^{-1}. Intensity normalised at 19,430 cm^{-1}.
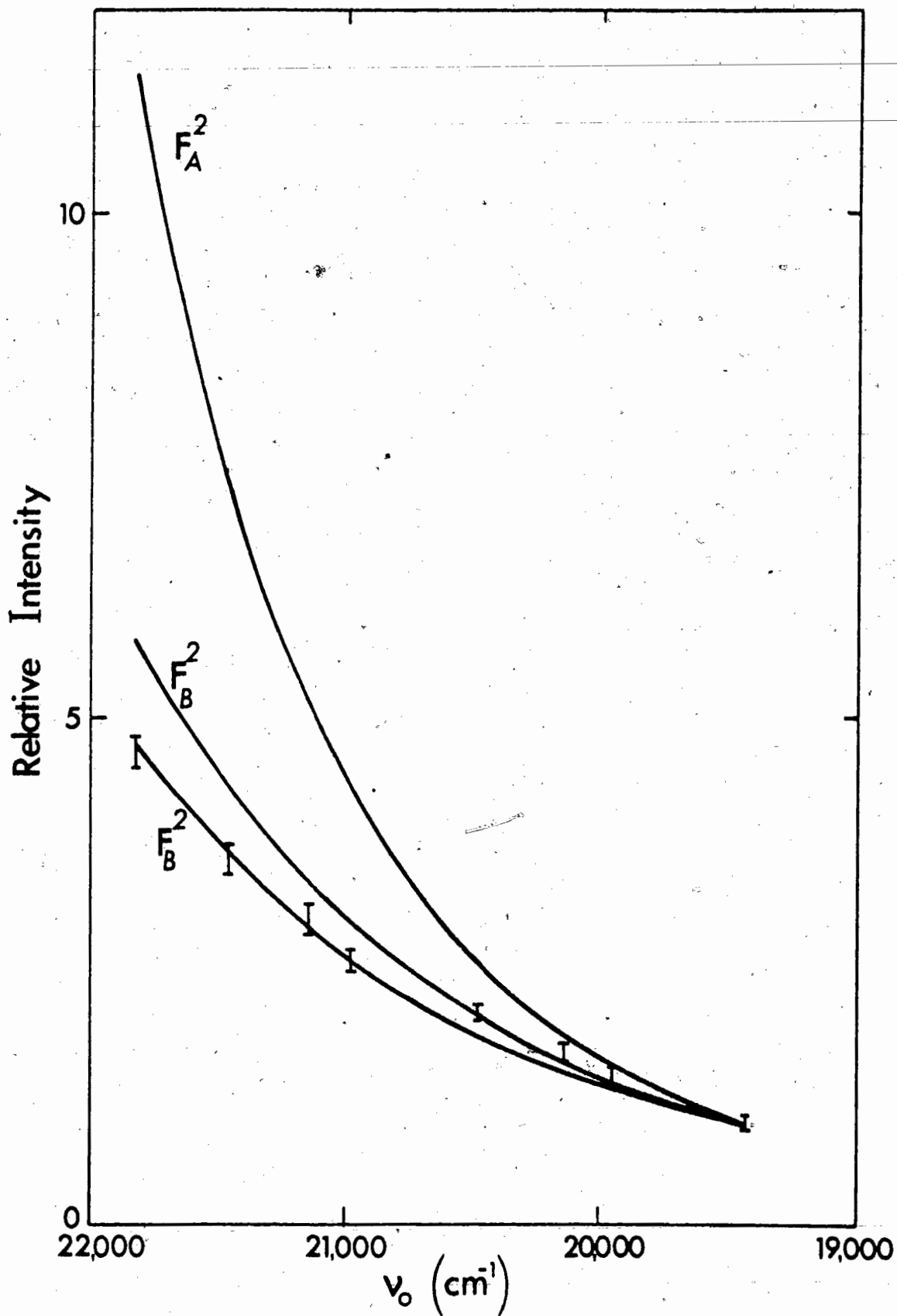
Fig. 7 Intensity of $\nu_{C\equiv N}$ as a function of excitation frequency for benzene/TCNE in CH_2Cl_2. Details are the same as in Fig. 6.
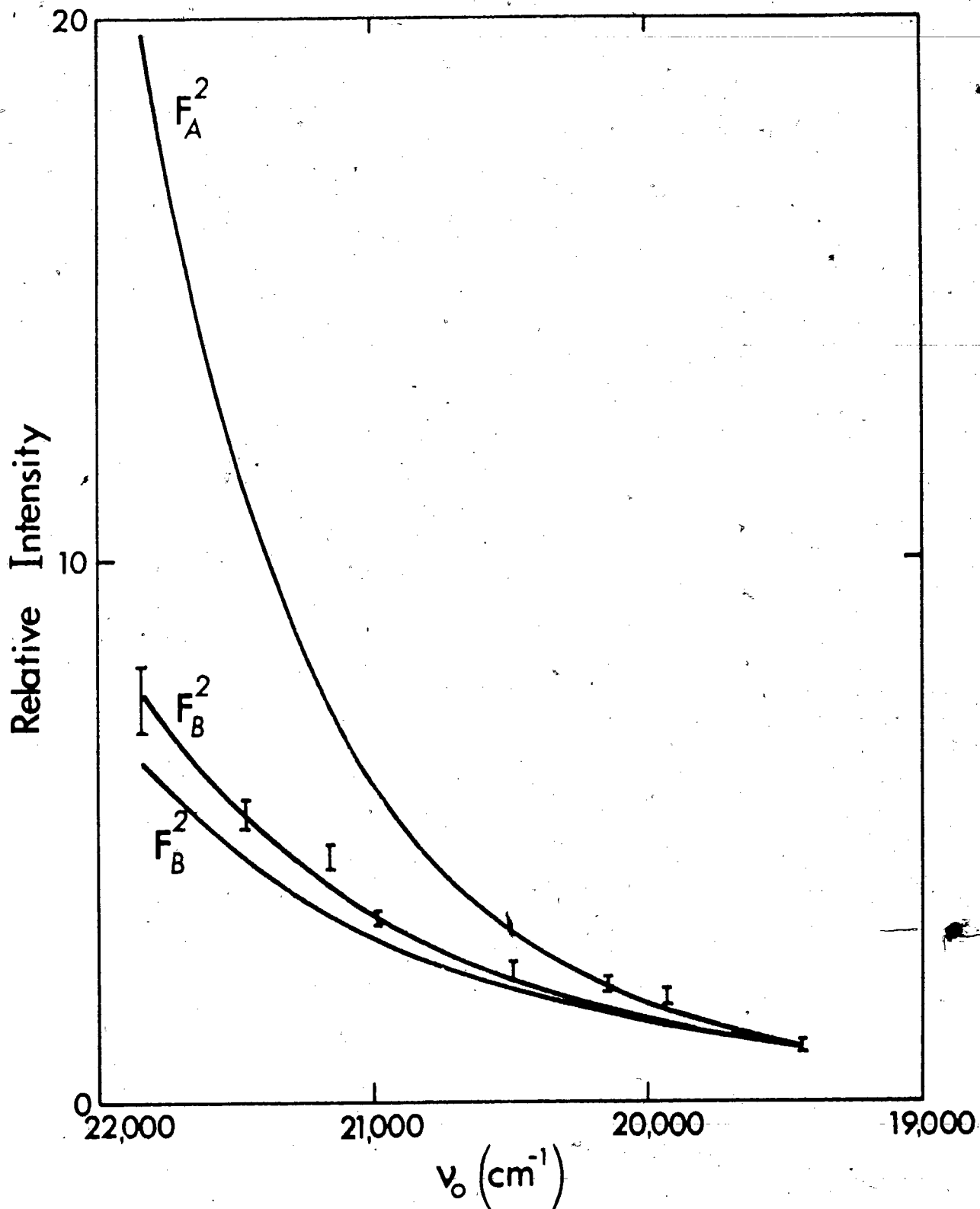
Fig. 8 Intensity of $\nu_{C=C}$ as a function of excitation frequency for toluene/TCNE in CH_2Cl_2. Details are the same as in Fig. 6.
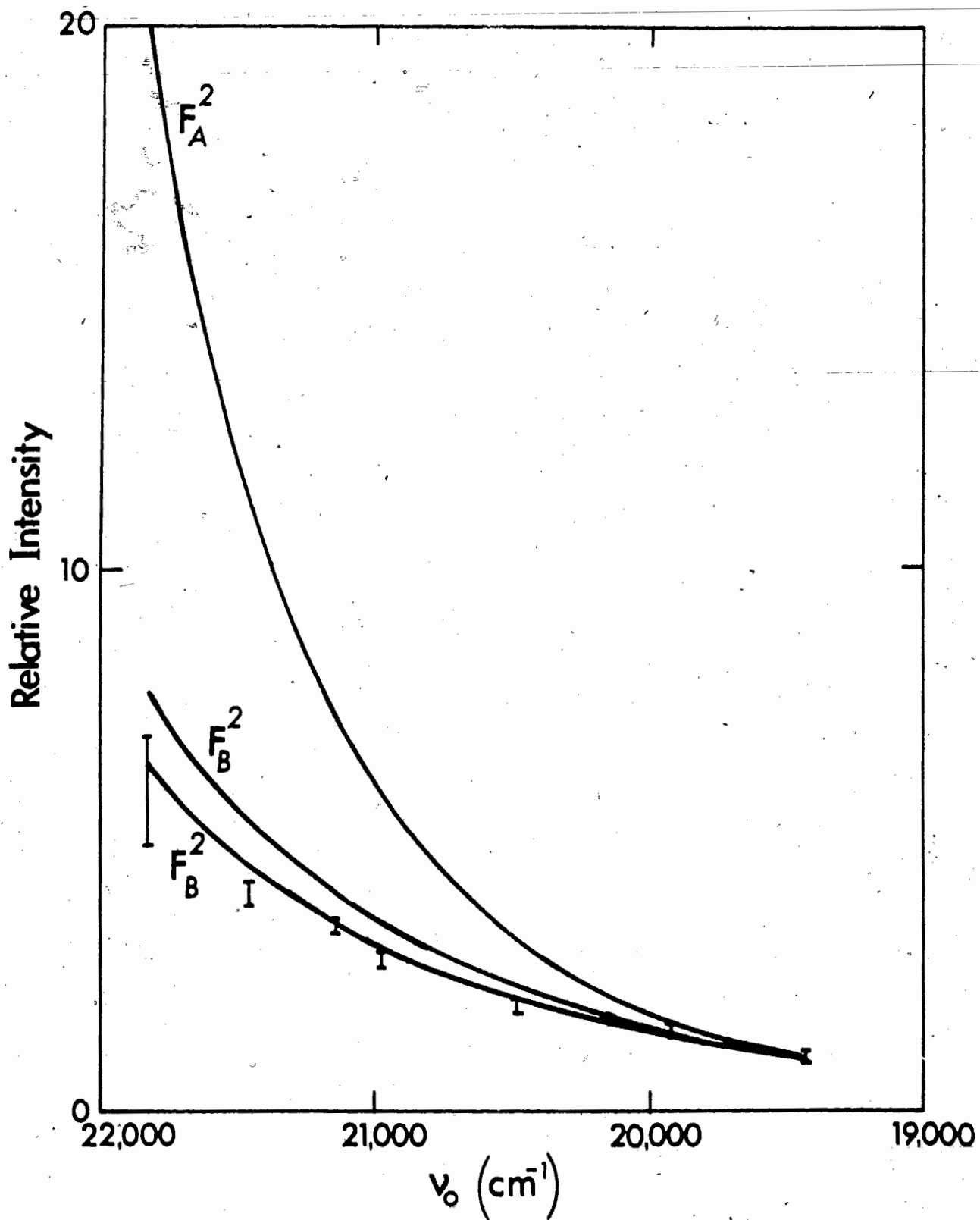
Fig. 9 Intensity of $\nu_{C \equiv N}$ as a function of excitation frequency for toluene/TCNE in CH_2Cl_2. Details are the same as in Fig. 6.
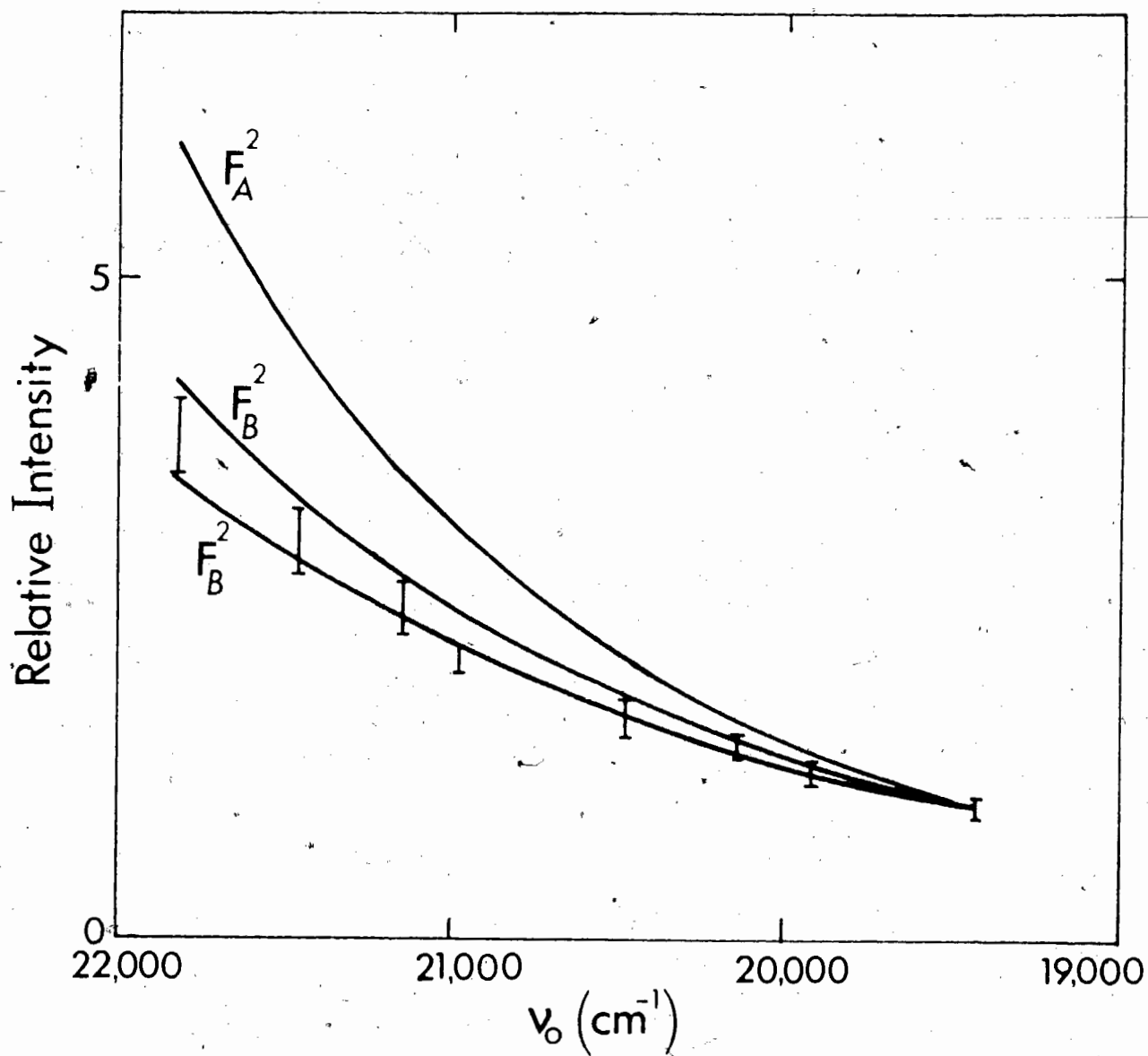
Fig. 10 Intensity of $\nu_{C=C}$ as a function of excitation frequency for fluorobenzene/TCNE. Details are the same as in Fig. 6.
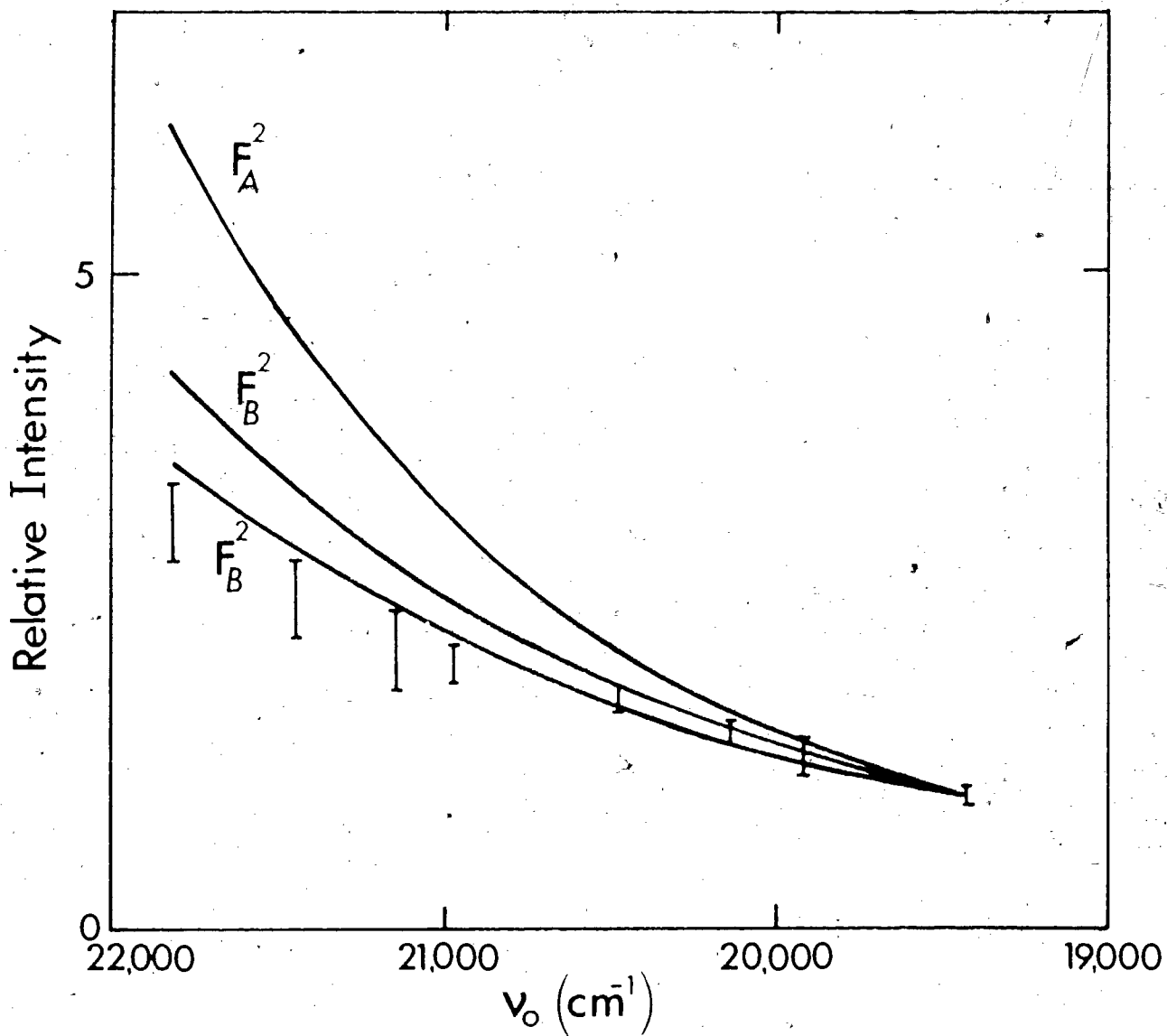
Fig. 11   Intensity of $\nu_{C\equiv N}$ as a function of excitation frequency for fluorobenzene/TCNE.   Details are the same as in Fig. 6.

lines are far enough from the absorption bands of these TCNE complexes that the preresonance Raman effect determines the intensities of the $\nu_{C=C}$ and $\nu_{C\equiv N}$ bands.

Because the frequency dependence of the lower F_B^2 curves is weaker than that of the upper F_B^2 curves, the intensity ratio $I(\nu_{C=C})/I(\nu_{C\equiv N})$ increases as ν_0 approaches the absorption maximum. This increase is observed in the Raman spectra of all three complexes, and is greatest for the complex with the strongest ν_0 dependence, toluene/TCNE.

The comparison of the preresonance Raman intensity data for the TCNE EDA complexes with the calculations based on the theory of Albrecht and Hutley[5] is summarised in Table VII. Inspection of this Table confirms the conclusions based on consideration of Figs. 6 to 11 given above. For fluorobenzene/TCNE, $\nu_{tk} = 36,170 \text{ cm}^{-1}$ and $\nu_{tk} = 55,560 \text{ cm}^{-1}$ give about the same agreement with the observed $\nu_{C=C}$ intensities; otherwise, the conclusions are the same as before.

As shown in Sec. 2.2.2, the depolarisation ratios of the preresonance-enhanced Raman bands approach limiting values which are characteristic of the degeneracy of the principal intermediate state. The depolarisation ratios for the $\nu_{C=C}$ Raman bands in the spectra of the TCNE EDA complexes are observed to increase from 0.21 for fluorobenzene/TCNE to 0.29 for benzene/TCNE and 0.35 for toluene/TCNE, parallel to the red shift in the absorption maximum with the change in the donor. Thus, the $\nu_{C=C}$ depolarisation ratio approaches 1/3; therefore, the first excited states of the above EDA complexes are not degenerate, with the possible exception of

benzene/TCNE. The fact that the a_g $\nu_{C\equiv N}$ depolarisation ratios have not increased measurably above the nonresonance value of .10 with complexation suggests that the $\nu_{C=C}$ mode is subject to a stronger preresonance effect than is the $\nu_{C\equiv N}$ mode.

The preresonance effect in the $\nu_{C=C}$ vibration apparently extends well beyond the CT absorption edges, as indicated by the fact that $I(\nu_{C=C})/I(\nu_{C\equiv N})$ for benzene/TCNE is still about 1.1 even when the excitation wavelength is 601.2 nm. If it is assumed that preresonance enhancement of the $\nu_{C=C}$ band is responsible for the increase in this ratio above the nonresonance value of 0.5, then one concludes that preresonance Raman scattering is important even when the excitation frequency is 9000 cm^{-1} away from the absorption maximum, presumably because of the considerable widths of the CT absorption bands, which in the case of benzene/TCNE extend to about 550 nm.

5.1.4 Discussion of the Results

Figures 6 to 11 show, as described above, that $I(\nu_{C=C})$ and $I(\nu_{C\equiv N})$ exhibit F_B^2 rather than F_A^2 frequency dependence of the intensity. Since both of the frequencies ν_{rk} and ν_{tk} occur in the expression for F_B, while only ν_{rk} is included in F_A, it can be concluded that state r (the first excited state of the EDA complex) is not the only important scattering state, since F_A^2 frequency dependence is not observed. In view of these results, the suggestion by Kaya et al.[4] that the first excited CT state is the dominant scattering state should therefore be clarified. The importance of this state is indicated by the fact that the frequencies ν_{rk} are essential in explaining the ν_0 dependence of

Table VII. Comparison of preresonance Raman intensities with the theory of Albrecht and Hutley[5]

fluorobenzene/TCNE

λ_0 (nm)	$I(\nu_{C=C})^a$ exp.	$(F_A^2)^b$ rel.	$(F_B^2)^c$ rel.	$(F_B^2)^d$ rel.	$I(\nu_{C\equiv N})^e$ exp.	$(F_A^2)^f$ rel.	$(F_B^2)^g$ rel.	$(F_B^2)^h$ rel.
514.5	1.00	1.00	1.00	1.00	1.00	1.00	1.00	1.00
501.7	1.25	1.13	1.06	1.02	1.30	1.09	1.02	.986
496.5	1.43	1.14	1.04	.990	1.49	1.10	1.01	.956
488.0	1.66	1.27	1.10	1.02	1.73	1.23	1.07	.987
476.5	2.11	1.45	1.16	1.04	2.00	1.54	1.24	1.11
472.7	2.56	1.39	1.09	.956	2.12	1.68	1.32	1.15
465.8	3.01	1.49	1.10	.944	2.52	1.81	1.35	1.15
457.9	3.83	1.59	1.10	.913	3.12	1.98	1.38	1.14

benzene/TCNE in CH_2Cl_2

λ_0 (nm)	$I(\nu_{C=C})^a$ exp.	$(F_A^2)^b$ rel.	$(F_B^2)^c$ rel.	$(F_B^2)^d$ rel.	$I(\nu_{C\equiv N})^e$ exp.	$(F_A^2)^f$ rel.	$(F_B^2)^g$ rel.	$(F_B^2)^h$ rel.
514.5	1.00	1.00	1.00	1.00	1.00	1.00	1.00	1.00
501.7	1.43	1.08	.962	.934	1.45	1.07	.958	.923
496.5	1.74	1.07	.911	.870	1.72	1.09	.932	.887
488.0	2.09	1.25	.967	.900	2.10	1.25	.977	.902
476.5	2.99	1.43	.967	.865	2.58	1.68	1.14	1.02
472.7	3.71	1.38	.885	.780	3.01	1.72	1.11	.974
465.8	4.65	1.56	.900	.774	3.62	2.03	1.18	1.01
457.9	5.28	2.11	1.07	.891	4.66	2.44	1.24	1.03

Table VII (cont.) Comparison of preresonance Raman intensities with the theory of Albrecht and Hutley[5]

toluene/TCNE in CH_2Cl_2

λ_0 (nm)	$I(\nu_{C=C})$[a] exp.	$\frac{F_A^2}{F_B^2}$[b] rel.	(F_B^2)[c] rel.	(F_B^2)[d] rel.	$I(\nu_{C\equiv N})$[e] exp.	(F_A^2)[f] rel.	(F_B^2)[g] rel.	(F_B^2)[h] rel.
514.5	1.00	1.00	1.00	1.00	1.00	1.00	1.00	1.00
501.7	1.95	.852	.736	.710	1.53	1.09	.943	.909
496.5	2.21	.942	.762	.723	1.72	1.22	.984	.935
488.0	2.40	1.30	.926	.855	1.91	1.64	1.17	1.08
476.5	3.42	1.67	.984	.874	2.77	2.09	1.23	1.09
472.7	4.52	1.59	.865	.757	3.42	2.12	1.16	1.01
465.8	5.29	2.11	.988	.843	4.02	2.82	1.32	1.13
457.9	7.39	2.67	1.02	.845	5.92	3.39	1.30	1.07

[a] $I(\nu_{C=C})/I(\text{donor}) \times \nu^4$ correction, normalised at 514.5 nm. Experimental uncertainties are indicated in Figs. 6, 8 and 10.

[b] F_A^2 divided by corrected $\nu_{C=C}$ data and normalised.

[c] F_B^2 (ν_{tk} = 36,170 cm^{-1}) divided by corrected $\nu_{C=C}$ data and normalised.

[d] F_B^2 (ν_{tk} = 55,560 cm^{-1}) divided by corrected $\nu_{C=C}$ data and normalised.

[e] $I(\nu_{C\equiv N})/I(\text{donor}) \times \nu^4$ correction, normalised at 514.5 nm. Experimental uncertainties are indicated in Fig. 7, 9 and 11.

[f] F_A^2 divided by corrected $\nu_{C\equiv N}$ data and normalised.

[g] F_B^2 (ν_{tk} = 36,170 cm^{-1}) divided by corrected $\nu_{C\equiv N}$ data and normalised.

[h] F_B^2 (ν_{tk} = 55,560 cm^{-1}) divided by corrected $\nu_{C\equiv N}$ data and normalised.

the Raman intensity; at the same time, the F_B^2 dependence of the intensity implies that one or more higher states of the components or of the complex are essential to account for the magnitudes of the observed preresonance Raman intensities.

In Sec. 2.2.1 the role of vibronic coupling in the pre-resonance Raman effect was discussed. Using the nomenclature introduced in that chapter, the F_B^2 dependence of the intensity which is observed in the Raman spectra of the TCNE EDA complexes implies that the preresonance Raman intensity is derived mostly from a vibronic coupling mechanism, rather than from a distortion of the C=C or C≡N bonds in the first excited CT states of the complexes. The vibronic coupling occurs via the matrix elements connecting states r and t; thus, the TCNE $\nu_{C=C}$ and $\nu_{C≡N}$ vibrations couple the first excited state of the complex with higher excited states of the acceptor, donor or complex. The UV absorption spectra of TCNE[7] indicate that the C=C distance also is not much changed in the first excited state of TCNE.

5.2   Resonance Raman (RR) Effect in EDA Complexes of TCNE[1,11]

When the Raman excitation wavelength falls within the region of strong absorption of a TCNE EDA complex, the RR effect is observed in some of the TCNE bands. These RR bands display changes in their absolute and relative intensities as compared with their intensities far from resonance. The depolarisation ratios of the affected bands are also changed with regard to their nonresonance values. Other features of the RR spectra which give useful information on the EDA complexes include the excitation profiles of the RR bands, the halfwidths of the Raman bands, and the fact

Table VIII. CT absorption maxima (CH_2Cl_2 solutions) of TCNE EDA complexes which display the resonance Raman effect

Donor	λ (nm)		
o-xylene	436		
m-xylene	440		
p-xylene	415,	470	
mesitylene	466		
durene	490		
isodurene	488		
pentamethylbenzene	521		
hexamethylbenzene	541		
anisole	383,	510	
o-dimethoxybenzene	429,	592	
m-dimethoxybenzene	441,	559	
p-dimethoxybenzene	380,	637	
1,2,3-trimethoxybenzene	515		
1,2,4-trimethoxybenzene	427,	685	
1,3,5-trimethoxybenzene	552		
acenaphthene	442,	654	
fluorene	402,	417,	571
naphthalene	427,	550	
pyrene	391,	495,	725

that resonance also occurs when the excitation falls within the second CT absorption band of these complexes. The excitation profiles also account for the wavelength dependence of the $I(\nu_{C=C})/I(\nu_{C \equiv N})$ intensity ratio which is observed for some complexes.

A large number of electron donors form EDA complexes with TCNE which have CT absorption bands in the same wavelength range as the output lines of the Argon laser. The donors studied here and the CT absorption maxima are listed in Table VIII. The Raman spectra of all of these complexes as obtained with this excitation source display at least some of the resonance characteristics mentioned above; the complexes studied most extensively with

regard to the RR effect are those in which methylbenzenes or methoxybenzenes are the electron donors, for reasons stated in Sec. 5.2.3. The greatest intensity changes on complexation are observed in the spectra of the methylbenzene/TCNE complexes; they will be discussed in the following sections.

5.2.1 Resonance in TCNE Vibrations

The increase in the intensities of the totally symmetric TCNE bands vis à vis the nontotally symmetric bands, first observed when the excitation frequency is several thousand cm^{-1} away from the CT transition (Sec. 5.1.1), also occurs in the region where the excitation source is in resonance with this transition. Because of absorption problems, the overall intensity of the RR spectra is low; the relative intensity increase of the a_g bands ensures that the only TCNE bands which can be identified are the totally symmetric ones (Table IX), whereas in the pre-resonance spectra nontotally symmetric TCNE bands are still observable.

The TCNE bands at 490 cm^{-1} and 532 cm^{-1} (Table II) cannot be identified in the present RR spectra of the TCNE EDA complexes because the quartz cuvettes used to contain the solutions produce a broad, strong quartz Raman band centred near 450 cm^{-1} (Sec. 4.1), which masks these weak TCNE bands. Since these two TCNE bands are of no special interest in this study, no further attempts to observe them have been made. On the basis of the preresonance Raman and resonance Raman activities of the 1526, 1567 and 2236 cm^{-1} TCNE bands (compare Tables II and IX), the bands at 490 and 532 cm^{-1} can be assumed to occur in the RR spectra of the

Table IX. TCNE vibrations active in the resonance Raman spectra
of TCNE EDA complexes

$\nu (cm^{-1})^a$	Description[b,c]
150	(CN)-C-(CN) scissoring
1526	combination band
1567	C=C stretch
2236	C≡N stretch.

[a]Band positions are for solid (uncomplexed) TCNE.
[b]All bands are of a_g symmetry.
[c]Assignments are discussed in Chapter 6.

TCNE EDA complexes, albeit with less intensity than those of the

other TCNE bands.

The RR spectra of the TCNE EDA complexes also contain

resonance-enhanced bands at 155-167 cm^{-1}, which are not detectable

in the preresonance Raman spectra. These bands are discussed in

detail in Sec. 5.4, where it is shown that the most likely origin

of them is the totally symmetric TCNE vibration ν_5. The assign-

ment of this TCNE vibration is also discussed in Sec. 6.1.

An increase in $I(\nu_{C=C})/I(\nu_{C\equiv N})$[†] above the nonresonance value

of 0.5 is observed in the RR spectra of the TCNE EDA complexes

(Table X); a typical spectrum showing these two TCNE bands is

given in Figure 12. For some of the complexes in Table X,

$I(\nu_{C=C})/(\nu_{C\equiv N})$ varies considerably within the wavelength range of

the Argon laser. The relationship of this result to the RR

[†]The absolute intensity increases with complexation (Tables XV-XVII)
quantify the RR intensification of these bands, whereas the
intensity ratios indicate only the relative intensity changes.

Fig. 12 Raman spectra of uncomplexed TCNE and of complexed TCNE. (a) TCNE in CH_2Cl_2; (b) durene/TCNE in CH_2Cl_2. TCNE concentration about .01 M; excitation at 514.5 nm.

(a)

(b)

1500

1600

2150

2250

$\Delta \nu$ (cm^{-1})

Intensity (photons/s)

100

0

100

0
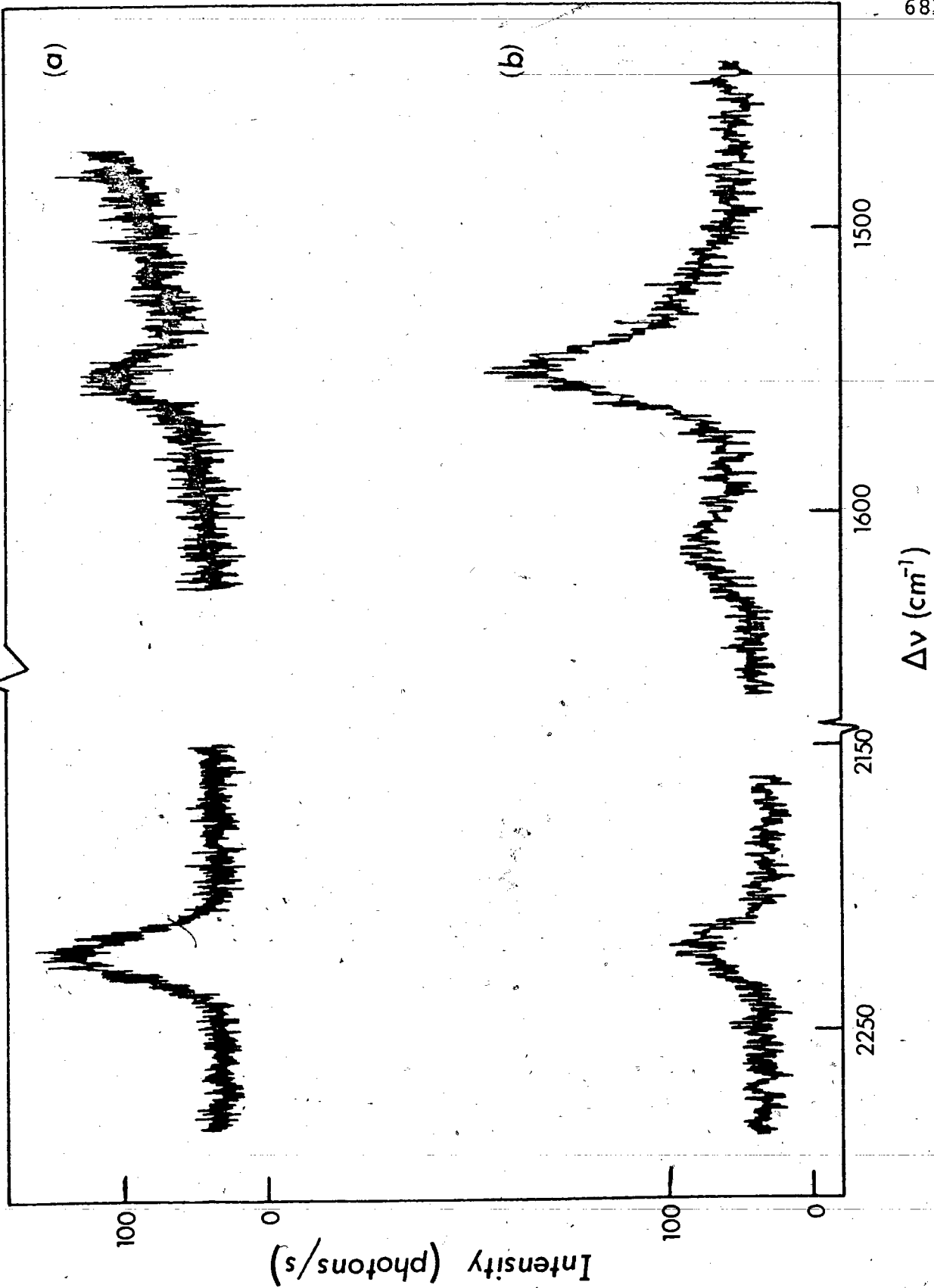
Table X. Intensity ratios for TCNE EDA complexes (excitation wavelength 488.0 or 514.5 nm)[a]

Donor[b]	[Donor], M[c]	[TCNE], M	$I(\nu_{C=C})/I(\nu_{C \equiv N})$[d]
o-xylene (ℓ)		.10	2.8
m-xylene (ℓ)		.083	3.4
p-xylene (ℓ)		.11	2.3
mesitylene (ℓ)		.083	2.6
durene (s)	.69	.10	3.5
isodurene (ℓ)		.056	2.3
pentamethylbenzene (s)	.74	.091	2.9
hexamethylbenzene (s)	1.1	.097	3.0
anisole (ℓ)		.099	2.0
o-dimethoxybenzene (ℓ)		.098	2.0
m-dimethoxybenzene (ℓ)		.094	2.2
p-dimethoxybenzene (s)	1.0	.086	1.9
1,2,3-trimethoxybenzene (s)	3.2	.18	1.9
1,2,4-trimethoxybenzene (ℓ)		.092	1.6
1,3,5-trimethoxybenzene (s)	1.1	.094	2.1
acenaphthene (s)	.94	.099	2.5
fluorene (s)	.20	.021	1.8
naphthalene (s)	.86	.099	1.3
pyrene (s)	.17	.011	3.1

[a]The ratio for uncomplexed TCNE is about 0.5.

[b](ℓ) = liquid; (s) = solid.

[c]Refers to CH_2Cl_2 solutions and solid donors. In all other solutions the donor is the solvent.

[d]Uncertainties in intensity ratios are ±.2 or less.

excitation profiles of the affected bands is discussed in Sec. 5.2.3. In addition, some of the ratios in Table X are misleading insofar as they are seriously affected by reabsorption of the scattered light (Sec. 5.2.5). Because of the concentration and wavelength dependence of the reabsorption effect, the intensity ratios in Table X should be regarded as characteristic of the complexes only at the specified excitation wavelengths and concentrations. When the concentration of a complex is reduced

to the point where reabsorption is no longer significant,
$I(\nu_{C=C})/I(\nu_{C\equiv N})$ may be changed considerably (Table XIV).

Because of the increased intensities of the totally symmetric
acceptor bands at resonance, the a_g $\nu_{C\equiv N}$ band is much stronger
than the b_{3g} $\nu_{C\equiv N}$ band; when a large excess of the donor is
present, only the a_g band can be identified. Therefore through-
out Sec. 5.2, '$\nu_{C\equiv N}$' is used only in reference to the a_g $\nu_{C\equiv N}$
vibration.

5.2.2 Observed Features of the Resonance Raman Effect

Before the RR excitation profiles of the $\nu_{C=C}$ and $\nu_{C\equiv N}$ bands
are discussed, some of the other features of the spectra will be
described. Particular attention is paid in this discussion to
those aspects of the spectra which supply information on the EDA
complexes.

As mentioned in Sec. 5.1, the depolarisation ratio of the
TCNE $\nu_{C=C}$ band increases from its nonresonance value of 0.21 to a
value approaching 1/3 in the preresonance Raman spectra of
TCNE EDA complexes. At resonance, depolarisation ratios
$\rho_\ell = 0.33 \pm .03$ are observed for the $\nu_{C=C}$ and $\nu_{C\equiv N}$ bands in the
TCNE EDA complexes with the electron donors p-xylene, mesitylene,
hexamethylbenzene (HMB), m-dimethoxybenzene and anisole, and for
the 167 cm^{-1} band in the spectrum of HMB/TCNE. The fact that the
depolarisation ratios of the $\nu_{C=C}$ and $\nu_{C\equiv N}$ bands equal 1/3 at
resonance has also been reported by other workers in the case of
m-xylene/TCNE[4]. These results imply that only one component of
the scattering tensor is enhanced in the case of each of these
three vibrations; it furthermore indicates, as mentioned in

Sec. 5.1.3, that the first excited states of these EDA complexes need not be degenerate. Since only one component of the scattering tensor is enhanced, the CT transition occurs in a well-defined direction with respect to the molecular complex, as discussed in Sec. 5.1.2. The fact that the $\nu_{C=C}$ and $\nu_{C \equiv N}$ depolarisation ratios are essentially equal to 1/3 for m-dimethoxybenzene/TCNE shows that the same limiting value occurs when the excitation falls between the two CT absorption maxima.

After the publication of these results[11], Jensen reported some surprising depolarisation data for the anisole/TCNE complex[12]. According to this paper, the depolarisation ratios of the $\nu_{C=C}$ and $\nu_{C \equiv N}$ bands in this complex are about 1/3 when the excitation is in resonance with the first CT absorption band, but rise to about .45 for the $\nu_{C=C}$ band and .70 for the $\nu_{C \equiv N}$ band when the excitation is between the two CT absorption maxima. These results were obtained for solutions where anisole is the solvent, i.e. under concentration conditions considerably different than those for the dilute CH_2Cl_2 solutions mentioned above. Because of the discrepancy between these two studies, the anisole/TCNE complex in which the donor is the solvent was investigated further to see if the results of Jensen[12] could be repeated. The $\nu_{C=C}$ depolarisation ratios found are .33 ± .03 for 514.5 nm excitation, .36 ± .03 for 488.0 nm excitation, and .36 ± .05 for 476.5 nm excitation. These data do not confirm the increases reported in Jensen's paper. It must be emphasized that these results for anisole/TCNE are not as accurate as those for some of the other complexes mentioned above, since the RR intensity enhancement is

weaker in anisole/TCNE. The experimental uncertainties quoted
for anisole/TCNE in this paragraph reflect this fact; therefore
it is concluded that within experimental uncertainty, the
depolarisation ratio does not rise above 0.33 for the $\nu_{C=C}$ band
in the spectrum of anisole/TCNE where the donor is the solvent.
The conclusions of Jensen therefore must be regarded with some
scepticism.

The proposal that the multiple CT bands of TCNE complexes
arise from different geometric isomers[13] is supported by the
observation that when the excitation falls within the second
absorption band of a complex (Figs. 20 and 21), an RR effect is
observed which has the same characteristics as those observed in
complexes where the excitation is in the first CT absorption band.
If the multiple CT bands of a complex are due to a single
geometric structure, they can both be expected to contribute
significantly to the scattering tensor, and produce an RR effect
which is different from that observed for complexes with a single
absorption band. The independent resonance observed for the CT
absorption bands therefore is consistent with the suggestion that
each band is due to a different species of the same complex.

The strength of the RR effect in the TCNE EDA complexes is
indicated by the fact that the $\nu_{C=C}$ and $\nu_{C\equiv N}$ intensities increase
by as much as two orders of magnitude in the transition from
nonresonance to resonance; however, a very common feature of the
RR effect, the appearance of overtones or combination bands
involving the enhanced bands, cannot be detected in these spectra.
According to the vibronic theory of RR scattering (Sec. 2.3.2),

the failure to observe overtones is due to small values of the vibrational overlap integrals $\langle v''|v'\rangle$ where the quantum number of the level on which the transition terminates is $v' = 2, 3$, etc. Alternatively, this failure may arise from the strong damping of the CT states (Sec. 5.2.3).

The RR enhanced TCNE bands are much broader than are their counterparts in the spectrum of uncomplexed TCNE. Specifically, in the spectrum of hexamethylbenzene/TCNE the halfwidth of the TCNE $\nu_{C=C}$ band is 16 ± 2 cm^{-1}, whereas the spectrum of a CH_2Cl_2 solution of TCNE shows a $\nu_{C=C}$ halfwidth of 9 ± 1 cm^{-1}. Similarly, in the spectrum of HMB/TCNE the 167 cm^{-1} band (attributed to TCNE vibration ν_5) has a halfwidth of 17 ± 1 cm^{-1}. These broad bands could be characteristic of the resonance scattering process, or they could be due to a change in the molecular motion of TCNE as a consequence of complexation. Since the resonance Raman condition cannot conveniently be separated from the complexation, the possible causes cannot be examined independently and the source of broadening identified. It should be mentioned that restricted rotational motion in solutions ordinarily leads to narrowing of vibrational bands; however, cases where such restricted motion is accompanied by band broadening have also been observed[14]. Further investigation of the broadening of the Raman bands requires their resolution into parallel and perpendicular polarised components[15].

5.2.3 Excitation Profiles of $\nu_{C=C}$ and $\nu_{C\equiv N}$ Bands

The RR excitation profile, i.e. the plot of RR intensity (divided by ν^4) vs. excitation frequency, shows the excitation frequency dependence of the scattering tensor $(\alpha_{\rho\sigma})_{vv'}$ and can

give information which leads to the simplification of the expression for the tensor. The excitation profiles of the TCNE $\nu_{C=C}$ and $\nu_{C\equiv N}$ bands also explain some of the features of the Raman spectra of the TCNE EDA complexes, and some of the details of the excited states of the complexes. The excitation profiles of these particular bands are studied because of their very noticeable intensity increases on complexation, and because the bands are sufficiently strong that quantitative measurements of their intensities with all of the excitation lines of the Argon laser are possible.

RR excitation profiles of the $\nu_{C=C}$ and $\nu_{C\equiv N}$ bands are shown in Figures 13 to 19 for the complexes where the excitation frequency falls in the first CT absorption band, and in Figures 20 and 21 for the complexes where the excitation is within the second CT absorption band. These Figures show that the excitation profiles roughly parallel the absorption spectra, except that the profiles are displaced by about $1000 - 2000$ cm^{-1} toward lower energy with respect to the corresponding absorption maxima. This unusual result is discussed in detail below, and is interpreted according to both existing and new RR theories. Not all of the complexes listed in Table VIII are included in the excitation profile data. Some of them are not suitable for study with Argon laser excitation because of the wavelengths of their CT absorption bands, while others give weak intensity enhancements which prohibit quantitative measurements.

In the complexes where the excitation profiles have identifiable maxima, for each complex the $\nu_{C=C}$ profile peaks at lower
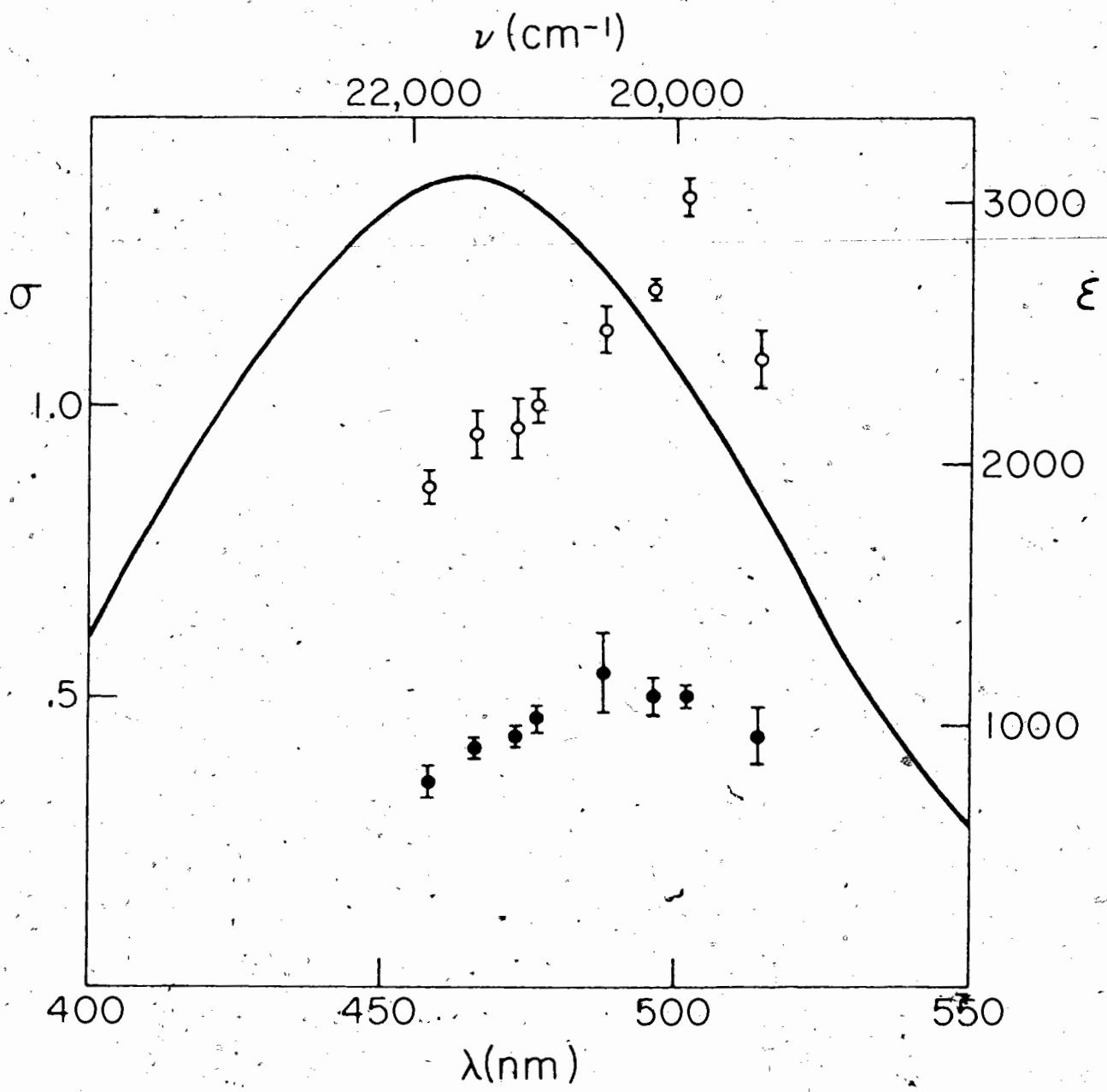
Fig. 13 Excitation profiles of the $\nu_{C=C}$ and $\nu_{C\equiv N}$ TCNE vibrations for mesitylene/TCNE in CH_2Cl_2. Open circles: $\nu_{C=C}$; filled circles: $\nu_{C\equiv N}$. The solid line is the absorption spectrum.
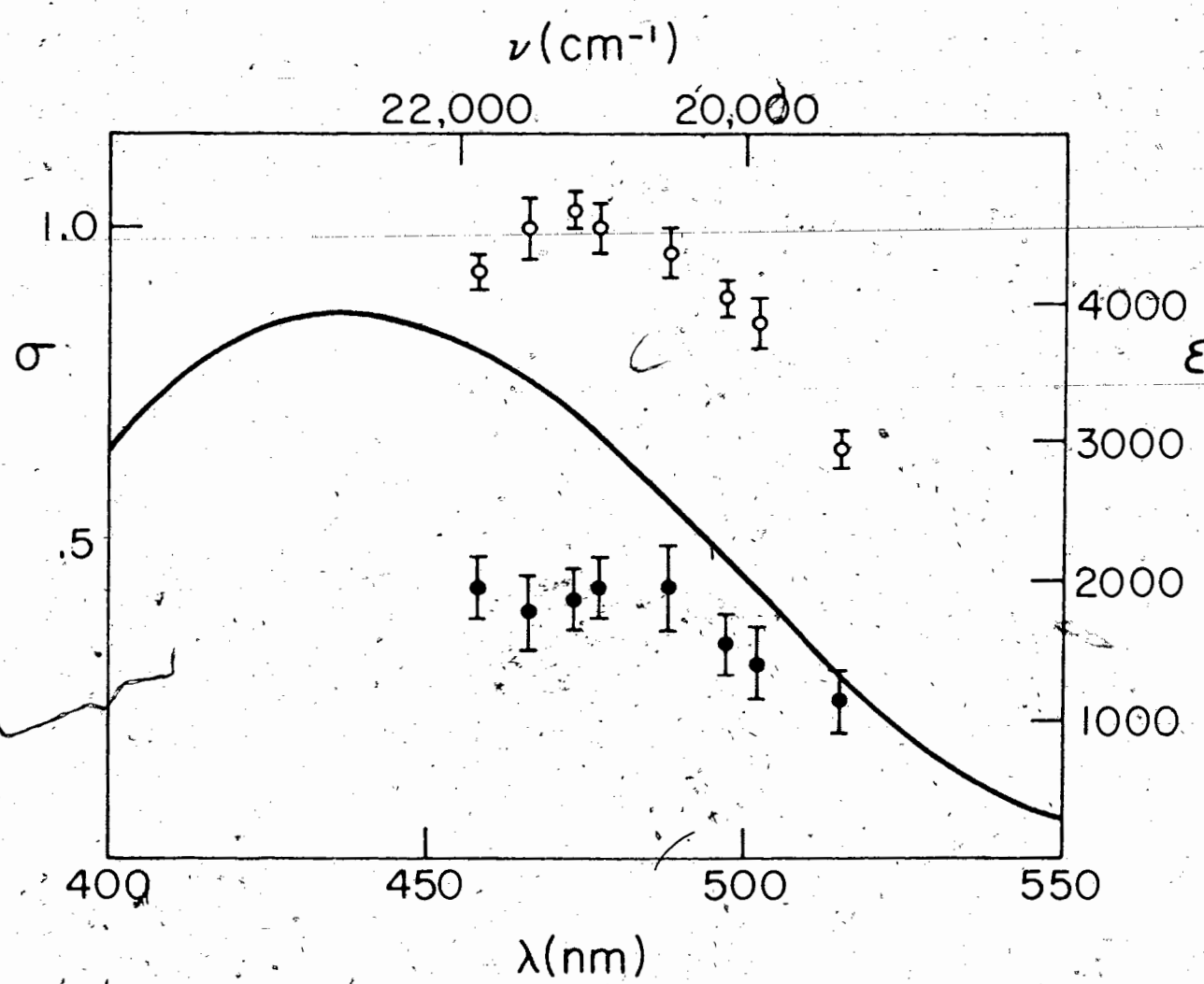
Fig. 14 Excitation profiles of the $\nu_{C=C}$ and $\nu_{C\equiv N}$ TCNE vibrations for o-xylene/TCNE in CH_2Cl_2. Details are the same as in Fig. 13.
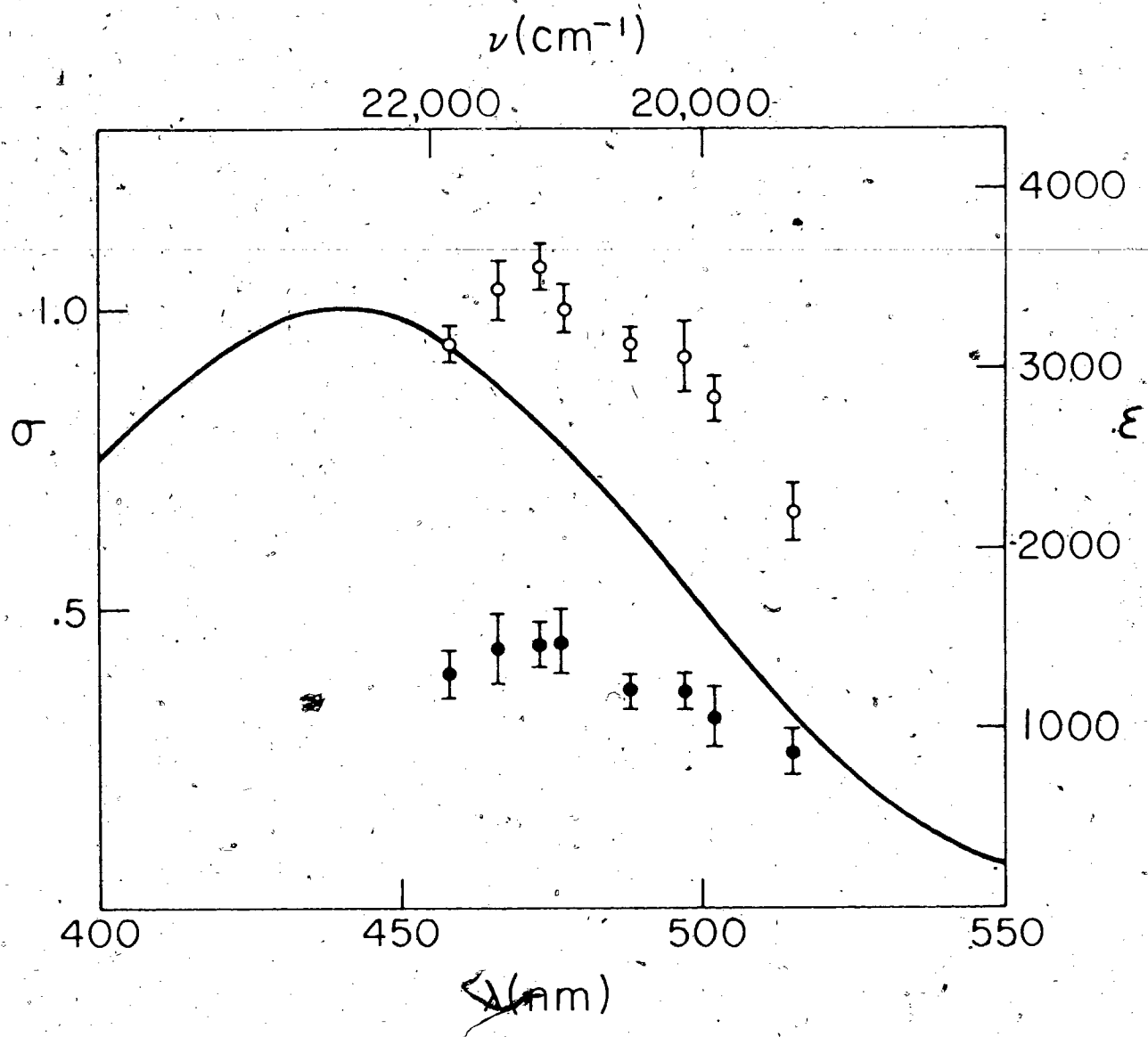
Fig. 15 Excitation profiles of the $\nu_{C=C}$ and $\nu_{C\equiv N}$ TCNE vibrations for m-xylene/TCNE in CH_2Cl_2. Details are the same as in Fig. 13.
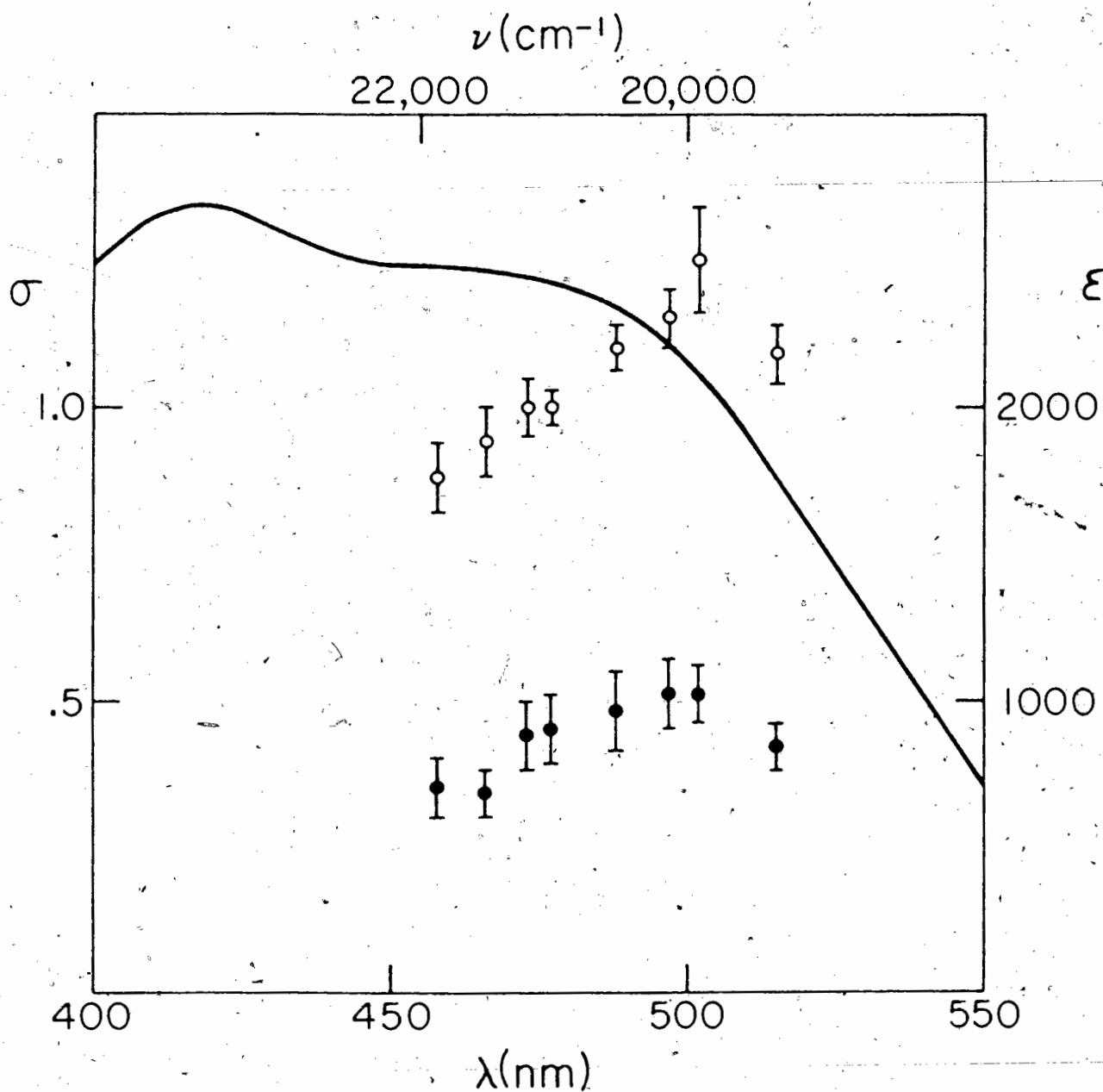
Fig. 16 Excitation profiles of the $\nu_{C=C}$ and $\nu_{C\equiv N}$ TCNE vibrations for p-xylene/TCNE in CH_2Gl_2. Details are the same as in Fig. 13.
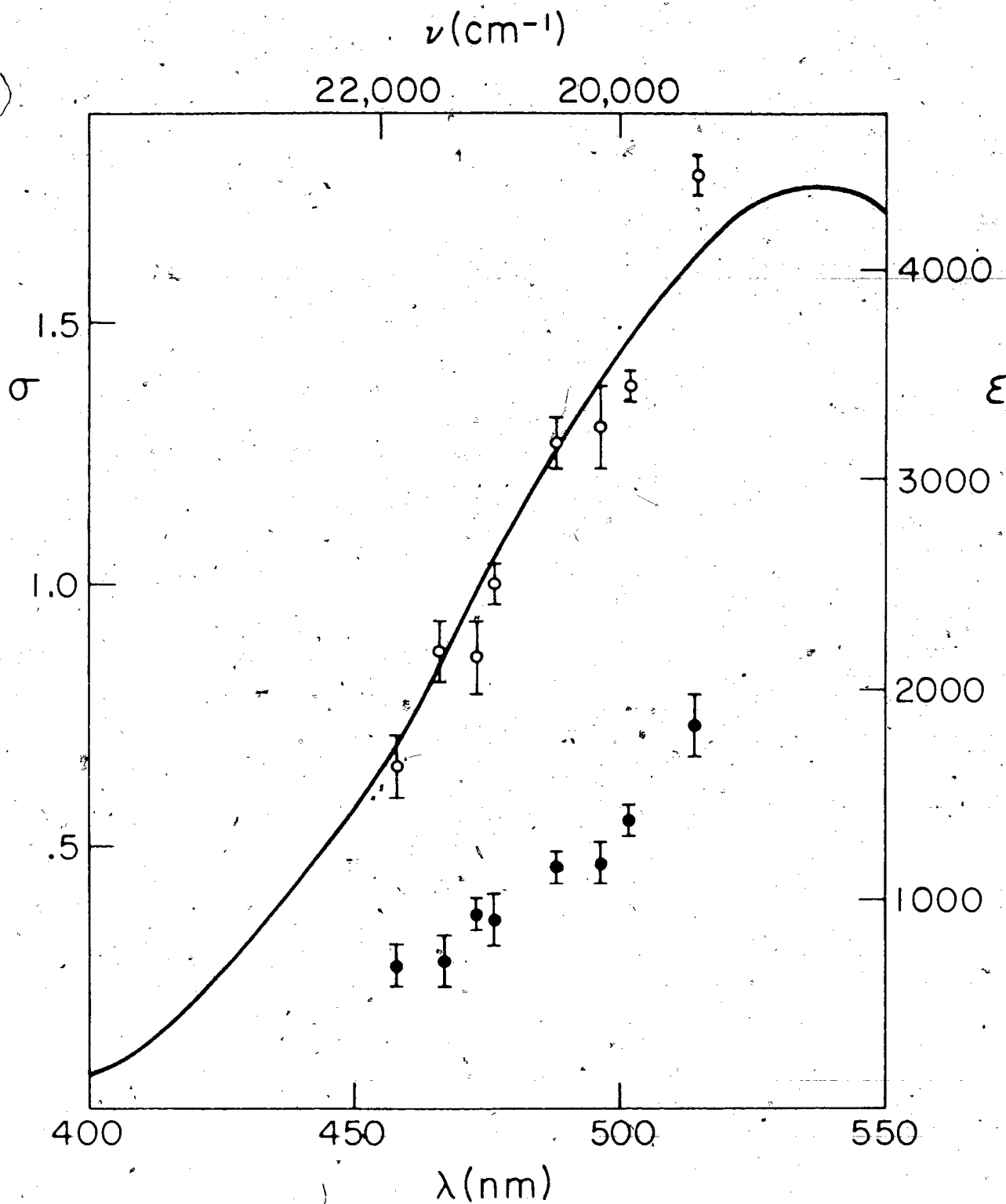
Fig. 17 Excitation profiles of the $\nu_{C=C}$ and $\nu_{C\equiv N}$ TCNE vibrations for hexamethylbenzene/TCNE in CH_2Cl_2. Details are the same as in Fig. 13.
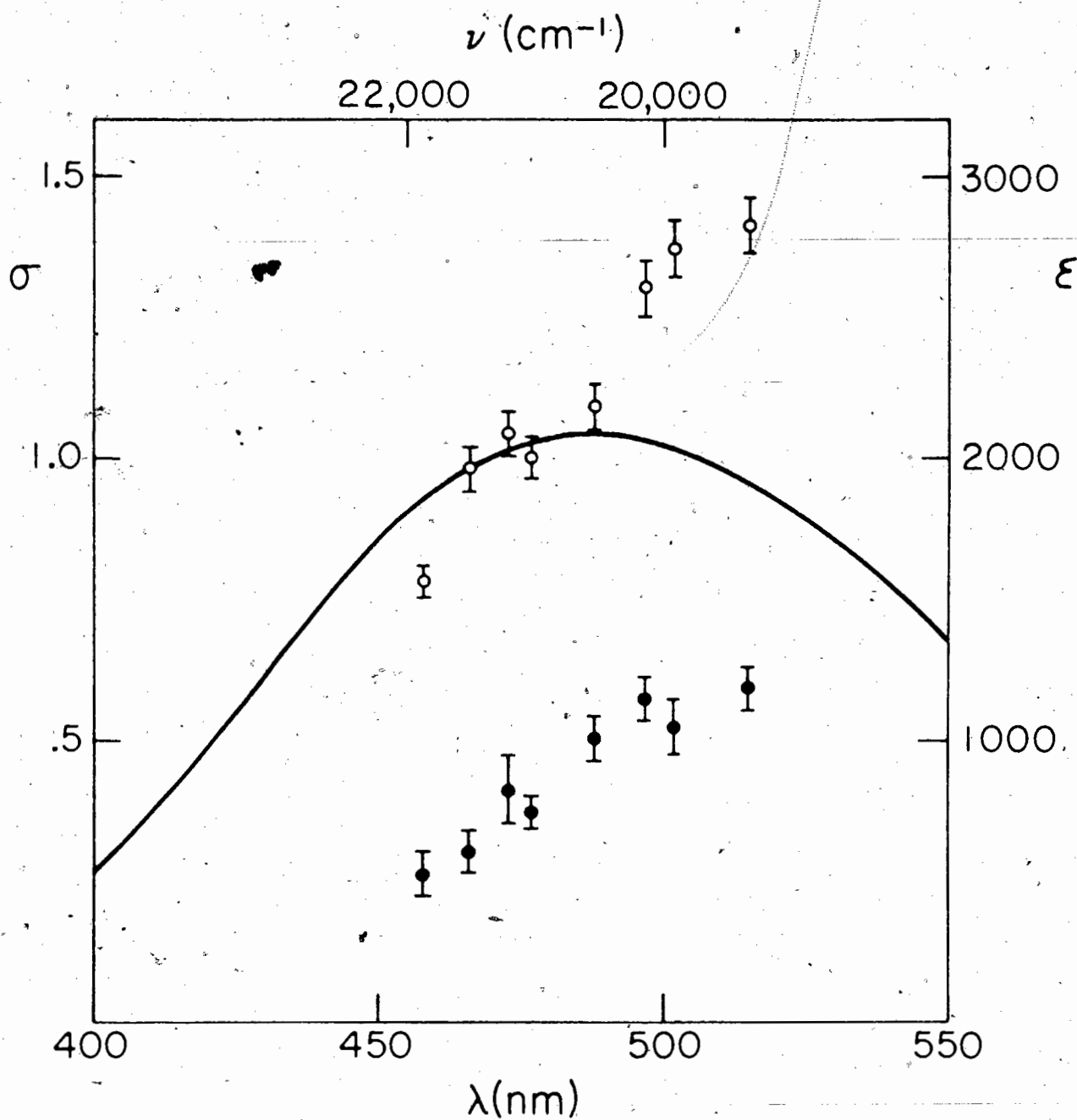
Fig. 18 Excitation profiles of the $\nu_{C=C}$ and $\nu_{C\equiv N}$ TCNE vibrations for isodurene/TCNE in CH_2Cl_2. Details are the same as in Fig. 13.
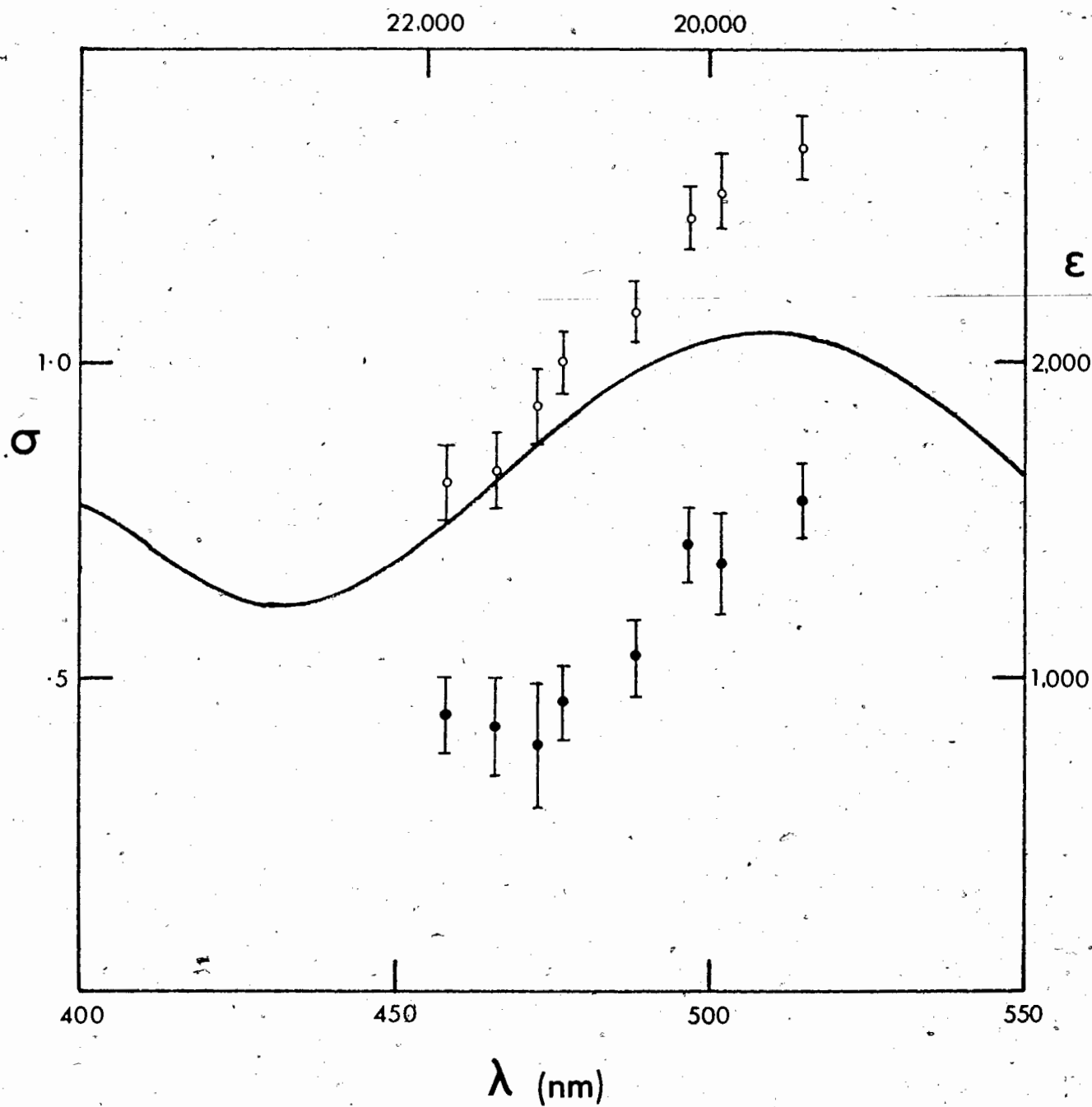
Fig. 19 Excitation profiles of the $\nu_{C=C}$ and $\nu_{C\equiv N}$ TCNE vibrations for anisole/TCNE in CH_2Cl_2. Details are the same as in Fig. 13.
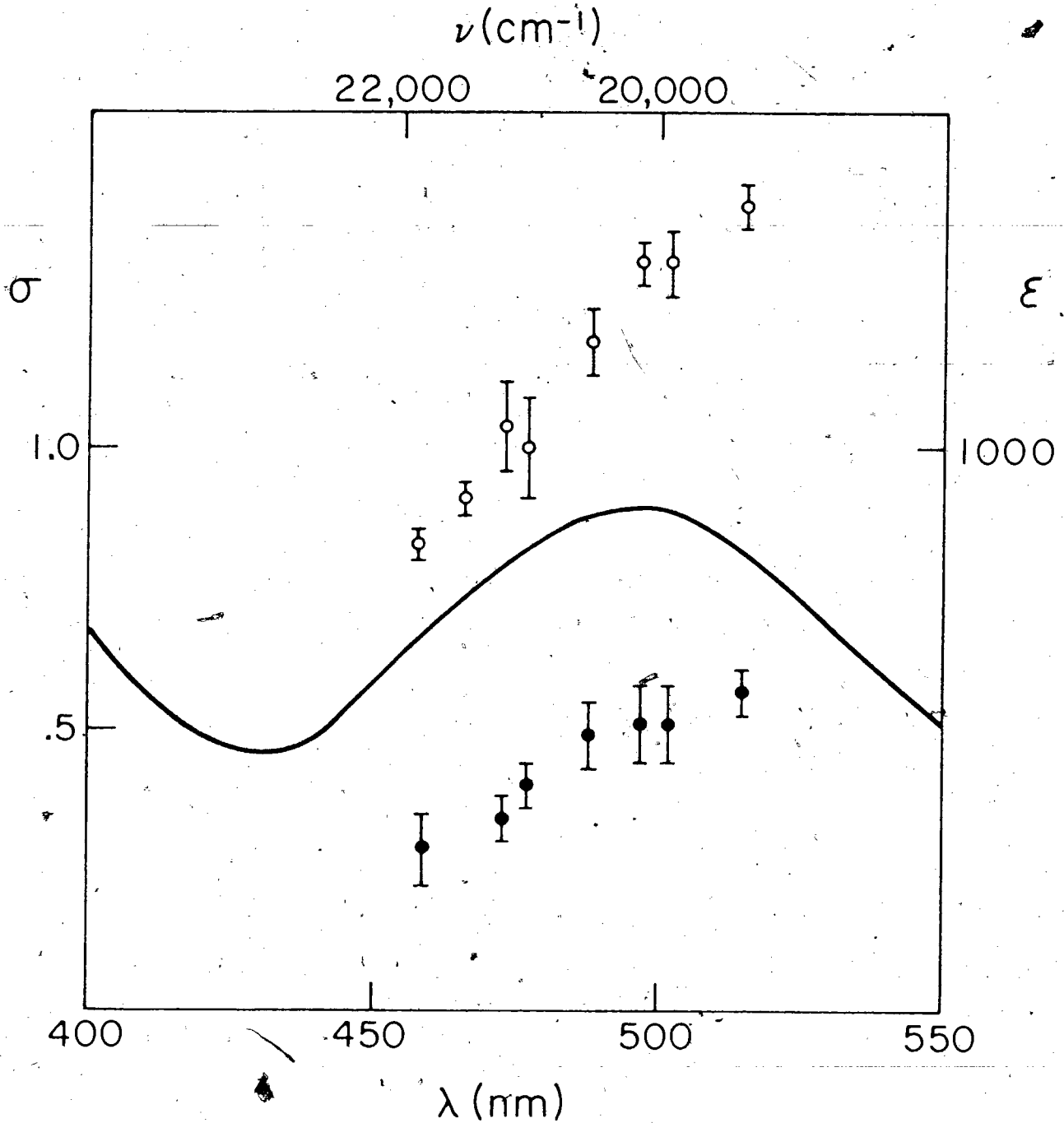
Fig. 20 Excitation profiles of the $\nu_{C=C}$ and $\nu_{C\equiv N}$ TCNE vibrations for the second CT transition of pyrene/TCNE in CH_2Cl_2. Details are the same as in Fig. 13.
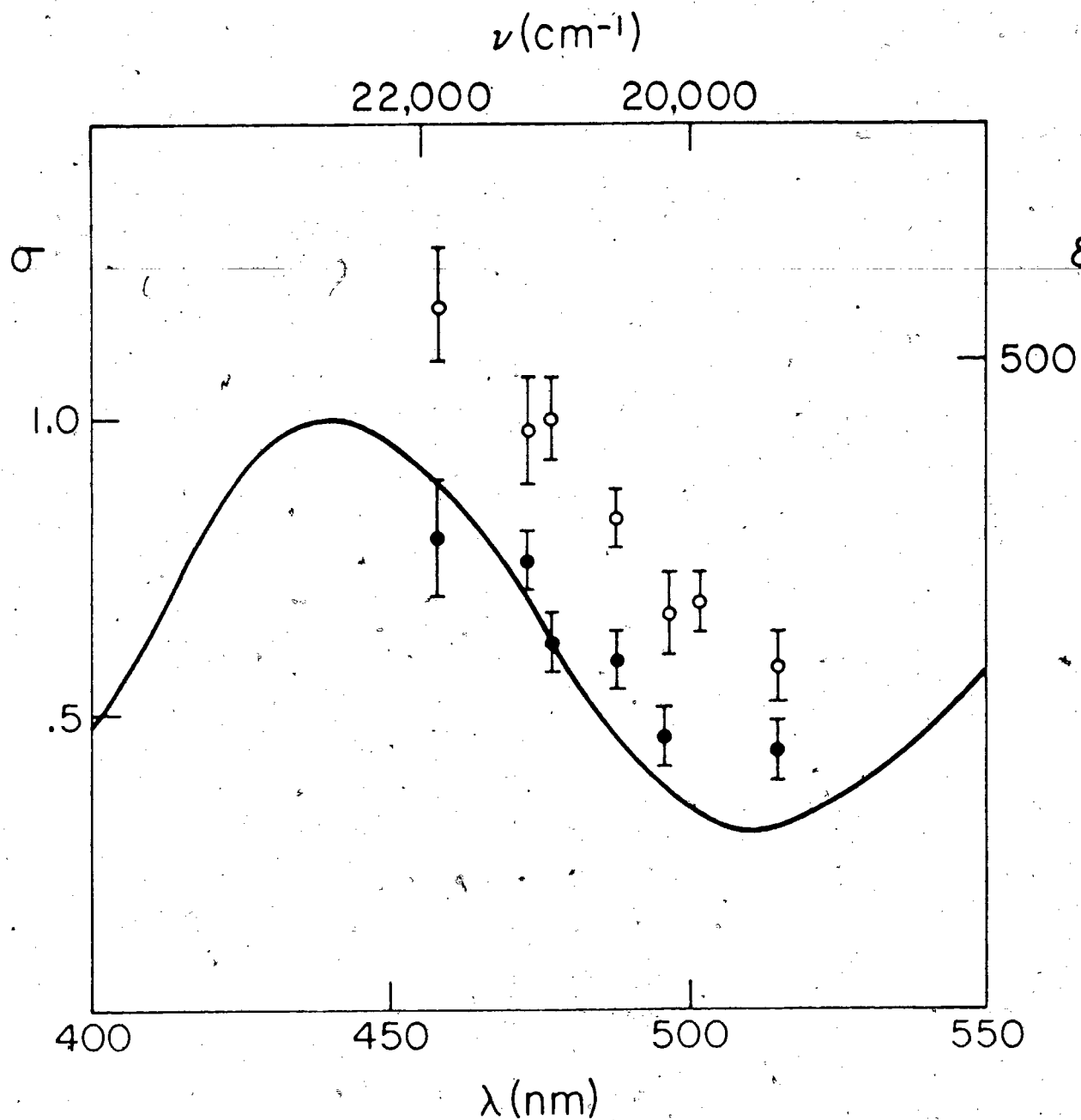
Fig. 21 Excitation profiles of the $\nu_{C=C}$ and $\nu_{C\equiv N}$ TCNE vibrations for the second CT transition of acenaphthene/TCNE in CH_2Cl_2. Details are the same as in Fig. 13.

Table XI. RR excitation profiles and 0-0 frequencies for some TCNE complexes[a]

Donor	Excitation profile maximum (cm^{-1})	Vibration[b]	ν_{0-0} (cm^{-1})[c]	$\nu_{m.p.}$ (cm^{-1})[d]	Fluorescence maximum (cm^{-1})
o-xylene	20,800	$\nu_{C=C}$	19,240	19,400	15,800
	21,100	$\nu_{C\equiv N}$	18,870		
m-xylene	20,800	$\nu_{C=C}$	19,240	19,100	15,500
	21,300	$\nu_{C\equiv N}$	19,070		
p-xylene	19,800	$\nu_{C=C}$	18,240	18,500	15,300
	20,200	$\nu_{C\equiv N}$	17,970		
mesitylene	19,800	$\nu_{C=C}$	18,240	18,300	15,000
	20,400	$\nu_{C\equiv N}$	18,170		

[a] Accuracies of all frequencies are ±200 cm^{-1} or better.

[b] The Raman frequencies for $\nu_{C=C}$ and $\nu_{C\equiv N}$ are about 1560 cm^{-1} and 2230 cm^{-1}, respectively.

[c] 0-0 frequencies estimated from the RR excitation profiles.

[d] Mirror point of CT absorption and fluorescence spectra.

Table XII.   Intensity ratios for mesitylene/TCNE in CH_2Cl_2.
Mesitylene concentration, 1.0 M[a]; TCNE concentration, .0092 M

λ_0 (nm)	$I(\nu_{C=C})/I(\nu_{C\equiv N})$[b]
514.5	6.0
501.7	5.0
496.5	3.7
488.0	3.1
476.5	3.0
472.7	3.1
465.8	2.8
457.9	2.6

[a] M = moles/litre.

[b] Uncertainties in intensity ratios are ± .2 or less.

frequency than does the $\nu_{C\equiv N}$ profile (Table XI). Because of this, at excitation frequencies close to the low frequency edges of the profiles, the $I(\nu_{C=C})/I(\nu_{C\equiv N})$ ratio is greater than that obtained when the excitation frequency is near the centres of the profiles. Therefore, the displacement of the excitation profiles leads to a wavelength dependence of $I(\nu_{C=C})/I(\nu_{C\equiv N})$ in the Raman spectra of complexes such as o-xylene/TCNE or mesitylene/TCNE (Table XII).

The Raman spectra of a number of different kinds of molecules[16-18] have RR excitation profiles which are approximately proportional to their respective absorption curves. Comparison with the excitation profiles of the TCNE EDA complexes shows that the approximate proportionality between the molar absorptivity and the excitation profile may occur over part of the spectrum, but once the maximum in the absorption curve is reached, the proportionality breaks down. Attempts to determine the maximum of the

Table XIII. TCNE complex absorption maxima in CH_2Cl_2 having excitation profiles without observed maxima

Donor	λ (nm)
durene	490[a]
isodurene	488[a]
hexamethylbenzene	541
anisole	510
m-dimethoxybenzene	441
pyrene	495
acenaphthene	442

[a] Two strongly overlapping CT absorption bands.

$\nu_{C=C}$ excitation profile for HMB/TCNE using the dye laser as the excitation source were unsuccessful, because of the poor signal-to-noise ratio in the spectra. The absorption maxima of this and other complexes for which the excitation profiles do not have maxima observable with Argon laser excitation are listed in Table XIII.

The anisole/TCNE and m-xylene/TCNE RR excitation profiles obtained by other authors[4,12] are in good agreement with those in Figs. 15 and 19. Both of the studies cited used different internal standards than the solvent band used in this work; the agreement of the published results with those reported here indicates that the excitation profiles in Figs. 13 to 21 actually reflect the excitation frequency dependence of the scattering tensor, and that they are not produced by experimental artifacts such as reabsorption of the scattered light or other effects.

In Table XI the excitation profiles are summarised for those

TCNE complexes included in the present study whose RR excitation profiles have identifiable maxima. For each complex, the excitation profile maximum for the $\nu_{C\equiv N}$ band occurs at higher energy than for the $\nu_{C=C}$ band. This can occur if the resonance is with the vibronic (electronic + vibrational) transitions involving these vibrations[19,20]. Since the vibrationless electronic transitions of these complexes are not active in their absorption spectra, their frequencies can be estimated by subtracting the frequency of the appropriate vibrational interval from each excitation profile maximum.[†] The 0-0 frequencies estimated by this method are entered in column 4 of Table XI. The comparison of these estimated frequencies with the pure electronic transition frequencies (column 5), calculated as the mirror point of CT absorption and fluorescence spectra[21], shows satisfactory agreement, and thus confirms that the excitation profiles are a result of resonance with the vibronic transitions involving the $\nu_{C=C}$ and $\nu_{C\equiv N}$ modes. Within the framework of the vibronic theory of RR spectra[22] (Sec. 2.3.2), this is equivalent to the statement that the vibrational quantum number v" of the intermediate electronic state in the RR scattering process has the value 1 for either vibration.

These results permit some comments on the form of the scattering tensor $(\alpha_{\rho\sigma})_{vv'}$. According to the vibronic theory of RR spectra, the scattering tensor in general contains three contributions, i.e. the three terms of equation (2.7). When totally symmetric vibrations such as $\nu_{C=C}$ and $\nu_{C\equiv N}$ are enhanced in

---

[†]Implicit in this analysis is the assumption that the vibrational frequency of each mode is the same in both electronic states.

intensity in RR spectra, the potential energy surfaces of the ground and first excited electronic states are generally different[23]; this is consistent with the implied differences in the potential surfaces of the ground and excited states of TCNE EDA complexes[21,24]. When the potential energy surfaces of electronic states k and r are different, all three terms of equation (2.7) can contribute to $(\alpha_{\rho\sigma})vv'$ and the excitation profile maximum need not coincide with either the 0-0 or the 0-1 frequencies[25]; however, the observed resonance with the 0-1 frequencies for the TCNE complexes suggests the dominance of certain terms in the expression for the scattering tensor.

The experimental results which are relevant to the simplification of the scattering tensor are (a) only totally symmetric vibrations are enhanced in intensity in the RR spectra; (b) depolarisation ratios of the RR bands are (within experimental uncertainty) equal to 1/3; (c) the resonance is with the first vibronic transitions; (d) the excitation frequency dependence of the preresonance Raman intensities follows the F_B^2 frequency factors. Results (a) and (b) imply that $\rho = \sigma$ and hence that the scattering tensor can be written $(\alpha_{\rho\rho})_{vv'}$[20]; the condition of resonance $v_{r,v'';k,v} - v_0 \approx 0$ described in (c) implies that v" = 1 and v = 0; and point (d) suggests the importance of the vibronic coupling operator h_{tr}^Q for the $v_{C=C}$ and $v_{C\equiv N}$ intensities. Therefore, the second term of equation (2.7) is the most important one for the intensities of the $v_{C=C}$ and $v_{C\equiv N}$ bands in the RR spectra of the TCNE EDA complexes, and the scattering tensor has the approximate form

$$(\alpha_{\rho\rho})_{vv'} = \frac{1}{h} \sum_{r,t,v''} \frac{h_{tr}^{Q} (M_{\rho}^{0})_{kt} (M_{\rho}^{0})_{rk} \langle v''|v'\rangle \langle v|Q|v'\rangle}{\nu_{r,v'';k,v} - \nu_{0} + i\gamma_{r,v''}} \tag{5.1}$$

where $v = 0$, $v' = 1$ and $v'' = 1$.

The red shift of the RR excitation profiles with respect to their respective absorption maxima can be interpreted in terms of equation (2.1), rather than the vibronic expansion described above. The asymmetry of the CT absorption bands and the large Stokes (red) shift (about 6000 cm^{-1}) between absorption and fluorescence maxima[11] indicate a considerable difference between the potential energy curves of the ground and excited states of each complex. The absorption intensity is governed by the matrix elements coupling the ground (initial) state to the excited (resonant) state, and the Raman intensity is determined by the product of the matrix elements coupling the ground and excited states and those coupling the excited and final states. Therefore, the shift in the potential energy curves produces a displacement of the Raman excitation profile with respect to the absorption profile in the same direction as the shift in the fluorescence spectrum. Furthermore, if the absorption band can be considered to arise from a superposition of highly damped Lorentzian vibronic transitions, whose damping increases with the energy of the transitions, the asymmetry of the absorption bands and of the RR excitation profiles is predictable. This description of the RR process in EDA complexes is the basis for the calculation of RR excitation profiles, fluorescence spectra and absorption spectra of a hypothetical system presented in Appendix C.

The physical mechanism for the frequency dependent damping is postulated to arise from interactions between the EDA complex and the solvent, which lead to a reduced lifetime for the higher vibrational levels of the ground and/or excited electronic states. In particular, nonradiative damping in the excited state may occur via ionic dissociation of the complex after its excitation, a process which is strongly solvent dependent[26,27]. An experimental test for the existence of this mechanism is described in Appendix D.

It is appropriate to mention here that red shifts of the RR excitation profiles for the visible iodine transition with respect to the absorption spectra for I_2 in complexing solvents have been observed, and have been attributed to a destructive interference between the contributions to the scattering tensor from the (resonant) I_2 state and the (preresonant) CT states in these complexes[28]. It is reasonable to expect higher lying states to make some contribution to the scattering tensor even at resonance[29]; however, the relative strengths of the preresonance and resonance Raman effects observed in the present study of TCNE EDA complexes implies that such an explanation is not likely in this case[11].

5.2.4 The Transition from Preresonance to Resonance Raman Scattering

It has been shown in Sections 5.1 and 5.2, that the frequencies of the excitation lines vis à vis the position of the CT absorption band for a given complex determine whether the preresonance or the resonance Raman effect is observed in the

TCNE $\nu_{C=C}$ and $\nu_{C\equiv N}$ bands. Thus it is logical to enquire just where the preresonance scattering is replaced by resonance scattering. The transition from the preresonance to the resonance region is illustrated in the study of the excitation frequency dependence of the $\nu_{C=C}$ and $\nu_{C\equiv N}$ intensities for the o-xylene/TCNE complex. This complex is chosen because its CT absorption maximum, 436 nm, is not too far from those of the complexes where the preresonance Raman effect is observed (Table I).

In Figure 22 the preresonance Raman frequency factors F_B^2 (divided by ν^4) are compared with the observed excitation profiles for the $\nu_{C=C}$ and $\nu_{C\equiv N}$ bands. In order to be consistent with the analysis of Sec. 5.1, the frequency factors are calculated using $\nu_{rk} = 23{,}000$ cm^{-1} (the CT absorption maximum), $\nu_{tk} = 36{,}170$ cm^{-1} for the $\nu_{C=C}$ band and $\nu_{tk} = 55{,}560$ cm^{-1} for the $\nu_{C\equiv N}$ band.

Fig. 22 shows that for the first few laser lines (beginning with the one at 514.5 nm), there is fair accord between the calculated frequency factors and the observed intensities; this agreement persists a little closer to the absorption maximum for the $\nu_{C\equiv N}$ intensity than it does for $\nu_{C=C}$. For both vibrations, as the excitation moves closer to the absorption maximum, the frequency factors diverge rapidly from the observed intensities. These results suggest that the preresonance regions for the $\nu_{C\equiv N}$ and the $\nu_{C=C}$ bands are slightly different, and that the transition from preresonance to resonance Raman scattering for the TCNE EDA complexes - at least as far as the TCNE $\nu_{C=C}$ and $\nu_{C\equiv N}$ vibrations are concerned - occurs when the excitation frequency is about 3000 to 4000 cm^{-1} away from the absorption maximum. When the
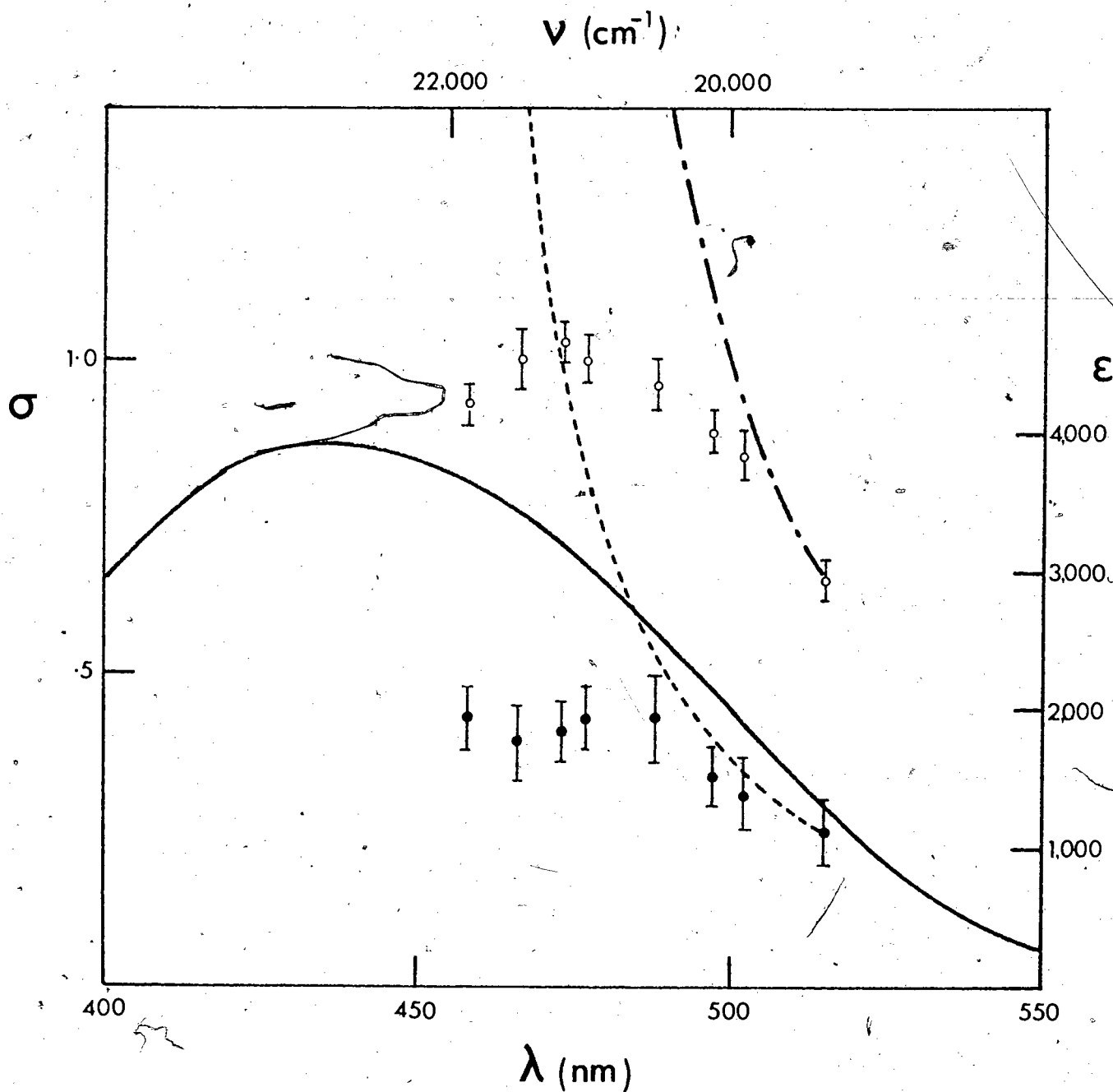
Fig. 22 Transition from preresonance to resonance Raman scattering for o-xylene/TCNE in CH_2Cl_2. Broken line: F_B^2/ν^4 for $\nu_{C=C}(\nu_{tk} = 36,170\ cm^{-1})$; dashed line: F_B^2/ν^4 for $\nu_{C\equiv N}$ $(\nu_{tk} = 55,560\ cm^{-1})$.

excitation is closer than this to the absorption band, damping can no longer be ignored and RR scattering occurs.

5.2.5 Reabsorption Effect on $I(\nu_{C=C}) I(\nu_{C\equiv N})$

Light scattered by absorbing solutions may be absorbed itself when the absorptivity at the wavelength of the scattered light is significant. This reabsorption (or self-absorption) effect occurs in many of the TCNE EDA complexes. The intensities of the $\nu_{C=C}$ and $\nu_{C\equiv N}$ Raman bands for a given complex are in general affected differently, and their observed ratio can be affected by reabsorption.

In Table XIV $I(\nu_{C=C})/I(\nu_{C\equiv N})$ ratios observed for the mesitylene/TCNE complex at several different excitation wavelengths and different acceptor concentrations are given. The data show that in solutions with higher TCNE concentration (and stronger absorption), the excitation wavelength dependence of the intensity ratio is diminished.[†] This concentration effect cannot be accounted for by a difference in the degree of complexation of TCNE (Sec. 5.3). Since the $\nu_{C=C}$ band is more apt to suffer intensity loss from reabsorption than is the $\nu_{C\equiv N}$ band (the molar absorptivity at the wavelength of the $\nu_{C=C}$ band is greater than that at the $\nu_{C\equiv N}$ wavelength for each excitation wavelength), this concentration dependence of $I(\nu_{C=C})/I(\nu_{C\equiv N})$ is concluded to arise from the reabsorption effect.

Similar results are obtained for other complexes in which the

---

[†]The wavelength dependence of this intensity ratio is discussed in Sec. 5.2.3.

Table XIV. $I(\nu_{C=C})/I(\nu_{C\equiv N})$ for mesitylene/TCNE in CH_2Cl_2 for several excitation wavelengths and TCNE concentrations.[a,b] Mesitylene concentration = 1.0 M

λ_0 (nm)	[TCNE], M	
	.029	.087
514.5	4.0	3.5
496.5	3.3	3.0
476.5	2.9	2.8
457.9	2.5	2.2

[a] Uncertainties in the intensity ratios are ± .2 or less.
[b] The CT absorption maximum for this complex is at 466 nm.

excitation is on the long wavelength side of the EDA complex absorption maximum. Because of the very significant effect of reabsorption on relative intensities, the interpretation of RR excitation profiles in Sec. 5.2.3 is confined to the results for dilute solutions, where reabsorption is much less troublesome (see below).

Whenever a complex absorbs the laser beam strongly, e.g. for mesitylene/TCNE and 514.5 nm excitation, measurement of the concentration dependence of the intensity ratio of two bands which are subject to reabsorption to different degrees makes possible the calculation of the depth of penetration of the beam into the solution[30]. For the $\nu_{C=C}$ and $\nu_{C\equiv N}$ bands the appropriate equation is

$$\log\left(\frac{I(\nu_{C=C})}{I(\nu_{C\equiv N})}\right)_{observed} = \log\left(\frac{I(\nu_{C=C})}{I(\nu_{C\equiv N})}\right)_{true} - bc\Delta\epsilon$$

(5.2)

where the subscripts "observed" and "true" denote the measured and intrinsic ratios respectively, b is the penetration depth, c is the concentration of the complex, and $\Delta\varepsilon$ is the difference between the molar absorptivities at the $\nu_{C=C}$ and $\nu_{C\equiv N}$ wavelengths. According to equation (5.2), a plot of observed intensity ratios vs. $c\Delta\varepsilon$ yields a straight line (provided that the scattering length is constant), with a slope equal to -b and the intercept, obtained by extrapolation to zero concentration, equal to the true intensity ratio. The data for mesitylene/TCNE in CH_2Cl_2, when analysed according to this equation, imply that the penetration depth of the 514.5 nm light is (.0085 ±.0011) cm, and that the true intensity ratio is 6.0 ± 1.0. Thus, according to Table XIV, even a TCNE concentration of .029 M is sufficient to cause significant reabsorption. The calculated penetration depth of about .0085 cm is reasonable in view of the molar absorptivities and the concentrations of mesitylene/TCNE used.

5.3 Equilibrium Constant Measurements by Raman Spectroscopy

In the preceding two sections, the intensity increases in the $\nu_{C=C}$ and $\nu_{C\equiv N}$ bands of TCNE on complexation with aromatic electron donors were discussed in detail and shown to result from preresonance or resonance Raman scattering. The preresonance or resonance conditions arise from the proximity of the Raman excitation frequencies to the CT absorption bands; the close relationship between the Raman intensity changes and the absorption intensities makes it possible to use the Raman intensities, instead of the absorption intensities, to calculate the concentration of the complex in solution and from there the equilibrium constant

(K_c^{AD}) for the complex formation. This constitutes a new method of determination of K_c^{AD} for $\pi-\pi$ EDA complexes.

The present determination of equilibrium constants by Raman spectroscopy is an application of some of the information gained in the investigation of the RR effect in TCNE EDA complexes. The K_c^{AD} are found for TCNE complexes in which various methyl or methoxy substituted benzenes are the electron donors; these complexes are chosen from among those discussed in Sections 5.1 and 5.2 because they display sufficiently large intensity changes in the TCNE $\nu_{C=C}$ and $\nu_{C\equiv N}$ bands with complexation when using the Argon laser for excitation. TCNE complexes which have comparatively small equilibrium constants are omitted, since the uncertainties in the K_c^{AD} for such complexes as calculated from the Raman spectra are of the same order of magnitude as the equilibrium constants themselves.

The solvents used for Raman studies of EDA complexes must be chosen so that they satisfy certain criteria. The most important of these are that the solvent dissolve both of the components of the complex in sufficient concentration that the Raman bands of interest are of reasonable intensity over a range of concentrations; that the solvent does not have Raman bands which interfere with the component bands to be analysed; and finally, that the solvent does not interact strongly with either of the components. Since dichloromethane meets all the above criteria, it was chosen as the principal solvent for this investigation. An additional factor in favour of this choice of solvent is the fact that equilibrium constants determined by other methods have been

reported for many TCNE EDA complexes in CH_2Cl_2, so that a

comparison of some of the Raman results with other published

results is possible. The other solvents used for the Raman

determination of K_C^{AD} are dibromomethane and 1,2-dichloroethane;

these solvents were chosen for the same reasons as was CH_2Cl_2.

5.3.1 The Intensity Ratio Method

The increase in the intensity of the $\nu_{C=C}$ band is greater

than the increase in the $\nu_{C\equiv N}$ band on complexation, which results

in an increase in the $I(\nu_{C=C})/I(\nu_{C\equiv N})$ intensity ratios. Quantita-

tive use of these intensity increases can then be made by measuring

the intensity ratios of these bands under various conditions.

Specifically, the measurement of intensity ratios for solutions of

appropriate known concentrations makes possible the calculation of

the equilibrium constants. As shown below, calculation of K_C^{AD} for

a complex only requires the measurement of one intensity ratio

once the intensity changes with complexation are known. Thus, the

$I(\nu_{C=C})/I(\nu_{C\equiv N})$ intensity ratios are obtained for solutions which

have suitable small fractions of the acceptor complexed; the

experimental ratios are then used to calculate these fractions

and the concentrations of the species in the solutions. This

allows calculation of the equilibrium constants for complex

formation.

The complexation of TCNE results in an increase in

$I(\nu_{C=C})/I(\nu_{C\equiv N})$ from the value for uncomplexed TCNE (about 0.5),

to a larger value characteristic of the complex and of the excita-

tion frequency used (Table X). In a solution where a small part

of the TCNE is complexed, the $\nu_{C=C}$ and $\nu_{C\equiv N}$ intensities originate

both from complexed and from uncomplexed TCNE, so that an intensity ratio somewhere between the two limiting values occurs. A mathematical relationship between this intensity ratio and the fraction of TCNE complexed is a prerequisite for the calculation of K_c^{AD}; such an equation is derived in the following paragraphs.

For a TCNE EDA complex in solution in which a fraction y of the TCNE is associated with the donor in the form of a 1:1 complex and if the TCNE $\nu_{C=C}$ and a_g $\nu_{C\equiv N}$ bands are denoted by the subscripts 1 and 2 respectively, then the observed intensities of these Raman bands are

$$I_1 = yI_{1c} + (1-y)I_{1u} \tag{5.3a}$$

$$I_2 = yI_{2c} + (1-y)I_{2u} \tag{5.3b}$$

where the subscripts c and u represent complexed TCNE and uncomplexed TCNE, respectively. From equations (5.3a) and (5.3b) one obtains

$$\frac{I_1}{I_2} = \frac{y}{y\frac{I_{2c}}{I_{1c}} + (1-y)\frac{I_{2u}}{I_{1c}}} + \frac{1-y}{y\frac{I_{2c}}{I_{1u}} + (1-y)\frac{I_{2u}}{I_{1u}}} \ . \tag{5.4}$$

The equilibrium constant for the formation of the complex according to the equilibrium $D + A \rightleftarrows AD$ is

$$K_c^{AD} = \frac{[AD]}{([D]_0 - [AD])([A]_0 - [AD])} = \frac{y}{([D]_0 - y[A]_0)(1-y)} \tag{5.5}$$

where $[D]_0$ and $[A]_0$ are the initial donor and acceptor concentrations, and the concentration ratio $y = [AD]/[A]_0$.

The intensity ratios on the right-hand side of equation (5.4)

are obtained as follows: I_{2u}/I_{1u} comes from the spectrum of uncomplexed TCNE; I_{2c}/I_{1c} is the limiting value characteristic of the particular complex and excitation frequency under consideration; the other two ratios are not measured directly, but are instead calculated as the products $I_{2u}/I_{1c} = (I_{2u}/I_{1u})(I_{1u}/I_{1c})$ and $I_{2c}/I_{1u} = (I_{2c}/I_{1c})(I_{1c}/I_{1u})$, where I_{1c}/I_{1u} is the relative increase in the intensity of the $\nu_{C=C}$ band on complexation. This intensity increase quantifies the resonance enhancement of this band, and is determined using a strong solvent band as internal standard in order to compensate for the loss in overall intensity resulting from the absorption of the excitation light by the EDA complex.

The I_1/I_2 intensity ratio, which varies between I_{1u}/I_{2u} and I_{1c}/I_{2c}, is for $y \ll 1$ approximately equal to

$$\frac{I_1}{I_2} \approx \frac{y}{y\frac{I_{2c}}{I_{1c}} + \frac{I_{2u}}{I_{1c}}} + \frac{1}{y\frac{I_{2c}}{I_{1u}} + \frac{I_{2u}}{I_{1u}}} \quad . \quad (5.6)$$

According to the data in Table XV, which are typical for the TCNE complexes, $\frac{I_{2c}}{I_{1c}} > y\frac{I_{2c}}{I_{1c}}$ and $\frac{I_{2u}}{I_{1u}} > y\frac{I_{2c}}{I_{1u}}$. When y is very small, equation (5.5) becomes simply $y \approx K_c^{AD}[D]_0$. With these approximations, the intensity ratio is given by

$$\frac{I_1}{I_2} \approx K_c^{AD} \frac{I_{1c}}{I_{2u}} \cdot [D]_0 + \frac{I_{1u}}{I_{2u}}, \quad y \ll 1 \quad .$$

$$(5.7)$$

When the kind of complex and the excitation frequency are fixed, K_c^{AD} and I_{1c}/I_{1u} are constant; thus, equation (5.7) predicts an

Table. XV. Intensity ratios used for the calculation of K_c^{AD} for TCNE EDA complexes in CH_2Cl_2 solutions[a,b,c]

Donor	Excitation wavelength (nm)	$\frac{I_{2c}}{I_{1c}}$	$\frac{I_{2u}}{I_{1c}}$	$\frac{I_{2c}}{I_{1u}}$	$\frac{I_{1c}}{I_{1u}}$
durene	488.0	.26	.031	15	59
	514.5	.23	.019	22	96
isodurene	488.0	.33	.043	14	43
	514.5	.30	.032	17	58
pentamethylbenzene	488.0	.31	.016	36	115
	514.5	.32	.010	61	188
hexamethylbenzene	488.0	.41	.012	62	150
	514.5	.41	.0068	110	275

[a] For both excitation wavelengths in this table, I_{2u}/I_{1u} is about 2.0.

[b] Uncertainties in the intensity ratios are less than 10% of their magnitudes.

[c] Subscripts 1 and 2 signify TCNE $\nu_{C=C}$ and a_g $\nu_{C\equiv N}$ bands respectively; c and u denote complexed and uncomplexed TCNE respectively.

approximate proportionality between I_1/I_2 and $[D]_0$ for each complex.

The graph of I_1/I_2 vs. $[D]_0/[A]_0$ for several different TCNE EDA complexes (Figure 23) shows that the expected proportionality between these two quantities occurs as long as the donor concentration (and therefore the fraction y) is comparatively low. As the donor concentration increases, the approximations used in the derivation of equation (5.7) lose their validity; therefore, the linear relationship no longer exists, and the exact equation
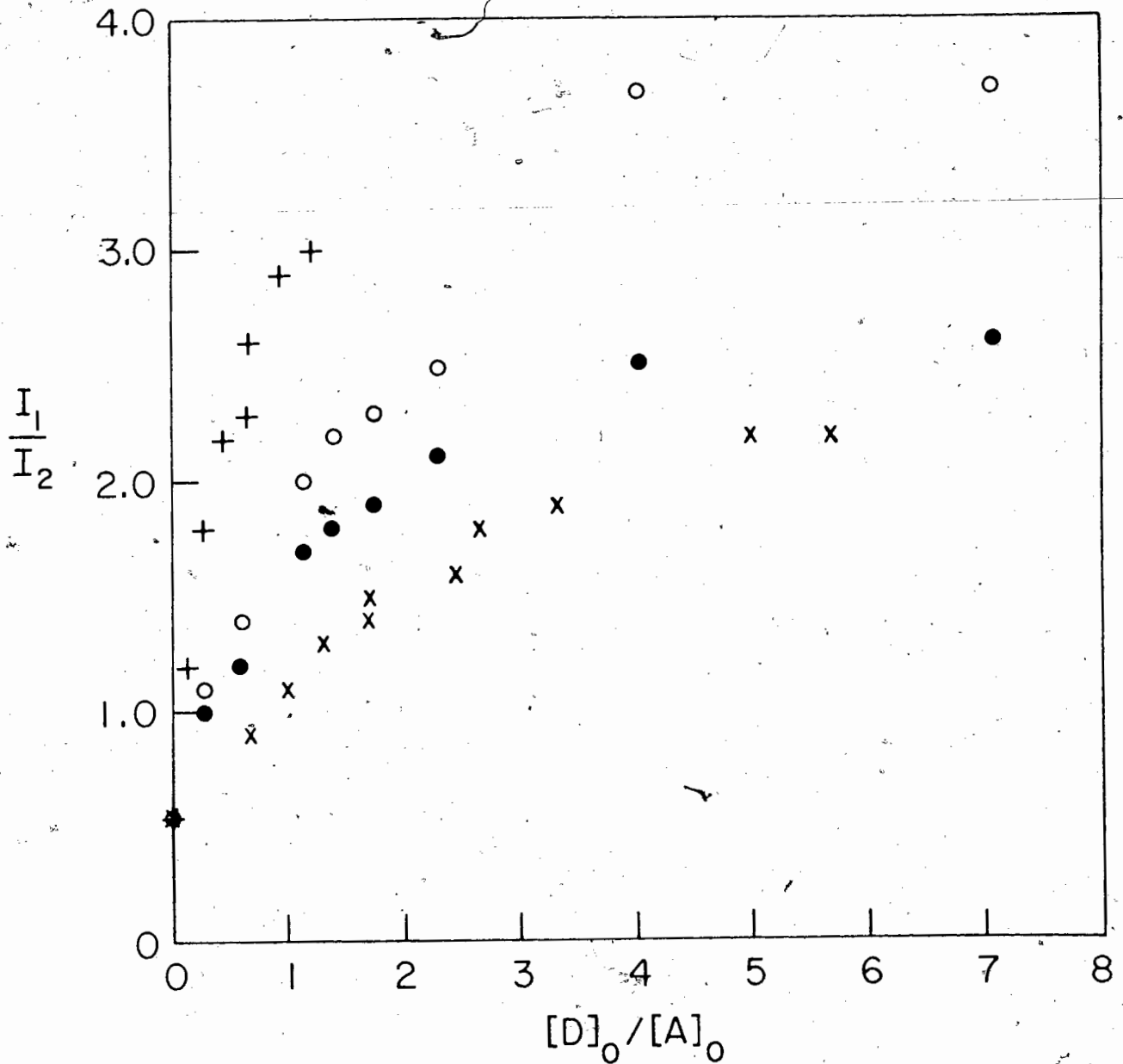
Fig. 23 Intensity ratio of TCNE $\nu_{C=C}$ and $\nu_{C\equiv N}$ bands as a function of relative donor concentration. Donors are o-xylene (x), mesitylene (o and ●), and durene (+). Excitation wavelength 514.5 nm in all cases except mesitylene/TCNE (●), 488.0 nm. The uncertainty in I_1/I_2 is ± .2 or less.

(5.4) governs the intensity ratios. In the region where I_1/I_2 is a slowly varying function of donor concentration, the precision in the calculated results is not very good, since significant variations in the donor concentration hardly affect the intensity ratio. Because of this, K_c^{AD} are best determined for solutions in which only a small fraction (less than 1/10) of the acceptor is complexed.

Figure 23 shows also, for the mesitylene/TCNE data for two excitation wavelengths that the rate of increase of I_1/I_2 with $[D]_0$ depends on the magnitudes of I_{1c}/I_{2u} and of K_c^{AD}, as is predicted by equation (5.7). For this complex, the I_{1c}/I_{2u} which is obtained with 514.5 nm excitation is greater than that found with 488.0 nm excitation; as expected, the slope of I_1/I_2 vs. $[D]_0$ is steeper with the 514.5 nm laser line. These results emphasise the fact that the complex and the excitation wavelength must be specified when equations (5.4) or (5.7) are to be used.

The final important feature of Fig. 23, the occurrence of steeper slopes for complexes with higher K_c^{AD}, is consistent with equation (5.7) in view of the intensity ratios in Table XV.

5.3.2 Results

The K_c^{AD} calculated from equations (5.4) and (5.5) are summarised for the TCNE complexes in CH_2Cl_2 solutions in Table XVI and for the CH_2Br_2 and dichloroethane solutions in Table XVII. The comparison of these results with the K_c^{AD} in the literature is discussed in Sec. 5.3.3. It should be noted that the equilibrium constant for the CH_2Cl_2/TCNE EDA complex[31,32] is less than about 0.2, i.e. it is considerably smaller than any of the K_c^{AD} in

Table XVI. Equilibrium constants for TCNE EDA complexes in CH_2Cl_2 solutions at room termperature (about 21°)

Donor	K_c^{AD} (M^{-1})	I_{1c}/I_{1u} [a,b]
o-xylene	.42 ± .15	75 ± 25
m-xylene	.50 ± .18	75 ± 25
p-xylene	.52 ± .19	75 ± 25
mesitylene	1.6 ± .6	75 ± 25
durene	3.3 ± .4	96
isodurene	4.7 ± .7	58
pentamethylbenzene	7.4 ± .6	188
hexamethylbenzene	17 ± 2	275
anisole	.52 ± .14	20 ± 5
o-dimethoxybenzene	1.0 ± .3	12 ± 3
m-dimethoxybenzene	1.0 ± .3	30 ± 10
p-dimethoxybenzene	1.0 ± .3	9 ± 3
1,2,3-trimethoxybenzene	.84 ± .30	30 ± 10
1,2,4-trimethoxybenzene	1.2 ± .3	12 ± 3
1,3,5-trimethoxybenzene	1.3 ± .3	45 ± 10

[a] Intensity increase of the TCNE $\nu_{C=C}$ band on complexation; excitation wavelength 514.5 nm.

[b] Values quoted with uncertainties are estimated (see text).

Table XVI:

The equilibrium constants in Table XVI are based on I_1/I_2 measured at several excitation wavelengths between 457.9 and 514.5 nm. Since I_1/I_2 for a solution varies with excitation wavelength, the data are analysed in terms of the appropriate equations (see above). The intensity ratios do not indicate any systematic variation of the calculated y with wavelength. Therefore for each solution, the average of the calculated y for the excitation wavelengths employed is used to calculate K_c^{AD}, and the K_c^{AD} for a series of solutions (5 to 15) of one complex are averaged and entered in Table XVI. Only one or two excitation

Table XVII. Equilibrium constants for TCNE EDA complexes in solvents other than CH_2Cl_2 at room temperature (about 21°)

Donor	Solvent	$K_c^{AD}(M^{-1})$	I_{1c}/I_{1u}[a]
p-dimethoxybenzene	CH_2Br_2	1.0 ± .3	9 ± 3[b]
hexamethylbenzene	CH_2Br_2	23 ± 2	206
hexamethylbenzene	$C_2H_4Cl_2$	19 ± 3	153

[a]Intensity increase of the TCNE $\nu_{C=C}$ band on complexation; excitation wavelength 514.5 nm.

[b]Estimated value (see text).

wavelengths were used to calculate the K_c^{AD} summarised in Table XVII since the results for the CH_2Cl_2 solutions showed that by using a wider range of laser lines no further information is obtained.

In addition to the calculated equilibrium constants, Tables XVI and XVII contain the $\nu_{C=C}$ intensity enhancements on complexation, as observed with 514.5 nm excitation. From equations (5.4) and (5.7), it can be seen that the determination of K_c^{AD} using Raman intensity ratios is only as accurate as are the measured I_{1c}/I_{1u}. Thus for completeness, both K_c^{AD} and I_{1c}/I_{1u} are entered in the Tables. Comparison of these ratios with the preresonance Raman results of Sec. 5.1 shows that the RR intensity increases are in most cases an order of magnitude larger than the preresonance Raman intensity enhancements in the TCNE EDA complexes. For this reason, the K_c^{AD} were obtained only for TCNE complexes in which the RR effect occurs with Argon laser excitation.

One limitation of the intensity ratio method is the

inaccessibility of accurate I_{lc}/I_{lu} ratios for complexes having

small K_C^{AD}. For such complexes the addition of even a large excess

of the donor to a TCNE solution does not bring about the complexa-

tion of most of the TCNE. Attempts to measure I_{lc}/I_{lu} for these

complexes yielded artificially low results, because the concentra-

tion of TCNE responsible for the band with intensity I_{lc} is less

than the concentration which produces intensity I_{lu}. (This

situation does not occur for complexes with higher K_C^{AD}, where

an excess of donor ensures the complexation of virtually all of

the TCNE). If a large amount of donor is added to a solution in

an attempt to complex all of the TCNE, a concentration gradient

within the cuvette sometimes develops, further complicating the

results.

Because of these considerations, the I_{lc}/I_{lu} observed

experimentally for the weaker complexes are used only as a basis

for the estimate of the true ratios. The I_{lc}/I_{lu} which are

estimated are those for which uncertainties are quoted in

Tables XVI and XVII. For example, mesitylene or one of the

xylenes, when added to a TCNE solution, produces an intensification

in the TCNE $\nu_{C=C}$ band by a factor between perhaps 50 and 100; for

one of these complexes, I_{lc}/I_{lu} is therefore about 75 ± 25. These

fairly wide limits are derived from the results of a number of

attempts to measure the ratios for these complexes, and from the

estimate that about .3 to .7 of the acceptor was actually complexed

in each solution. Obviously, the K_C^{AD} calculated using estimated

I_{lc}/I_{lu} are not as reliable as those calculated for complexes in

which I_{lc}/I_{lu} is known more accurately.

The Raman method of determining K_c^{AD} of EDA complexes was successfully applied to TCNE EDA complexes in the solvents CH_2Cl_2, CH_2Br_2 and dichloroethane (Tables XVI and XVII). Readily available conventional nonpolar solvents could not be used partly because of the limited solubility of TCNE in these solvents, and partly because of interfering solvent bands. Solvents such as cyclohexane and CCl_4 were tried, but in order to dissolve sufficient TCNE in one of them to produce a reliable Raman spectrum, an excess of the electron donor had to be added. In that case, however, the resulting solution is not suitable for equilibrium constant determination by the Raman intensity ratio method, since it has much more than 1/10 of the dissolved TCNE complexed (see above). Because of this, the Raman method was not applied to TCNE complexes in such solvents, despite the desirability of such data for comparison with results in solvents such as CH_2Cl_2.

5.3.3 Comparison with Other Methods

In Table XVIII the K_c^{AD} for CH_2Cl_2 solutions as determined from the Raman intensity ratios are compared with published K_c^{AD} obtained by absorption spectroscopy. The results of the Raman spectra agree very well with those of the absorption method, showing that the application of Raman spectroscopy to the determination of K_c^{AD} of EDA complexes is viable. For the other solvents, the HMB/TCNE K_c^{AD} determined from the Raman spectra (Table XVII) are equal, within experimental uncertainty, to the values obtained from absorption spectra[33,34]. The results of the Raman and the absorption methods for obtaining K_c^{AD} are greatly at

Table XVIII. Comparison of equilibrium constants for TCNE EDA complexes in CH_2Cl_2 solutions obtained by various methods

Donor	Raman	This work[a] Absorption[b]	Literature Absorption
o-xylene	.42 ± .15	.41	.45[c]
m-xylene	.50 ± .18	---	.38[c]
p-xylene	.52 ± .19	.47	.49[c]
mesitylene	1.6 ± .6	1.2	1.1[c]; 1.5[d]
durene	3.3 ± .4	---	3.4[c]
isodurene	4.7 ± .7	4.7	---
pentamethylbenzene	7.4 ± .6	---	7.9[c]
hexamethylbenzene	17 ± 2	---	16.8[c]; 21.6[d]
anisole	.52 ± .14	---	.28[e]

[a] Room temperature (about 21°).

[b] Obtained under the concentration condition [D] = [A] according to the method of ref. 34.

[c] Ref. 8; obtained for relative concentrations [D] >> [A] at 22°.

[d] Ref. 31; obtained for relative concentrations [D] > [A] at 25°.

[e] Calculated from the K_x^{AD} value in ref. 32, measured at 22°.

variance with those derived from a calorimetric method[35].

The equilibrium constants calculated from the Raman spectra, for solutions with [D] ~ [A] (column 2, Table XVIII), agree well with those obtained from absorption spectra for solutions having [D] = [A] (column 3) or [D] >> [A] (column 4). Since only 1:1 complexes are likely to occur when the donor concentration is comparable to that of the acceptor, and when the overall concentration is low, the consistency of these results supports the assumption that only 1:1 complexes occur under the condition

[D] >> [A] for the complexes studied.

Further comment on the accuracy of the K_c^{AD} determined from Raman spectra is possible in view of the results of the NMR measurements of K_c^{AD} for $\pi-\pi$ EDA complexes using, however, acceptors other than TCNE. The K_c^{AD} calculated from absorption spectra for solutions with [D] = [A] agree well with the NMR results, which are independent of the relative concentration [D]/[A][8]. The lack of relative concentration dependence in the NMR data implies that the same kind of complex is detected in each solution; by inference, this is the 1:1 complex. This supports the assumption that the K_c^{AD} determined by absorption spectroscopy for solutions with [D] = [A] are the true equilibrium constants for the formation of the 1:1 complexes. Since the absorption and Raman results tend to agree, the Raman results are thus supported by the NMR data. The goal of this investigation has been to show that the application of Raman spectroscopy to the study of EDA complex equilibria is feasible, and the agreement of the Raman K_c^{AD} and the absorption K_c^{AD} (as well as those from NMR) indicates that this is so.

5.4 Low Energy Spectra[36]

As mentioned in Chapter 1, an important aspect of the Raman spectra of EDA complexes is the low energy region of their spectra, because it is in this region that one expects a new band or bands to appear, characteristic of the complex but not of either of its components. Intermolecular stretching and bending vibrations are expected to occur below about 150 cm^{-1} for $\pi-\pi$ complexes, because of the weak intermolecular interaction in the ground state.

The EDA complexes investigated here also deserve special attention in the low energy region because of the existence of several low energy Raman bands in the spectrum of uncomplexed TCNE whose assignments are not very well established (Chapter 6). The activity of these TCNE vibrations in the preresonance or resonance Raman spectra of the complexes can help identify totally symmetric vibrations and therefore simplify the situation. Because of the lack of a satisfactory assignment for TCNE in this region, the low energy Raman spectrum of uncomplexed TCNE as well as of complexed TCNE is discussed in this section.

5.4.1 Low Energy Raman Bands of TCNE

Since a thorough investigation of the low frequency Raman spectrum of TCNE has not been published prior to this work, it is necessary to examine this spectrum before interpreting the low energy spectra of the complexes. In Fig. 24a the low energy spectrum of polycrystalline TCNE is shown. The spectrum has two bands in the region of immediate interest, at 134 cm^{-1} and 150 cm^{-1}. When TCNE is dissolved in noncomplexing solvents, the 134 cm^{-1} band is not of sufficient intensity to be observed in the solution spectra (Chapter 6). Since the totally symmetric vibration ν_5 (Fig. 25a) is expected in this region, the 150 cm^{-1} band is assigned to ν_5 and the 134 cm^{-1} band is attributed to a nontotally symmetric vibration, consistent with its depolarised character.

The fact that the 150 cm^{-1} band is observed only in the spectrum of solid TCNE might be considered as evidence that it arises from a lattice vibration; since no assignment of the
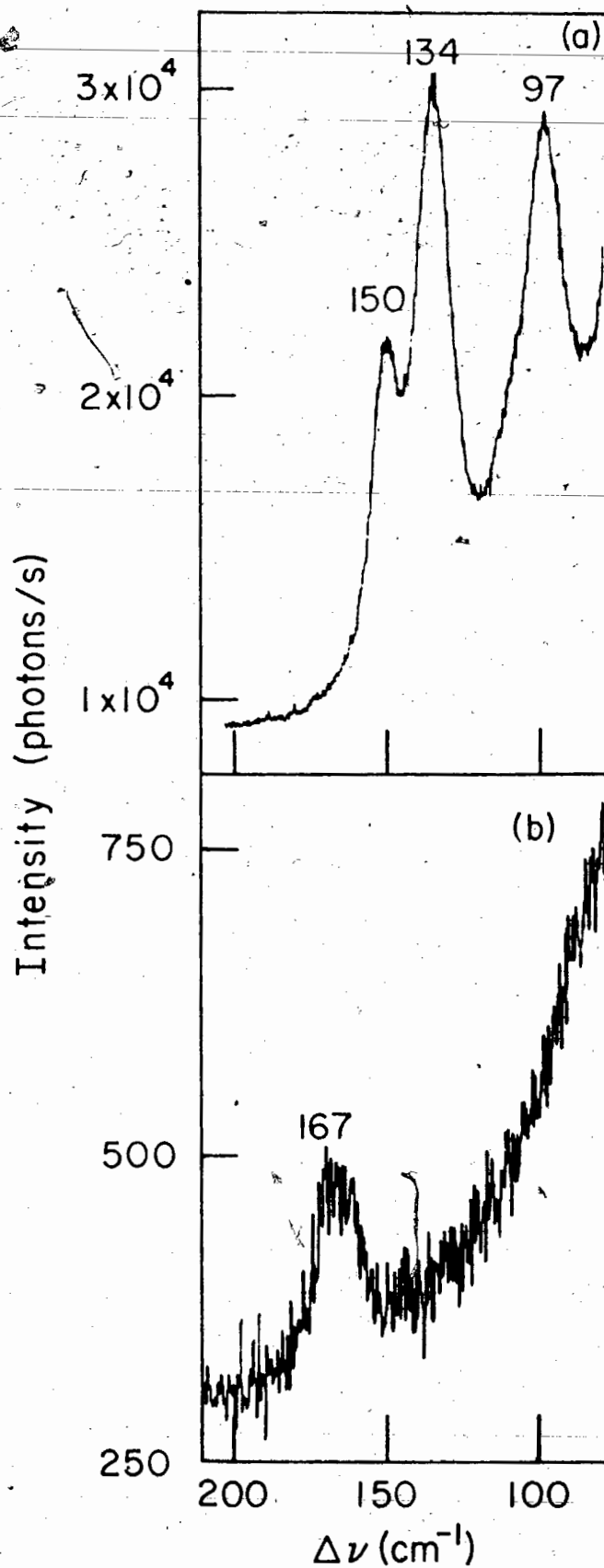
Fig. 24 Low energy Raman spectra of uncomplexed TCNE and of complexed TCNE. (a) solid TCNE; (b) hexamethylbenzene/TCNE in CH_2Cl_2.
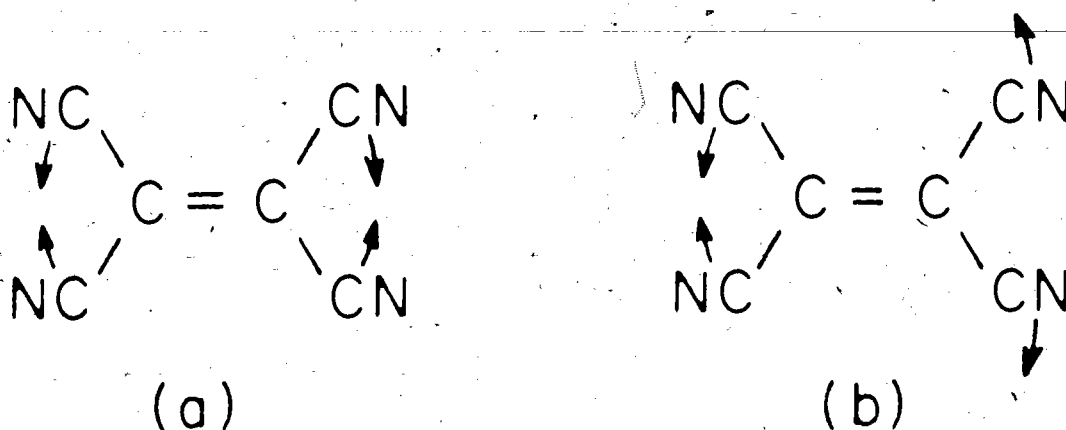
Fig. 25   Planar scissoring vibrations of TCNE.
(a) ν_5;   (b) ν_{12}.

lattice modes of TCNE has been published, this possibility cannot
be ruled out with certainty.   However, the presence of this band
in the solution spectra of the complexes (Sec. 5.4.2) strongly
suggests the existence of a TCNE fundamental near 150 cm^{-1}.   Thus
the data are consistent with the assignment of the 150 cm^{-1} band
to ν_5.

5.4.2   Low Energy Raman Bands of EDA Complexes of TCNE

As shown in Table XIX, a Raman band is found between 155 cm^{-1}
and 167 cm^{-1} in the spectrum of each TCNE complex having a methyl-
benzene or a methoxybenzene electron donor.   These are the only
bands in the spectra of the complexes in the accessible low energy
region (about 90 cm^{-1} to 200 cm^{-1}), except for a few unshifted
donor bands near 200 cm^{-1}.   For most of the complexes, these low
energy bands are very weak (signals as small as 10 photons/s); an
exception to this is the 167 cm^{-1} band of HMB/TCNE, whose intensity
is of the order of 100 photons/s (Fig. 24b), or about 2/3 that of
the TCNE $\nu_{C=C}$ band at 1547 cm^{-1}.   Since the 167 cm^{-1} band is the

Table XIX. Low energy Raman bands of TCNE EDA complexes and of uncomplexed donors between 100 cm^{-1} and 200 cm^{-1}

Donor	Neat Donor		TCNE complex[a,c]
	This work[a]	Low temp.[b]	
benzene	none		none
toluene	none		155
o-xylene	179		158
m-xylene	none		160
p-xylene	none		157
mesitylene	none		159
durene	101	161	160
isodurene	none		157
pentamethylbenzene	104		163
hexamethylbenzene	114	165	167
anisole	none		157
o-dimethoxybenzene	171		158
m-dimethoxybenzene	none		159
p-dimethoxybenzene	114		156
1,2,3-trimethoxybenzene	106, 149		162
1,2,4-trimethoxybenzene	197		161
1,3,5-trimethoxybenzene	128, 192		161

[a] Uncertainties in band positions are ± 2 cm^{-1} or less.

[b] Literature values; refs. 39 and 40.

[c] Solvent used was CH_2Cl_2. Donor and acceptor concentrations were adjusted so that the complex concentration in each solution was between 10^{-3} and 10^{-2} M.

strongest low energy band observed, it was selected for the more detailed investigations described below which attempt to ascertain the origin of these low energy bands.

The 155 - 167 cm^{-1} bands in the spectra of the TCNE EDA complexes may have one or more of the following origins: (a) the bands arise from the totally symmetric TCNE vibration ν_5, and appear because of resonance enhancement; (b) the (infrared active) TCNE vibration ν_{12} is activated in the Raman spectra of the

complexes; (c) torsional vibrations of the methyl or methoxy donor substituent groups are the source of the bands; (d) the bands are due to the stretching vibrations of the complexes. These possibilities are discussed below, and the first one is shown to be the most likely source of the bands in the spectra of the complexes.

(a) Resonance Raman effect in the TCNE vibration ν_5.

Accepting the proposition that the 150 cm^{-1} TCNE band is due to ν_5, the activity in the spectra of the complexes of the other totally symmetric vibrations of TCNE suggests that the 150 cm^{-1} band might also be resonance enhanced in the spectra. Indeed, the 155 – 167 cm^{-1} bands display several characteristics of RR scattering, including the following:

·(1) Using the CH_2Cl_2 band at 283 cm^{-1} as an internal standard, the intensities of the bands are weaker for complexes in which the resonance effect is weaker (e.g. p-xylene/TCNE) than for complexes in which the resonance effect is stronger (e.g. HMB/TCNE). (The strength of the resonance is indicated by the intensity increases of the $\nu_{C=C}$ and $\nu_{C\equiv N}$ bands on complexation; Table XVI).

(2) As shown in Figure 26, the excitation profile of the HMB/TCNE 167 cm^{-1} band is very similar to that of the $\nu_{C=C}$ and the $\nu_{C\equiv N}$ bands in this complex, which are also shown in this figure.

(3) The depolarisation ratio of the 167 cm^{-1} band is $\rho_\ell = .33 \pm .03$, the same as those of the $\nu_{C=C}$ and $\nu_{C\equiv N}$ bands, and indicative of the RR effect where the resonating state is not degenerate (Sec. 2.2.2).
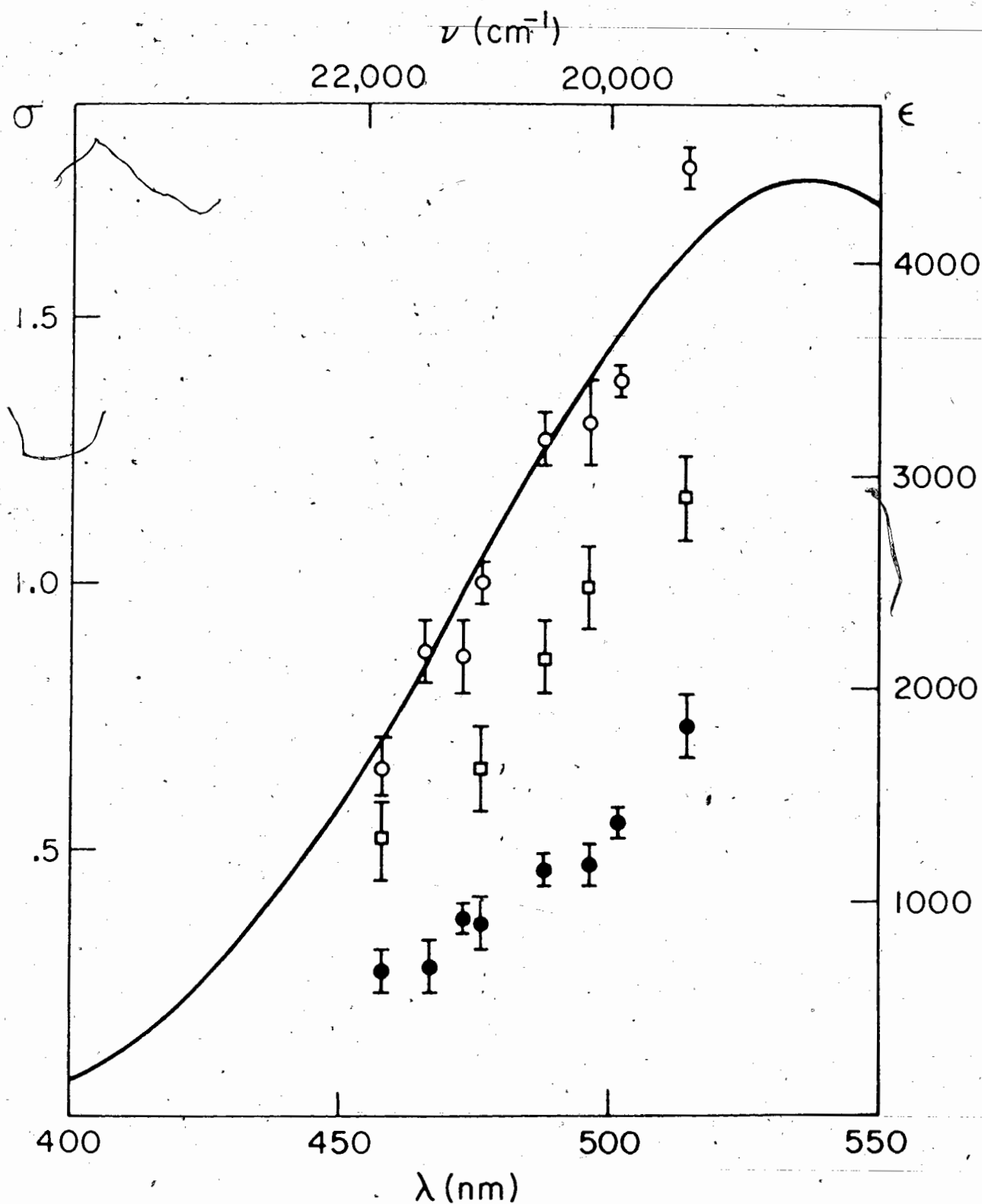
Fig. 26 Excitation profiles of the 167 cm^{-1} band and the $\nu_{C=C}$ and $\nu_{C\equiv N}$ TCNE vibrations for hexamethylbenzene/TCNE in CH_2Cl_2. Squares: 167 cm^{-1} band; open circles: $\nu_{C=C}$; filled circles: $\nu_{C\equiv N}$.

(4) Partial excitation profiles for the m-xylene/TCNE and durene/TCNE low frequency bands are consistent with the $\nu_{C=C}$ and $\nu_{C \equiv N}$ profiles for these complexes.

(5) Again using the 283 cm^{-1} solvent band as internal standard, the 157 cm^{-1} p-xylene/TCNE band is found to be more than five times weaker when excited at 632.8 nm than when excited at 488.0 nm. Since the first CT absorption band of this complex is at 470 nm, this result implies an increased resonance enhancement of the 157 cm^{-1} band as the Raman excitation wavelength approaches the CT absorption maximum.

Low energy RR bands have also been observed in the spectra of TCNE anion salts[37]. It is not certain that these bands have an analogous origin to those observed in the spectra of the TCNE EDA complexes, but the similarity of the results in the two studies is consistent with a TCNE origin in both cases. The 150 - 180 cm^{-1} TCNE anion salt bands were attributed to lattice modes[37,38], but such an assignment is ruled out for spectra of EDA complexes in solution.

(b) Raman activation of the TCNE vibration ν_{12}.

The small donor dependence of the positions of the 155 - 167 cm^{-1} bands implies that they have a TCNE origin and as an alternative to ν_5, the TCNE vibration ν_{12} (Fig. 25b) can be considered a possible source of the bands. Vibration ν_{12} is active only in the infrared spectrum of uncomplexed TCNE[37], and must be somehow activated in order to appear in the Raman spectra of the complexes. The data do not contain any evidence of such an activation; furthermore, extensive investigation of the Raman

spectra of these complexes has not revealed any other examples of Raman activated ungerade TCNE vibrations. Therefore it is unlikely that the 155 - 167 cm^{-1} bands are due to the TCNE vibration ν_{12}.

(c) Torsional vibrations of donor methyl or methoxy groups.

Both durene and HMB have low temperature Raman bands which are of essentially the same frequency as those observed at ordinary temperatures in the spectra of their respective TCNE complexes (Table XIX). These low temperature bands have been assigned to torsional vibrations of the methyl groups on the basis of their ν_H/ν_D isotopic ratios[39,40].

The UV absorption spectra of HMB[41] and of the dimethoxy-benzenes[42,43] have vibrational intervals of about 150 - 165 cm^{-1}, which in the case of the dimethoxybenzenes have been assigned to torsional vibrations[43]. Of these compounds, only o-dimethoxy-benzene has a Raman band below 200 cm^{-1} at room temperature (Table XIX).

The fact that the Raman spectrum of benzene/TCNE does not have a measurable band near 160 cm^{-1} is not inconsistent with the assignment to substituent torsional vibrations of the 155 - 167 cm^{-1} bands in the spectra of complexes having substituted benzenes as donors. However, the preresonance Raman intensity increases in the benzene/TCNE $\nu_{C=C}$ and $\nu_{C\equiv N}$ bands (Figs. 8 and 9) are weaker than those in the toluene/TCNE bands (Figs. 10 and 11), and much weaker than the RR intensity increases observed for the other complexes in Table XIX. If the 155 - 167 cm^{-1} bands appear by virtue of resonance enhancement associated with (a) or (b) above,

the weaker resonance effect in benzene/TCNE would probably produce a band below the limits of detection. Therefore, the absence of a low energy band for this complex cannot really be considered as evidence in favour of the assignment of the 155 - 167 cm^{-1} bands to substituent torsional vibrations.

(d). Intermolecular vibrations of the complexes.

The least likely of the origins considered here for the low energy bands in the spectra of the complexes is that they arise from the intermolecular stretching vibrations of the complexes. Although the trend in the frequencies of these bands as the donor is changed is consistent with that expected for such vibrations, this assignment is very improbable, since the intermolecular vibrations of these weak complexes are expected to occur at much lower energies, and to vary more in energy depending on the strength of the complex than the 12 cm^{-1} observed.

In view of the evidence presented under (a) to (d), the most likely origin of the 155 - 167 cm^{-1} bands in the Raman spectra of the EDA complexes of TCNE having substituted benzenes as donors is the TCNE vibration ν_5. The observed RR characteristics of the bands, similar to those of the $\nu_{C=C}$ and $\nu_{C\equiv N}$ bands, imply that they arise from such a totally symmetric vibration. The decrease in the frequencies of the bands with the strength of the complexes can be explained in terms of the charge redistribution on the CN groups in the complexes, and the effect of these charges on the vibration which brings the groups closer together.

5.5 Frequency Shifts on Complexation[1]

In this section, the positions of the Raman bands of the donor

and acceptor molecules in the spectra of the complexes are compared to the positions in the spectra of the uncomplexed compounds. This comparison shows the effects of complexation on the bond strengths of the component molecules. The frequencies observed arise from transitions between the vibrational levels of the ground electronic states, and no specific consideration of the participation of the excited states in the scattering is necessary. Donor vibrations and acceptor vibrations are discussed separately; particular attention is paid to the TCNE frequency shifts with complexation, since they allow an estimation of the dative character of the ground electronic states of the complexes.

5.5.1 Frequency Shifts in Donor Bands

In Tables XX and XXI all of the Raman bands in the spectra of the TCNE complexes with benzene or substituted benzenes which are attributable to donor vibrations are listed. Since the vibrational spectra of some of these donors have not been completely assigned, and because no systematic shift of donor bands is observed on complexation, no attempt is made here to identify all of the donor vibrations which are active in the spectra of the complexes. The vibrational assignments of many of the compounds used as electron donors have been summarised by Varsanyi[44].

Comparison of Tables XX and XXI shows that the preresonance Raman spectra of TCNE EDA complexes are somewhat richer in donor bands than are the resonance Raman spectra. This mainly results from the fact that the absorption and reabsorption effects are less troublesome in the preresonance Raman spectra.. The complexes which strongly absorb the laser beam yield very weak Raman spectra, and

Table XX.   Donor bands in the preresonance Raman spectra of
TCNE EDA complexes (donor as solvent)

Donor	Band positions $(cm^{-1})^{a,b}$
fluorobenzene	241(249); 519(517); 613(611); 804(803); 1010(1010); 1157(1158); 1219(1220); 3076(3075)
benzene	408(405); 607(608); 671(680); 802(802); 845(845); 992(992); 1176(1177); 1588(1585); 1604(1604); 2948(2948); 3057(3057)
toluene	526(526); 624(626); 790(790); 1009(1010); 1036(1035); 1211(1214); 1378(1380); 1598(1602); 2925(2922); 3052(3055)

[a] The first of each pair of numbers is the band position observed
in the spectrum of the complex; the second (in parentheses) is
the band position in the spectrum of the neat donor.

[b] Uncertainty in band positions is ± 3 cm^{-1} or less.

therefore only the strongest donor bands (usually those assigned

to totally symmetric vibrations) can be identified. The donors

which produce strong RR effects in the TCNE bands, e.g.

pentamethylbenzene (PMB), give complexes with strong CT absorption

bands; only a few donor bands can be identified in their spectra

(Table XXI).

. Jensen[12] recently reported a resonance effect for some of the

totally symmetric donor bands in the spectrum of anisole/TCNE. If

such an effect occurs in the spectra of other TCNE complexes, it

might account for the predominance of totally symmetric bands in

Table XXI. A thorough investigation of the donor bands which are

active in the RR spectra of the TCNE EDA complexes would elucidate

Table XXI. Donor bands in the resonance Raman spectra of
TCNE EDA complexes[a]

Donor[b]	Band positions (cm^{-1})[c,d]
o-xylene (ℓ)	738(734); 1053(1053); 1221(1223); 3050(3048)
m-xylene (ℓ)	532(536); 724(723); 998(999); 1249(1248); 1378(1377)
p-xylene (ℓ)	825(826); 1199(1204); 1606(1615); 2926(2924)
mesitylene (ℓ)	233(228); 272(273); 520(514); 578(576); 997(996); 1296(1299); 1368(1378) 1604(1605); 2873(2868); 2916(2919); 2999(3008)
durene (s)	734(735); 1266(1266); 1614(1617)
isodurene (ℓ)	1205(1208); 1293(1284); 1607(1608); 2912(2910)
pentamethylbenzene (s)	894(897); 1288(1290); 1599(1603)
hexamethylbenzene (s)	1290(1297); 1388(1393)
anisole (ℓ)	996(996); 1168(1176); 1244(1247); 1298(1304); 1439(1455); 1595(1594) 3058(3060)
o-dimethoxybenzene (ℓ)	745(748); 1055(1052); 1165(1164); 1252(1256); 1329(1330); 1450(1456); 1505(1504); 1586(1591); 3006(3005); 3074(3074).
m-dimethoxybenzene (ℓ)	728(719); 990(992); 1288(1287); 1340(1334); 1457(1455); 1588(1596)
p-dimethoxybenzene (s)	1177(1174); 1260(1267)
1,2,3-trimethoxybenzene (s)	1296(1297)
1,2,4-trimethoxybenzene (ℓ)	613(618); 1204(1185); 1333(1340); 1451(1454); 1597(1607); 2839(2837); 2946(2943); 3003(3004); 3078(3080)

Table XXI. (cont.) Donor bands in the resonance Raman spectra of TCNE EDA complexes[a]

Donor	Band positions (cm^{-1})[c,d]
1,3,5-trimethoxybenzene (s)	986(990); 1212(1209); 1349(1337) 2990(3004)

[a]Band positions for complexes having solid donors are for CH_2Cl_2 solutions; for complexes having liquid donors, the donor serves as the solvent.

[b](ℓ) = liquid; (s) = solid

[c]The first of each pair of numbers is the band position observed in the spectrum of the complex; the second (in parentheses) is the band position in the spectrum of the neat donor.

[d]Uncertainty in band positions is ± 3 cm^{-1} or less.

this situation, but is beyond the scope of this work.

The data in Tables XX and XXI indicate that virtually all of the donor bands in the spectra of the TCNE complexes are shifted by less than 10 cm^{-1} with respect to the band positions in the spectra of the uncomplexed donors.[†] Many of the bands in these tables are (within experimental uncertainty) unshifted by complexation. These results are in accord with those reported for the infrared[45,46] and Raman[3,4,12] spectra of TCNE EDA complexes. As mentioned in Chapter 3, the effects of complexation of π electron donors are expected to be small consistent with the data in Tables XX and XXI. Since the spectra from which the data in these tables are taken are for solutions in which the donor is in excess, the donor bands mostly originate from the uncomplexed donors. The donor bands would have to be significantly affected by complexation to be identified as shifted bands, and this is not observed.

5.5.2 Frequency Shifts In Acceptor Bands[1]

Tables XXII and XXIII summarise the observed TCNE band positions in the spectra of its EDA complexes; the low energy bands (Sec. 5.4) are not included. For most of the complexes, only the totally symmetric $\nu_{C=C}$ and $\nu_{C\equiv N}$ bands (and in some cases the 1526 cm^{-1} band) of TCNE can be identified outside of the low energy region (Table XXIII). Because the data in these tables are for solutions having a large excess of the donor, they correspond to

[†]The Raman spectra of the electron donors studied are given in Appendix B.

Table XXII.   Band positions for complexed and for uncomplexed
              TCNE[a]

| benzene/TCNE | Band positions (cm^{-1})[b] | |
	TCNE (solid)	TCNE (solution)[c]
487	490	494
531	532	533
1524	1526	1522
1564	1567	1559
2228	2236	2224
2234	2247	2233

[a]Assignments are discussed in Chapter 6.
[b]Uncertainties in band positions are ±3 cm^{-1} or less.
[c]Noncomplexing solvents used were CH_2Cl_2 and CH_3CN.

the band positions of complexed TCNE.

Table XXII shows that the TCNE bands in the spectrum of benzene/TCNE tend to occur at lower energies than they do in the spectrum of solid TCNE, but only in the case of the two C≡N stretching vibrations are these shifts definitely greater than the experimental uncertainty in the band positions. Thus, the TCNE frequency shifts for benzene/TCNE relative to solid TCNE are comparable to those observed for the spectra of TCNE in non-complexing solvents. Together with the results described in Sec. 5.5.1, this implies that the Raman spectrum of an EDA complex such as benzene/TCNE - if only band positions are considered - consists of a superposition of the spectra of the components, with only minor changes in the vibrational frequencies as a consequence of complexation.

The $\nu_{C=C}$ and $\nu_{C\equiv N}$ band positions in the spectra of the TCNE EDA

complexes (Table XXIII) are red shifted by up to 20 cm^{-1} with respect to the band positions for solid TCNE (Table XXII) or for solutions of TCNE in noninteracting solvents[1]. Because the a_g and the b_{3g} $\nu_{C\equiv N}$ bands are of comparable intensity in the spectrum of uncomplexed TCNE, the interpretation of the shifts of the $\nu_{C\equiv N}$ bands must consider the fact that (with four exceptions) only the a_g band is observed in the spectra of the complexes (Table XXIII). The $\nu_{C\equiv N}$ band position in the low resolution spectrum of uncomplexed TCNE cannot be compared with the low resolution spectra of most of the complexes, since this would suggest an exaggerated red shift. Thus, the $\nu_{C\equiv N}$ band positions in the spectra of the complexes as summarised in Table XXIII are arranged according to their symmetry species (determined by depolarisation ratios), to facilitate the comparison with the band positions for uncomplexed TCNE.

The increases in the magnitudes of the $\nu_{C=C}$ and a_g $\nu_{C\equiv N}$ frequency shifts with change of donor parallel each other and in the case of the methylbenzene donors, tend to increase with increasing free energy of formation of the complexes in CH_2Cl_2 solutions[32]; this is also the case for the methoxybenzene donors[47]. The greatest shifts are observed in the spectra of HMB/TCNE, which on the basis of its free energy of formation as reflected in the equilibrium constant for complex formation (Table XVI) is the strongest complex investigated. The smallest shifts in the band positions occur for 1,2,3-trimethoxybenzene/TCNE, and are attributed to steric hindrance associated with the three adjacent methoxy groups which prevents full conjugation of these groups with

Table XXIII. Band positions for complexed TCNE[a,b] (cm^{-1})

Donor[c]	$\nu_{C=C}$	$\nu_{C\equiv N}(a_g)$[d]	$\nu_{C\equiv N}(b_{3g})$[d]
benzene (ℓ)	1564	2228	2234
toluene (ℓ)	1564	2230	---
o-xylene (ℓ)	1562	2226	---
m-xylene (ℓ)	1557	2222	---
p-xylene (ℓ)	1559	2223	---
mesitylene (ℓ)	1560	2227	---
durene (s)	1552	2222	---
isodurene (ℓ)	1556	2220	---
pentamethylbenzene (s)	1552	2223	---
hexamethylbenzene (s)	1547	2223	---
anisole (ℓ)	1558	2227	---
o-dimethoxybenzene (ℓ)	1557	2228	---
m-dimethoxybenzene (ℓ)	1554	2226	---
p-dimethoxybenzene (s)	1553	2226	---
1,2,3-trimethoxybenzene (s)	1564	2233	---
1,2,4-trimethoxybenzene (ℓ)	1550	2227	---
1,3,5-trimethoxybenzene (s)	1553	2226	---
fluorobenzene (ℓ)	1559	2230	2238
hexafluorobenzene (ℓ)	1560	2226	2235
acenaphthene (s)	1556	2232	---
chrysene (s)	1556	2227	2234
fluorene (s)	1557	2226	---
naphthalene (s)	1558	2231	---
pyrene (s)	1556	2229	---

[a]Band positions for complexes having solid donors are for CH_2Cl_2 solutions; for complexes having liquid donors, the donor serves as the solvent.

[b]Excess donor was present in each solution.

[c](ℓ) = liquid; (s) = solid.

[d]Symmetry species refer to uncomplexed TCNE.

the benzene π electron system, and also interferes with the close approach of TCNE to the donor required for strong interaction[13].

The observed red shifts of the $\nu_{C=C}$ and $\nu_{C\equiv N}$ Raman bands on complexation are in the same direction as the shifts of the infrared activated $\nu_{C=C}$ and $\nu_{C\equiv N}$ bands in the spectrum of the TCNE anion[46,48]: in the anion spectra these bands occur at about 1380 cm^{-1} and 2190 cm^{-1}, respectively. Comparing the band shifts for $\nu_{C=C}$ in Table XXIII with the 180 cm^{-1} shift observed in the transition from TCNE to the TCNE anion, and assuming that the magnitude of the shift is proportional to the degree of electron transfer to TCNE, one calculates the ground states of the stronger complexes to have up to 10% dative character, while for the weaker complexes the ground state is less than 5% ionic. These estimates of the ionic character are about the same as those based on dipole moments of the methylbenzene/TCNE complexes[49] or on infrared spectra of glassy HMB/TCNE samples[48]. The red shifts in the $\nu_{C=C}$ and $\nu_{C\equiv N}$ bands for the complexes in solution can be attributed to the fact that the electron accepted by the TCNE molecule goes into an antibonding π orbital; since this orbital is localised on the C=C bond, the bond is weakened and its stretching frequency is lowered. This effect is also manifested in the C$\equiv$N bonds, probably because of conjugation in the TCNE molecule.

REFERENCES

1. K.H. Michaelian, K.E. Rieckhoff and E.M. Voigt, Chem. Phys. Lett. 23, 5 (1973).

2. K.H. Michaelian, K.E. Rieckhoff and E.M. Voigt, Chem. Phys. Lett. 30, 480 (1975).

3. L. M. Fraas, J.E. Moore and R.E. Bruns, Chem. Phys. Lett. 21, 357 (1973).

4. K. Kaya, A. Nakatsuka, N. Kubota and M. Ito, J. Raman Spectrosc. 1, 595 (1973).

5. A.C. Albrecht and M.C. Hutley, J. Chem. Phys. 55, 4438 (1971).

6. J. Halper, W.D. Closson and H.B. Gray, Theoret. Chim. Acta 4, 174 (1966).

7. J. Prochorow and A. Tramer, Bull. Acad. Polon. Sci., Ser. Sci. Math. Astr. Phys. 12, 429 (1964).

8. R. Foster, Organic Charge Transfer Complexes, (Academic Press, London, 1969).

9. H. Kuroda, I. Ikemoto and H. Akamatu, Bull. Chem. Soc. Japan 39, 1842 (1966).

10. J. Prochorow and A. Tramer, J. Chem. Phys. 47, 775 (1967).

11. K.H. Michaelian, K.E. Rieckhoff and E.M. Voigt, Proc. Natl. Acad. Sci. USA 72, 4196 (1975).

12. P.W. Jensen, Chem. Phys. Lett. 39 138 (1976).

13. E.M. Voigt, J. Am. Chem. Soc. 86, 3611 (1964).

14. J. Yarwood, in Spectroscopy and Structure of Molecular Complexes, J. Yarwood, ed. (Plenum Press, London, 1973).

15. S. Bratoz and E. Marechal, Phys. Rev. 4A, 1078 (1971).

16. M.C. Hutley and D.J. Jacobs, Chem. Phys. Lett. 6, 269 (1970).

17. A. Ranade and M. Stockburger, Chem. Phys. Lett. 22, 257 (1973).

18. R.S. Chao, R.K. Khanna and E.R. Lippincott, J. Raman Spectrosc. 3, 121 (1975).

19. T.G. Spiro and T.C. Strekas, Proc. Natl. Acad. Sci. USA 69, 2622 (1972).

20. J.A. Koningstein, *Opt. Spektrosk.* 35, 260 (1973).

21. J. Prochorow, *Bull. Acad. Polon. Sci., Math. Astr. Phys.* 15, 37 (1967).

22. A.C. Albrecht, *J. Chem. Phys.* 34, 1476 (1961).

23. J.A. Koningstein, *Introduction to the Theory of the Raman Effect*, (D. Reidel, Dordrecht, Holland, 1972).

24. J. Prochorow, *Bull. Acad. Polon. Sci., Ser. Sci. Math. Astr. Phys.* 22, 1283 (1974).

25. J.A. Koningstein and B.G. Jakubinek, *J. Raman Spectrosc.* 2, 317 (1974).

26. M. Shimada, H. Masuhara and N. Mataga, *Chem. Phys. Lett.* 15, 364 (1972).

27. H. Masuhara, M. Shimada and N. Mataga, *Bull. Chem. Soc. Japan* 43, 3316 (1970).

28. S. Matsuzaki and S. Maeda, *Chem. Phys. Lett.* 28, 27 (1974).

29. J. Friedman and R.M. Hochstrasser, *Chem. Phys. Lett.* 32, 414 (1975).

30. T.C. Strekas, D.H. Adams, A. Packer and T.G. Spiro, *Appl. Spectrosc.* 28, 324 (1974).

31. R.X. Ewall and A.J. Sonnessa, *J. Am. Chem. Soc.* 92, 2845 (1970).

32. R.W. Merrifield and W.D. Phillips, *J. Am. Chem. Soc.* 80, 2778 (1958).

33. P.J. Trotter and D.A. Yphantis, *J. Phys. Chem.* 74, 1399 (1970).

34. R. Foster and I.B. Matheson, *Spectrochim. Acta* 23A, 2037 (1967).

35. W.C. Herndon, J. Feuer and R.E. Mitchell, *Chem. Comm.*, 435 (1971).

36. K.H. Michaelian, K.E. Rieckhoff and E.M. Voigt, *Chem. Phys. Lett.* 39, 521 (1976).

37. J.J. Hinkel and J.P. Devlin, *J. Chem. Phys.* 58, 4750 (1973).

38. D.L. Jeanmaire, M.R. Suchanski and R. P. Van Duyne, *J. Am. Chem. Soc.* 97, 1699 (1975).

39. P.N. Prasad and R. Kopelman, J. Chem. Phys. 58, 5031 (1973).

40. M. Suzuki, J. Raman Spectrosc. 1, 371 (1973).

41. O. Schnepp, J. Chem. Phys. 29, 56 (1958).

42. D. Marjit, P.K. Bishui and S.B. Banerjee, Indian J. Phys. 46 49 (1972).

43. D. Marjit, P.K. Bishui and S.B. Banerjee, Indian J. Phys. 46 457 (1972).

44. G. Varsanyi, Assignments for Vibrational Spectra of Seven Hundred Benzene Derivatives, (John Wiley and Sons, New York, 1974).

45. B. Moszynska, Bull. Acad. Polon. Sci., Ser. Sci. Math. Astr. Phys. 17, 99 (1969).

46. J. Stanley, D. Smith, B. Latimer and J.P. Devlin, J. Phys. Chem. 70, 2011 (1966).

47. K.H. Michaelian, K.E. Rieckhoff and E.M. Voigt, unpublished work.

48. J.C. Moore, D. Smith, Y. Youhne and J.P. Devlin, J. Phys. Chem. 75, 325 (1971).

49. R.K. Chan and S.C. Liao, Can. J. Chem. 48, 299 (1970).

6. ASSIGNMENT OF THE RAMAN SPECTRUM OF TETRACYANOETHYLENE

The investigation of the Raman spectra of the EDA complexes
of TCNE has made apparent the need for an improved assignment of
the TCNE Raman spectrum. In particular, the published assignments
of three of the totally symmetric vibrations and several of the
low energy nontotally symmetric vibrations need to be reevaluated.
Thus, in this chapter, a new assignment of the Raman active
fundamental vibrations of TCNE is proposed. It contains changes
to some of the previous assignments, including those for the
out-of-plane vibrations, which are consistent with published and
new polarisation and intensity data. Moreover, it is based on
the resonance Raman and preresonance Raman intensity behaviour of
the totally symmetric TCNE bands in the spectra of TCNE complexes,
as described in Chapter 5. New Raman spectra of TCNE, which
augment the previously published data, are also reported. The
infrared absorption spectra of some TCNE EDA complexes as published
by several authors are also taken into consideration.

A number of authors have published vibrational assignments of
TCNE[1-8]. The early paper of Miller et al.[3], together with the
recent one on the Raman spectra of TCNE and TCNE anion by Hinkel
and Devlin[8], are the most representative works and therefore serve
as the starting point for the improved assignment given in this
chapter.

The TCNE molecule belongs to the D_{2h} point group. Taking the
x axis perpendicular to the molecular plane and the z axis
parallel to the C=C bond, the 24 molecular vibrations are
divided into the symmetry classes

$$5a_g + 2a_u + 1b_{1g} + 4b_{1u} + 2b_{2g} + 4b_{2u} + 4b_{3g} + 2b_{3u},$$

where the gerade vibrations are predicted by group theory to be Raman active, and the ungerade vibrations (except a_u) are allowed in the infrared spectrum. According to the X-ray analysis of Bekoe and Trueblood[9], a TCNE molecule in the crystal occupies a site of symmetry C_i; the mutual exclusion rule therefore should govern the activities of the bands in the vibrational spectra of solid TCNE. A comparison of the Raman bands observed for solid TCNE in the present work (Table XXIV) with the published infrared spectra[2-4,6] shows no bands common to both kinds of spectra, consistent with this statement.

In the following discussion, the band positions referred to are those observed in the Raman spectrum of solid TCNE. The numbering of the TCNE vibrations (Table XXV) is the same as that suggested by Miller et al.[3]

6.1 a_g Vibrations

The assignments of ν_1 and ν_2 in Table XXV are the same as the previously published ones[3,5,7,8]. Both of these vibrations give rise to Raman bands which are resonance-enhanced on complexation; similar intensity behaviour is used as evidence in the assignment of some of the other TCNE bands to totally symmetric vibrations.

In a change from the published assignments, the 592 cm^{-1} band is now attributed to ν_3. This new assignment is suggested by the appearance of bands near 580 cm^{-1} in the infrared spectra of crystalline TCNE complexes[10,11].

The IR spectra of TCNE EDA complexes are of special interest

Table XXIV.   Raman spectrum of tetracyanoethylene

Band positions (cm^{-1}) [a]		
Solid[b]	Solution[c,d]	Assignments[e]
27 s		Lattice mode
64 s		Lattice mode
74 sh		Lattice mode
97 s		Lattice mode
134 s	130 dp	ν_{14}
150 m		ν_5
251 m	247 dp	ν_{22}
360 m	360 dp	ν_{13}
490 w	494 p	$134 + 360 = 494$ (ν_4)
508 w		ν_{21} ($150 + 360 = 510$)
532 w	533 p	ν_4 (ν_3)
592 w	589 p?	ν_3
674 s	674 dp	ν_8
1262 w		
1278 s	1274 dp	ν_{20}
1507 w		
1526 m	1522 p	$251 + 1278 = 1529$
1537 w		
1567 s	1559 p	ν_2
1581 w		
2191 w		TCNE anion?
2236 s	2224 p	ν_1
2247 s	2233 p	ν_{19}
2309 w		

[a] Uncertainty in band positions is $\pm 3\ cm^{-1}$ or less.
[b] s = strong; m = medium; w = weak; sh = shoulder.
[c] Solvents used were CH_2Cl_2, CH_3CN and acetone.
[d] p = polarised; dp = depolarised.
[e] Alternate assignments are given in parentheses.

since they show the activation of the ν_1 and ν_2 vibrations of TCNE. This activation is generally thought to be due to the "electron vibration" mechanism first suggested by Ferguson[12], wherein the vibration is activated because of its influence on the ionisation energy of the donor or on the electron affinity of the acceptor. From the discussion in Chapter 3, it can be seen that such a vibration is necessarily related to the interaction of the components in the complex. The result is a charge oscillation between donor and acceptor, occurring with the frequency of the vibration. For a complex in which donor and acceptor planes are parallel (the approximate configuration of the TCNE EDA complexes), this oscillation is perpendicular to the molecular planes, and the associated infrared absorption band is therefore polarised in this direction[10]. Only totally symmetric vibrations of components can be enhanced as electron vibrations in the spectra of EDA complexes[13].

Returning to the assignment of ν_3, the results obtained for the polarised infrared spectra of solid HMB/TCNE[10,11,13] and PMB/TCNE[10] can now be considered. These complexes form needle-like crystals, with the donor and acceptor planes perpendicular to the needle axis[10,11]. Once the crystals are appropriately oriented, the dichroic behaviour of their IR absorption bands allows their correlation with in-plane or out-of-plane vibrations; the activated TCNE in-plane vibrations ν_1 and ν_2 also appear with out-of-plane polarisation, consistent with the electron vibration model described above. The infrared spectra of both complexes also have bands near 580 cm^{-1}, each of which are comprised of an

Table XXV. Assignments of Raman active fundamental vibrations of tetracyanoethylene[a,b]

Species (D_{2h})	Number	Description[c]	Miller et al.[3] calcd.	obsd.	Hinkel & Devlin[8] calcd.	obsd.	This work[d] obsd.
a_g	1	C≡N stretch	2236	2236 p	2235	2235	2236 p
	2	C=C stretch	1603	1569 p	1569	1569	1567 p
	3	C-C stretch	607	679 dp?	558	535 p	592 p? (532 p)
	4	C-C≡N bend	500	541 p	489	490 p	532 p (490 p)
	5	(CN)-C-(CN) scissoring	125	127 dp	133	130	150
b_{1g}	8	C-C≡N o.p. bend	---	416?	---	---	674 dp
b_{2g}	13	C-C≡N o.p. bend	---	596?	---	679 dp	360 dp
	14	(CN)-C-(CN) o.p. wag	---	360?	---	---	134 dp
b_{3g}	19	C≡N stretch	2236	2247 dp	2257	2247	2247 dp
	20	C-C stretch	1352	1280 p?	1287	1282	1278 dp
	21	C-C≡N bend	512	510	452	510e	508
	22	(CN)-C-(CN) rocking	278	253	245	254	251 dp

[a]Observed frequencies are for solid samples.

[b]p = polarised; dp = depolarised (refers to solution spectra).

[c]o.p. = out-of-plane.

[d]Alternate assignments are given in parentheses.

[e]The 510 cm^{-1} band was not observed by these authors, but was apparently taken from the literature.

out-of-plane polarised component and an in-plane component. The in-plane band is probably due to a planar TCNE vibration[10], and is of no special interest. On the other hand, Moszynska[11] attributed the out-of-plane component to an electron vibration, but did not assign this frequency to a particular totally symmetric mode.

These results suggest that there is a totally symmetric electron vibration near 580 cm^{-1} in these spectra. Both donors have totally symmetric vibrations nearby, as indicated by the polarised Raman bands at 550 cm^{-1} and 567 cm^{-1} for HMB and PMB respectively[14]; however, these donor band positions do not agree well with the observed 580 cm^{-1} frequency in the spectra of the complexes, and the existence of a TCNE a_g vibration near 580 cm^{-1} is intimated. The Raman band of TCNE at 592 cm^{-1} thus can be assigned to ν_3, consistent with the calculation[3] which places ν_3 at 607 cm^{-1}. The original assignment of the 674 cm^{-1} band to ν_3[3,5,7] is clearly unsatisfactory, since the solution spectra show that this band is depolarised[8] (see Table XXIV).

Because of the change in the assignment of ν_3, the 532 cm^{-1} TCNE band is now attributed to ν_4, consistent with early assignments[3,5,7]. There is no doubt that this band must be placed in the a_g class, since it is polarised and furthermore has considerable resonance Raman intensity in the spectra of KTCNE and NaTCNE[8]. In addition, preresonance Raman results for the benzene/TCNE complex (see Chapter 5) show that this band has an excitation frequency dependence similar to those of ν_1 and ν_2. Since the 532 cm^{-1} band cannot be explained as a combination or

overtone band, it must therefore be due to a totally symmetric TCNE fundamental.

As indicated by the data in Tables XXIV and XXV, the polarised character of the 490 cm^{-1} band is consistent with its assignment as a combination of the bands at 134 cm^{-1} and 360 cm^{-1}, provided that both of the latter two bands arise from b_{2g} vibrations. The preresonance Raman intensity study for benzene/TCNE shows that the intensity of this band is increased when the excitation frequency approaches the absorption maximum; this fact, however, does not require its assignment as a fundamental, since combination bands in the a_g class also can be resonance or preresonance enhanced (see Tables II and IX). Therefore, the 490 cm^{-1} band need not be assigned to an a_g fundamental vibration, as was suggested by Hinkel and Devlin[8].

As an alternative to the assignments of ν_3 and ν_4 given here, the 532 cm^{-1} and 490 cm^{-1} bands can be assigned to ν_3 and ν_4 respectively[8]. This is a plausible assignment; however, it does not explain the electron vibration infrared bands in the spectra of the complexes described above.

The final TCNE a_g vibration, ν_5, is assigned here to the band at 150 cm^{-1}. This is a change from the previous assignments of the 134 cm^{-1} band to ν_5[3,5,7]; Miller et al.[3] made the latter assignment in spite of the fact that their solution data showed that the band is depolarised. The 150 cm^{-1} band is the only other band in this region and therefore must be considered as a possibility for ν_5.

Experimental evidence supporting the assignment of the 150 cm^{-1}

band to ν_5 is found in the low energy Raman spectra of TCNE EDA complexes, which contain resonance-enhanced bands at 155 - 167 cm^{-1} (Sec. 5.4.2). As discussed in Sec. 5.2, the RR effect in the spectra of these complexes manifests itself in the totally symmetric vibrations of TCNE. Thus, as shown in Sec. 5.4, these bands are most likely to originate from the TCNE vibration ν_5.

6.2 b_{1g} Vibrations

The only TCNE vibration of b_{1g} symmetry, ν_8, is assigned to the depolarised 674 cm^{-1} band. Although the present work provides no positive verification of this assignment, the strength of this band indicates that it almost certainly arises from a fundamental vibration; the assignment of the 674 cm^{-1} band to ν_8, together with the other assignments in this chapter, ensures that no strong or medium intensity bands are ignored. At the present time, no calculated frequencies for the nonplanar TCNE vibrations have been published, so there is no other way to check on this assignment.

6.3 b_{2g} Vibrations

The bands at 360 and 134 cm^{-1} are assigned to the nonplanar vibrations ν_{13} and ν_{14} respectively, consistent with the fact that both bands are depolarised in the solution spectra. Furthermore, this assignment means that the combination $\nu_{13} + \nu_{14}$, which has a_g symmetry, can account for the polarised 490 cm^{-1} band. Since no normal coordinate calculations have been reported for the TCNE b_{2g} vibrations, the correlation of these bands to the particular b_{2g} vibrations in Table XXV is based on the assumption that the bending vibration occurs at higher frequency than does the wagging mode.

6.4 b_{3g} Vibrations

The assignments of the b_{3g} vibrations in Tables XXIV and XXV agree with several of the previously published ones[3,7,8]. The only new result in support of these assignments is the observation that the 251 cm^{-1} and 1278 cm^{-1} bands are depolarised, which is compatible with their assignment to nontotally symmetric vibrations.

REFERENCES

1. C.E. Looney and J.R. Downing, J. Am. Chem. Soc. 80, 2840 (1958).

2. D.A. Long and W.O. George, Spectrochim. Acta 19, 1717 (1963).

3. F.A. Miller, O. Sala, P. Devlin, J. Overend, E. Lippert, W. Luder, H. Moser and J. Varchmin, Spectrochim. Acta 20, 1233 (1964).

4. T. Takenaka and S. Hayashi, Bull. Chem. Soc. Japan 37, 1216 (1964).

5. A. Rosenberg and J.P. Devlin, Spectrochim. Acta 21, 1613 (1965).

6. P. Heim and F. Dörr, Ber. Bunsengesell. Phys. Chem. 69, 453 (1965).

7. E.M. Popov, I.P. Yakovlev, G.A. Kogan and V.V. Zhogina, Teor. Eksp. Khim. 2, 464 (1966).

8. J.J. Hinkel and J.P. Devlin, J. Chem. Phys. 58, 4750 (1973).

9. D.A. Bekoe and K.N. Trueblood, Z. Krist. 113, 1 (1960).

10. J. Stanley, D. Smith, B. Latimer and J.P. Devlin, J. Phys. Chem. 70, 2011 (1966).

11. B. Moszynska, Acta Phys. Polon. 33, 959 (1968).

12. E.E. Ferguson, J. Chim. Phys. 61, 257 (1964).

13. B. Moszynska and A. Tramer, J. Chem. Phys. 46, 820 (1967).

14. G. Durocher, J. Chim. Phys. 66, 988 (1969).

7. CONCLUSIONS

The first detailed investigation of the Raman spectra of a series of π-π EDA complexes has been described in the preceding chapters. Emphasis was placed on the effects of complexation on the vibrations of the acceptor (TCNE) molecule observed for room temperature solutions in either the (liquid) donor or an inert solvent.

Strong absorption of the Argon laser excitation light by the TCNE complexes was found to produce preresonance and resonance Raman intensity effects in the bands assigned to the totally symmetric vibrations of TCNE. These effects lead to intensity changes (both absolute and relative) and depolarisation ratio changes for the affected bands.

The excitation frequency dependence of the intensities of the above-mentioned TCNE bands was studied in both the preresonance and the resonance Raman regions. The frequency dependence observed for the preresonance Raman spectra establishes the role of the first excited states of the complexes as intermediate states and also shows that the higher excited states of the components or of the complex take part in the scattering, thereby establishing the role of vibronic coupling in the Raman scattering process in these molecules. The resonance Raman excitation profiles of the C=C and C≡N stretching bands were observed to be shifted by about $1000 - 2000 \text{ cm}^{-1}$ toward the low energy side of the absorption bands whether the excitation falls within the first or the second CT absorption band of the complex. This red shift was interpreted in terms of the vibronic theory of RR scattering, and shown to

occur as a result of resonance with the vibronic absorption bands involving the $\nu_{C=C}$ and $\nu_{C\equiv N}$ vibrations. A model of the RR scattering in the EDA complexes in which the higher vibronic levels of the ground and first excited CT states are nonradiatively damped was suggested as the explanation of the shifts of the profiles.

The intensity increases in the TCNE $\nu_{C=C}$ and $\nu_{C\equiv N}$ bands on complexation were used quantitatively to calculate the equilibrium constants for complex formation, thus establishing a new method for the determination of equilibrium constants of π-π complexes. The results obtained using Raman intensities were found to agree very well with the published results as obtained by absorption spectroscopy.

Low energy Raman spectra of the complexes were investigated above about 90 cm^{-1}. Bands at 155 - 167 cm^{-1} were observed and by virtue of their RR characteristics assigned to the lowest energy totally symmetric TCNE vibration, which necessitated a new assignment of the low energy Raman bands of uncomplexed TCNE. A Raman band which is definitely attributable to the intermolecular stretching vibration does not occur in the spectra of the complexes.

The band positions in the spectra of the complexes were found to be nearly the same as those in the spectra of the respective uncomplexed compounds. Systematic red shifts of up to 20 cm^{-1} for the TCNE $\nu_{C=C}$ and $\nu_{C\equiv N}$ bands were observed and related to a degree of electron transfer approaching 10% in the ground state of the complexes. No systematic shifts in the donor bands with complexation occur.

The Raman spectrum of uncomplexed TCNE was investigated partly to improve the assignments of the low energy vibrations, and later extended to include the entire spectrum. This lead to a new assignment of the TCNE Raman spectrum in which about half of the previously published assignments were changed.

7.1 Suggestions for Further Work

Because this research was the first extensive investigation of the Raman spectra of TCNE EDA complexes, it has perhaps posed as many questions as it has answered. The results described in Chapter 5 were obtained in the attempt to elucidate certain aspects of these spectra; however, other important points remain to be considered. In this section, the most important of these topics are briefly discussed, as are some other interesting subjects which have arisen out of this work.

The reader is aware of the emphasis which was placed on the acceptor bands in the spectra of the complexes studied here. Donor bands were also observed, but these were not studied to the same extent. Therefore, further investigation of the Raman spectra of TCNE EDA complexes might well begin with an analysis of the effects of complexation on the positions and intensities of the donor bands. Such data would provide valuable information on geometric and electronic structure changes in the donors with complexation. These spectra would be most informative if obtained for solutions in which a sizeable fraction of the donor is complexed, i.e. under different concentration conditions than those in the present investigation. The spectra already obtained

have shown that the effects of complexation on the donor bands
are not as great as those observed for the acceptor, emphasising
the importance of the relative donor and acceptor concentrations
in the solutions used for any study of donor bands.

Dichloromethane was used as the solvent for most of the
samples which were investigated here, especially where the effects
of reabsorption were found to be significant; resonance Raman
excitation profiles were obtained in most cases using CH_2Cl_2 bands
as internal intensity standards. Since the red shift of the
excitation profiles with respect to the CT absorption bands was
interpreted to be a consequence of interactions between the
electronically excited complex and the solvent, further investi-
gation of the excitation profiles ought to include a check for
any solvent dependence of the profiles. As suggested by the
results in Appendix D, a nonpolar solvent such as cyclohexane may
result in a much different solvent-complex interaction and there-
fore certainly should be included in such a study.

The good results obtained from the Raman intensity ratio
method for calculating equilibrium constants are very encouraging.
Further experiments in this area should involve temperature control
in order that equilibrium constants can be obtained for a series
of temperatures and the enthalpy of formation of the complexes
calculated. The latter quantity is an important measure of the
strength of a complex and as such has been obtained by absorption
spectroscopy, so that as in the case of the equilibrium constants
a comparison of the Raman results with published results is
possible.

The methyl and methoxy substituted benzenes employed here as electron donors comprise but one group of donors which interact with TCNE to form EDA complexes. Many other TCNE EDA complexes absorb in the visible region, and resonance Raman scattering is expected to occur for many of these. As shown by the results of the present work, a considerable amount of information on the excited electronic states of EDA complexes can be obtained from their RR spectra, and this conclusion should remain valid for a large number of TCNE EDA complexes.

The photoconductivity experiment described in Appendix D has established the existence of the ionic dissociation process in a number of electronically excited TCNE complexes. Further investigations of the photoconductivity behaviour of TCNE EDA complexes should attempt to quantify parameters such as rates of ion production, lifetimes of ions in solution, and recombination of ions. These data would provide valuable insight into energy transfer processes in these complexes.

The experiments proposed in this section should answer some of the more interesting questions which persist regarding the nature of EDA complexes. Although these complexes have been studied extensively by a variety of methods, they are not fully understood. The future application of Raman spectroscopy to this field will certainly improve this situation.

APPENDIX A

NOTATION

Table XXVI. Abbreviations used in the thesis

Abbreviation	Meaning
A	acceptor
CT	charge transfer
D	donor
EDA	electron donor/acceptor
HMB	hexamethylbenzene
K_c^{AD}	equilibrium constant for complex AD
M	molar
PMB	pentamethylbenzene
RR	resonance Raman
TCNB	tetracyanobenzene
TCNE	tetracyanoethylene

APPENDIX B

RAMAN SPECTRA OF ELECTRON DONORS

The Raman spectra of the compounds used as electron donors in
the EDA complexes of TCNE are summarised in tabular form in this
appendix. All of the methyl and methoxy substituted benzenes
investigated in this work are presented for completeness, although
some of these spectra have already been reported in the literature.
The band positions for the uncomplexed donors as given in
Sec. 5.5.1 are taken from this appendix.

The donor Raman spectra were measured in the frequency region
from about 100 cm^{-1} to 3100 cm^{-1} and are reported in Tables XXVII
to XXXII. The uncertainties in the band positions in these tables
are generally within $\pm 3 \text{ cm}^{-1}$. The relative intensities of the
bands observed are also included. It should be noted that no
special effort was made to observe all the weak donor bands; such
bands generally cannot be identified in the spectra of the TCNE
EDA complexes, because of the overall low intensity of such
spectra.

Table XXVII. Raman spectra of benzene and monosubstituted benzenes[a,b]

benzene	toluene	fluorobenzene	anisole
405 vw	526 m	249 m	266 w
608 m	626 m	517 w	443 m
680 vw	734 vw	611 w	511 vw
802 vw	790 s	803 s	554 vw
845 w	844 sh	1010 s	612 w
992 s	892 vw	1158 m	782 w
1177 m	1010 m	1220 m	996 s
1404 vw	1035 w	1602 m	1030 m
1585 m	1167 m	3075 s	1176 m
1604 m	1214 m		1247 w
2948 w	1331 w		1304 w
3057 s	1380 m		1455 m
	1441 w		1594 m
	1584 m		1606 s
	1602 m		2838 m
	2922 m		2916 sh
	2984 sh		2942 m
	3055 s		3003 m
			3060 s

[a] s = strong; m = medium; w = weak; vw = very weak; sh = shoulder
[b] Band positions in cm^{-1}.

Table XXVIII. Raman spectra of xylenes[a,b]

o-xylene	m-xylene	p-xylene
181 w	202 m	310 m
256 w	227 m	384 w
505 w	279 w	462 s
582 m	516 m	647 s
643 vw	536 s	703 w
734 s	723 s	826 m
987 w	767 vw	1042 vw
1053 m	999 s	1204 s
1158 w	1035 w	1312 w
1223 m	1095 w	1378 w
1291 vw	1167 w	1448 w
1385 m	1248 m	1576 vw
1451 w	1262 w	1615 w
1584 m	1377 m	2924 m
1608 m	1590 w	3025 m
2921 m	1610 w	3054 m
2942 sh	2726 w	
2977 sh	2860 m	
3048 m	2910 s	
	3041 m	

[a]Abbreviations are the same as in Table XXVII.
[b]Band positions in cm^{-1}.

Table XXIX. Raman spectra of higher methylbenzenes.[a,b]

mesitylene	durene	isodurene
228 m	101 s	230 m
273 w	271 m	276 w
514 m	352 m	326 m
576 s	433 vw	452 m
996 s	505 m	497 vw
1036 w	735 s	510 vw
1164 vw	1266 m	544 m
1299 s	1377 w	572 s
1378 s	1390 w	731 m
1440 w	1444 w	877 vw
1605 m	1617 m	892 vw
2729 w	2914 m	956 m
2868 m	2960 m	1140 m
2919 s	2981 w	1208 w
3008 m	3023 w	1284 m
		1376 m
		1440 w
		1480 vw
		1576 vw
		1608 m
		2722 vw
		2858 m
		2910 m
		2958 sh
		3005 m

[a]Abbreviations are the same as in Table XXVII.

[b]Band positions in cm^{-1}.

Table XXX. Raman spectra of pentamethylbenzene and hexamethylbenzene[a,b]

pentamethylbenzene	hexamethylbenzene
104 s	113 m
301 m	364 m
355 m	452 m
446 w	556 m
484 m	1297 s
554 sh	1366 m
570 s	1393 m
681 m	1572 m
897 vw	2910 s
1214 vw	2985 m
1290 m	
1364 m	
1388 m	
1440 vw	
1562 vw	
1574 vw	
1603 vw	
2856 sh	
2906 m	
2932 sh	
2956 sh	
2990 w	

[a]Abbreviations are the same as in Table XXVII.

[b]Band positions in cm^{-1}.

Table XXXI. Raman spectra of dimethoxybenzenes[a,b]

o-dimethoxybenzene	m-dimethoxybenzene	p-dimethoxybenzene
171 w	207 m	114 sh
208 w	254 m	278 w
381 m	292 sh	382 w
476 w	370 m	406 w
578 w	426 sh	552 w
748 m	462 m	634 w
1052 m	532 w	708 w
1164 m	580 vw	804 sh
1256 m	621 m	816 m
1330 s	719 s	846 w
1456 w	764 w	1026 w
1504 vw	992 m	1057 vw
1591 m	1038 w	1152 vw
2839 m	1085 w	1168 sh
2951 m	1157 sh	1174 sh
3005 s	1186 w	1267 m
3074 s	1208 sh	1306 vw
	1287 m	1448 sh
	1334 m	1466 sh
	1455 m	1585 w
	1596 m	1611 w
	1609 m	2842 w
	2837 m	2918 sh
	2943 s	2949 m
	3008 s	3016 s
	3076 s	3056 m
		3078 s

[a]Abbreviations are the same as in Table XXVII.
[b]Band positions in cm^{-1}.

Table XXXII. Raman spectra of trimethoxybenzenes[a,b]

1,2,3-trimethoxybenzene	1,2,4-trimethoxybenzene	1,3,5-trimethoxybenzene
106 w	197 m	128 m
149 w	361 m	192 m
206 m	389 sh	214 sh
224 m	496 w	246 m
274 w	555 w	318 w
367 m	618 m	368 m
406 w	710 m	443 m
490 vw	764 s	482 w
526 m	920 m	536 vw
608 w	1024 m	592 m
697 s	1152 vw	614 m
739 w	1185 w	912 vw
802 m	1260 vw	990 s
1002 m	1315 sh	1035 m
1034 w	1340 m	1065 w
1058 vw	1454 m	1192 w
1096 m	1511 vw	1209 w
1192 m	1607 m	1315 w
1232 w	2837 m	1337 m
1297 s	2943 m	1429 sh
1442 w	3004 m	1449 m
1459 m	3080 m	1465 sh
1499 vw		1587 m
1584 s		2845 m
2849 m		2942 s
2949 m		2960 sh
2999 s		3004 s
3084 s		

[a] Abbreviations are the same as in Table XXVII.
[b] Band positions in cm^{-1}.

APPENDIX C

CALCULATION OF ABSORPTION SPECTRA, FLUORESCENCE SPECTRA AND
RESONANCE RAMAN EXCITATION PROFILES

The observed red shifts of the RR excitation profiles of the CT transitions with respect to the absorption bands of the complexes, described for the TCNE $\nu_{C=C}$ and $\nu_{C\equiv N}$ Raman bands in Sec. 5.2.3, was interpreted in terms of a model of the EDA complexes wherein the CT absorption bands consist of a super-position of Lorentzian vibronic transitions with frequency dependent damping. In this appendix, absorption spectra, fluorescence spectra and RR excitation profiles are calculated by applying some of the features of this model to a hypothetical case. The results are compared to those of the existing RR theories, as summarised in Chapter 2.

The electronic spectra and the RR excitation profiles calculated here are for a single vibrational coordinate and two electronic states. The results for this assumed system are relevant in that the electronic states are assigned properties similar to those of the ground and the first excited electronic states of the TCNE EDA complexes, in particular a deeper potential energy curve and a shorter internuclear distance in the excited state than in the ground state[1,2]. Since the potential energy surfaces of the TCNE EDA complexes are much more complicated than those considered here, an interpretation of the spectra of the complexes in terms of the results of the present calculations is not attempted. Instead, the calculations are intended to illustrate the importance of a specific arrangement of the

potential energy surfaces for the RR effect as well as for the absorption and the fluorescence spectra.

In Fig. 27, a typical arrangement of the potential energy curves used in the calculations is shown. The Raman active vibration is assumed harmonic in both states, and the vibrational frequency ν_m is lower in the ground state k than in the excited state r. The vibrational levels which enter into the Raman scattering and absorption processes are shown with the vibrational wavefunctions superimposed on the energy levels. Only the first four vibrational levels in states k and r are considered; the third and fourth vibrational levels of the ground state, which appear in the expression for the fluorescence intensity, are not shown.

The transitions between the two electronic states are assumed to obey the Franck-Condon principle, i.e. they are assumed vertical[3]. This implies that the absorption and Raman scattering processes occur at some internuclear distance which is characteristic of the ground electronic state vibrational wavefunction for which $v = 0$; the most probable internuclear separation at which these transitions occur is therefore Q_k. Assuming that the nuclei are able to achieve the equilibrium excited state configuration before fluorescence, then this transition takes place at a reduced internuclear distance corresponding to the excited electronic state vibrational wavefunction for $v'' = 0$.

As stated above, both absorption and fluorescence spectra are calculated assuming that they are each comprised of the profiles
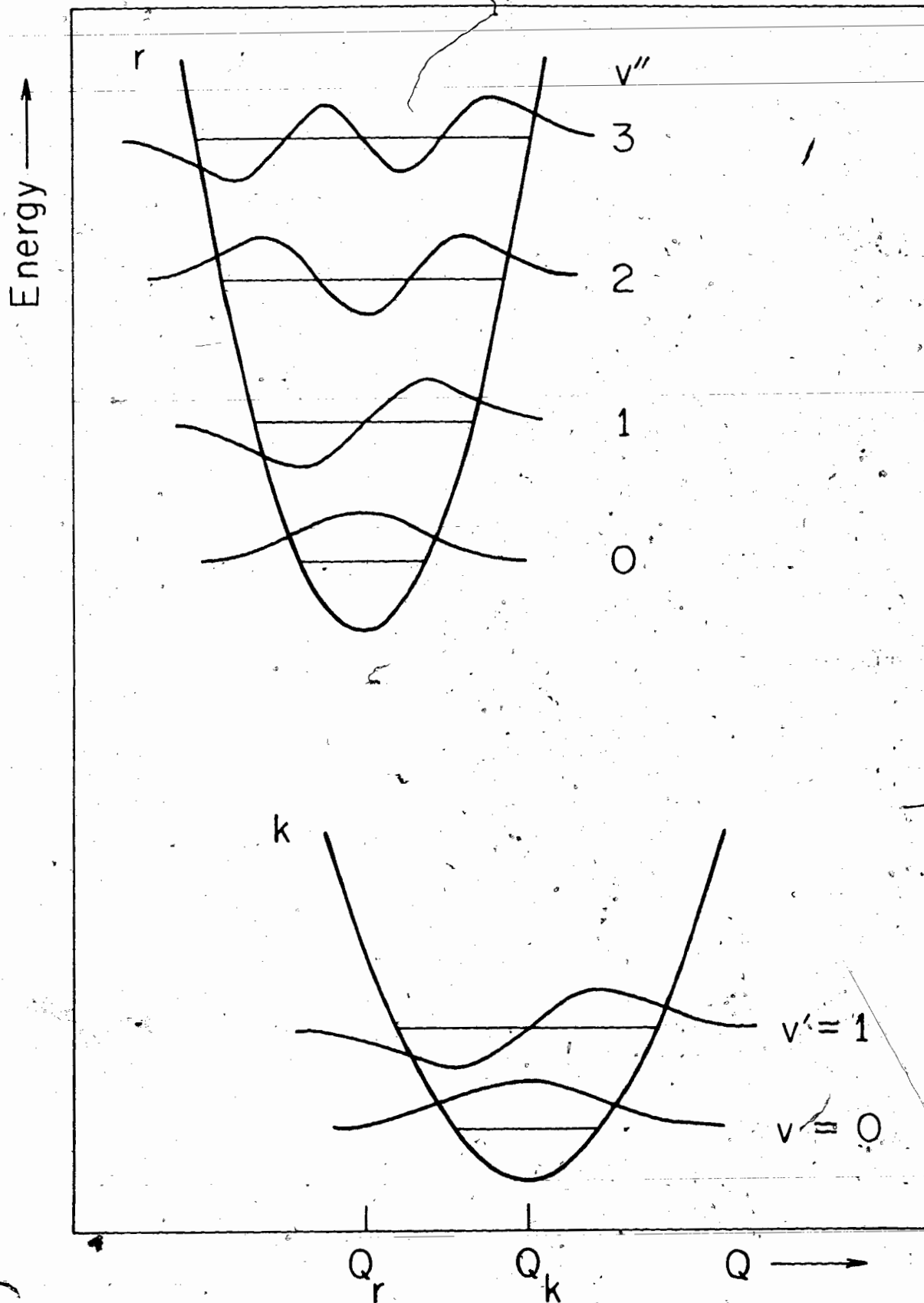
Fig. 27 Potential energy curves used for the calculation of resonance Raman excitation profiles, absorption spectra and fluorescence spectra.

for four Lorentzian vibronic transitions. The intensity distribution $I(\nu)$ of each Lorentzian profile is that of the natural line width of a damped oscillator,[4]

$$I(\nu) = I_0 \frac{\gamma}{2\pi} \frac{1}{(\nu - \nu_i)^2 + \gamma^2/4} \qquad (C.1)$$

where I_0 is the total integrated intensity, ν_i is the resonant frequency, and γ is the halfwidth. The contribution of each vibronic transition to the overall absorption or emission intensity is determined by its transition probability; according to the Franck-Condon principle this probability is proportional to the square of the overlap integral for the initial and final vibrational levels involved in the transition. Labelling the lowest vibrational level of the ground state $v = 0$ and the excited state vibrational levels v'' (Fig. 27), the total absorption intensity distribution is therefore

$$I(\nu) = \sum_{v''=0}^{3} \frac{|<v|v''>|^2}{(\nu_{r,v'';k,v} - \nu)^2 + \delta_{r,v''}^2} \qquad (C.2)$$

where the symbols have the same meanings as in Chapter 2, and $\delta_{r,v''} = \gamma_{r,v''}/2$. The damping terms $\delta_{r,v''}$ in general vary with the $\nu_{r,v'';k,v}$ and the form of this dependence is linked to the kind of damping (radiative or nonradiative) which occurs. Equation (C.2) explicitly assumes that only the lowest vibrational level of the ground electronic state is populated at ordinary temperatures; this is an excellent approximation for the ground state vibrational frequencies considered here, 500 cm^{-1} and 1000 cm^{-1}.

Using reasoning analogous to that described for the
absorption spectrum, the fluorescence intensity distribution is

$$I(\nu) = \sum_{v=0}^{3} \frac{|\langle v''|v\rangle|^2}{(\nu_{r,v'';k,v} - \nu)^2 + \delta_{r,v''}^2} \tag{C.3}$$

where it is assumed that the emission originates only from the
vibrational level $v'' = 0$.

The expression for the RR excitation profile is derived using
the reasoning that only the first term of equation (2.1), after
introduction of the damping term, contributes significantly to the
intensity. Again assuming that the electronic transition moment
is proportional to the vibrational overlap integral, the scattering
tensor is written

$$(\alpha_{\rho\sigma})_{vv'} = \frac{1}{h} \sum_{v''=0}^{3} \frac{\langle v|v''\rangle\langle v''|v'\rangle}{\nu_{r,v'';k,v} - \nu_0 + i\delta_{r,v''}} \tag{C.4}$$

$$(\alpha_{\rho\sigma})_{vv'} = \frac{1}{h} \sum_{v''=0}^{3} \frac{\langle v|v''\rangle\langle v''|v'\rangle(\nu_{r,v'';k,v} - \nu_0)}{(\nu_{r,v'';k,v} - \nu_0)^2 + \delta_{r,v''}^2}$$

$$- \frac{i}{h} \sum_{v''=0}^{3} \frac{\langle v|v''\rangle\langle v''|v'\rangle\delta_{r,v''}}{(\nu_{r,v'';k,v} - \nu_0)^2 + \delta_{r,v''}^2} \tag{C.5}$$

where $v = 0$ and $v' = 1$. Equation (C.5) is very similar to the result derived by Behringer {equation (2.6)} except for the appearance of the vibrational overlap integrals in equation (C.5). From equation (2.2), the RR excitation profile in the present case is given by

$$\left|(\alpha_{\rho\sigma})_{vv'}\right|^2 = \frac{1}{h^2}\left|\sum_{v''=0}^{3}\frac{\langle v|v''\rangle\langle v''|v'\rangle(\nu_{r,v'',k,v} - \nu_0)}{(\nu_{r,v'';k,v} - \nu_0)^2 + \delta_{r,v''}^2}\right|^2 +$$

$$+ \frac{1}{h^2}\left|\sum_{v''=0}^{3}\frac{\langle v|v''\rangle\langle v''|v'\rangle\delta_{r,v''}}{(\nu_{r,v'';k,v} - \nu_0)^2 + \delta_{r,v''}^2}\right|^2 \qquad (C.6)$$

The overlap integrals which appear in equations (C.2) and (C.4) to (C.6) are summarised in Table XXXIII; the integrals for equation (C.3) are in Table XXXIV. These integrals are calculated graphically between the limits defined by the extents of the wavefunctions v or v'' (see above). Negative overlap occurs when the wavefunctions have opposite signs in a particular region, and in some cases outweighs the positive overlap, resulting in the negative overlap integrals.

Absorption spectra, fluorescence spectra and RR excitation profiles calculated according to equations (C.2), (C.3) and (C.6), using the overlap integrals in Tables XXXIII and XXXIV, are presented in Figs. 28 to 31. Figures 28 and 29 correspond to the potential energy curves in Fig. 27, for which $\nu_m = 1000$ cm^{-1} and the excited state vibrational interval is 1400 cm^{-1}; Figures 30

Fig. 28 Resonance Raman excitation profile, absorption spectrum and fluorescence spectrum calculated from the potential energy curves in Fig. 27 assuming frequency dependent damping.

Legend:
- —·— Fluorescence
- —— Raman
- --- Absorption

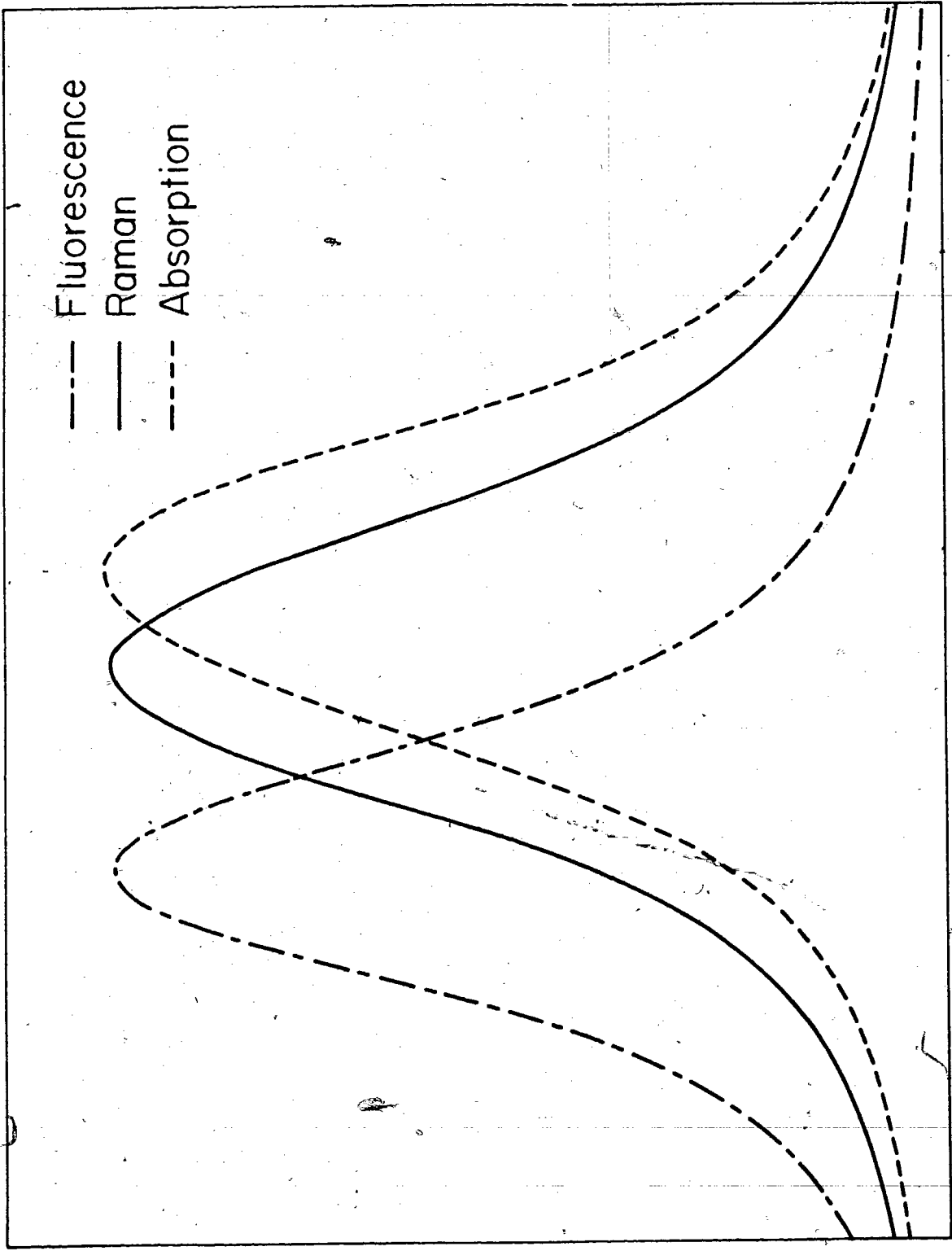Y-axis: Intensity (arbitrary scale)

X-axis: ν (cm^{-1})
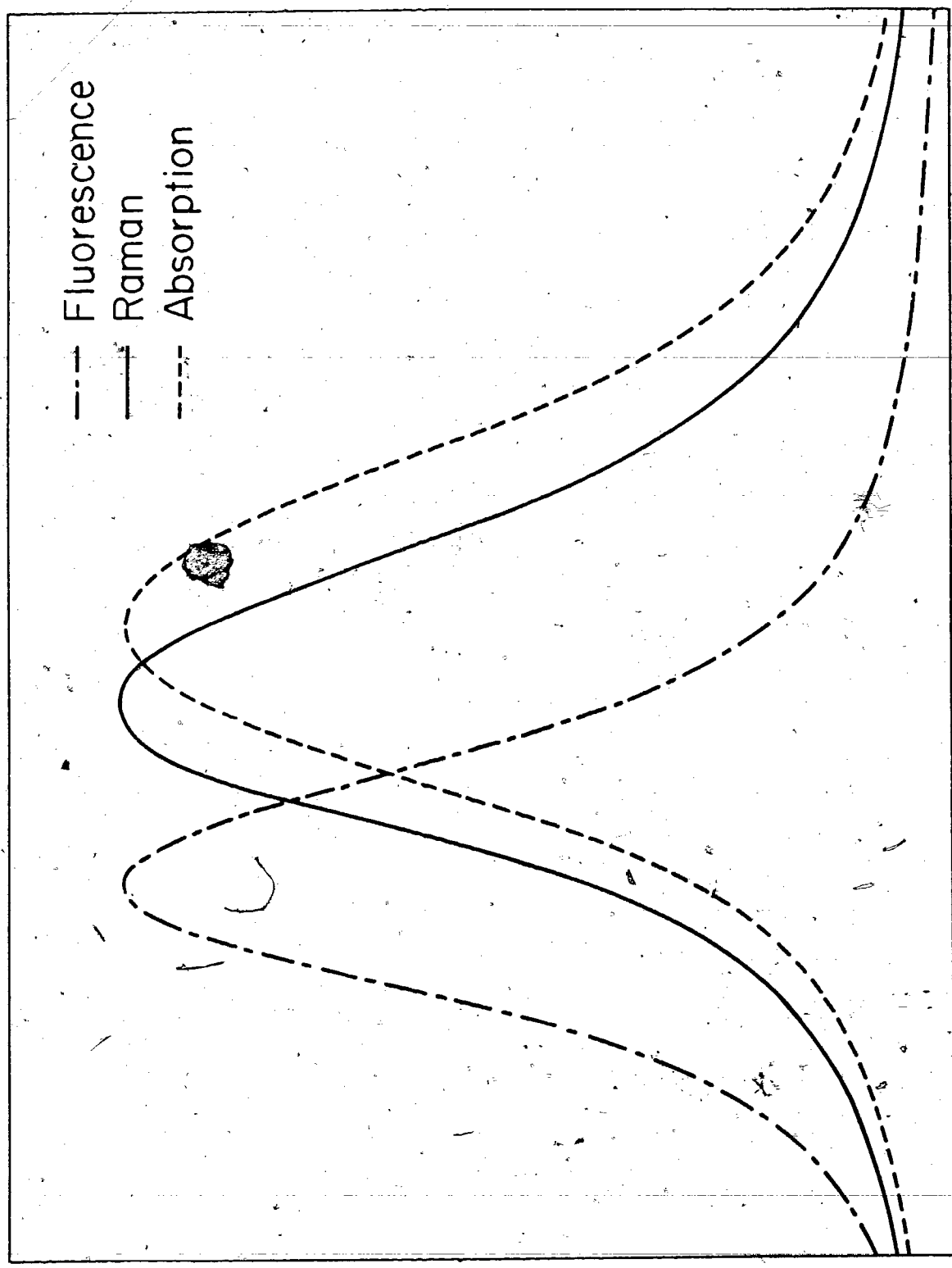
X-axis values: 10,000 ... 30,000

159b

Fig. 29 Resonance Raman excitation profile, absorption spectrum and fluorescence spectrum calculated from the potential energy curves in Fig. 27 assuming constant damping.

Fig. 30 Resonance Raman excitation profile, absorption spectrum and fluorescence spectrum calculated for $\nu_m = 500 \ cm^{-1}$ assuming frequency dependent damping.

Fluorescence
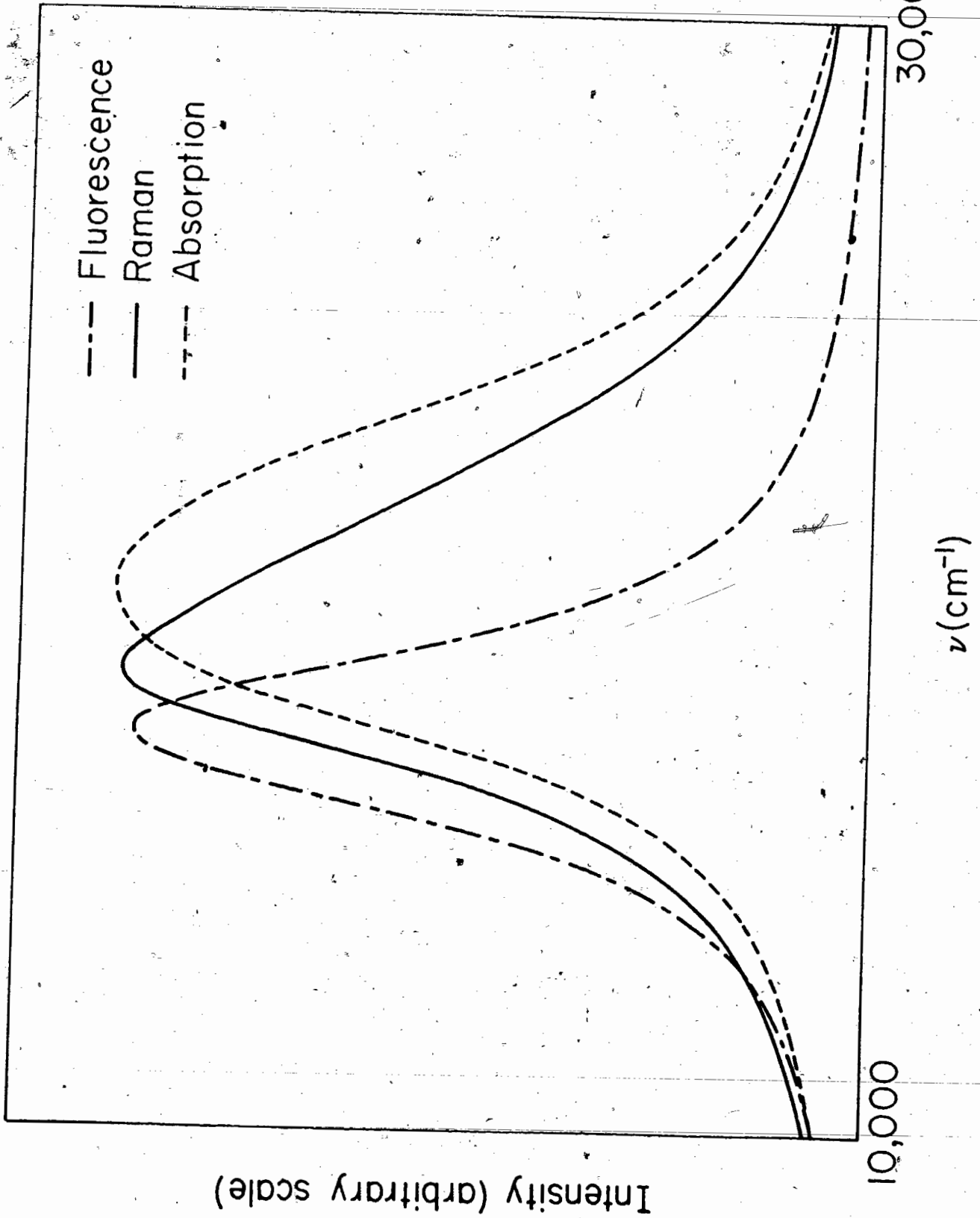Raman
Absorption

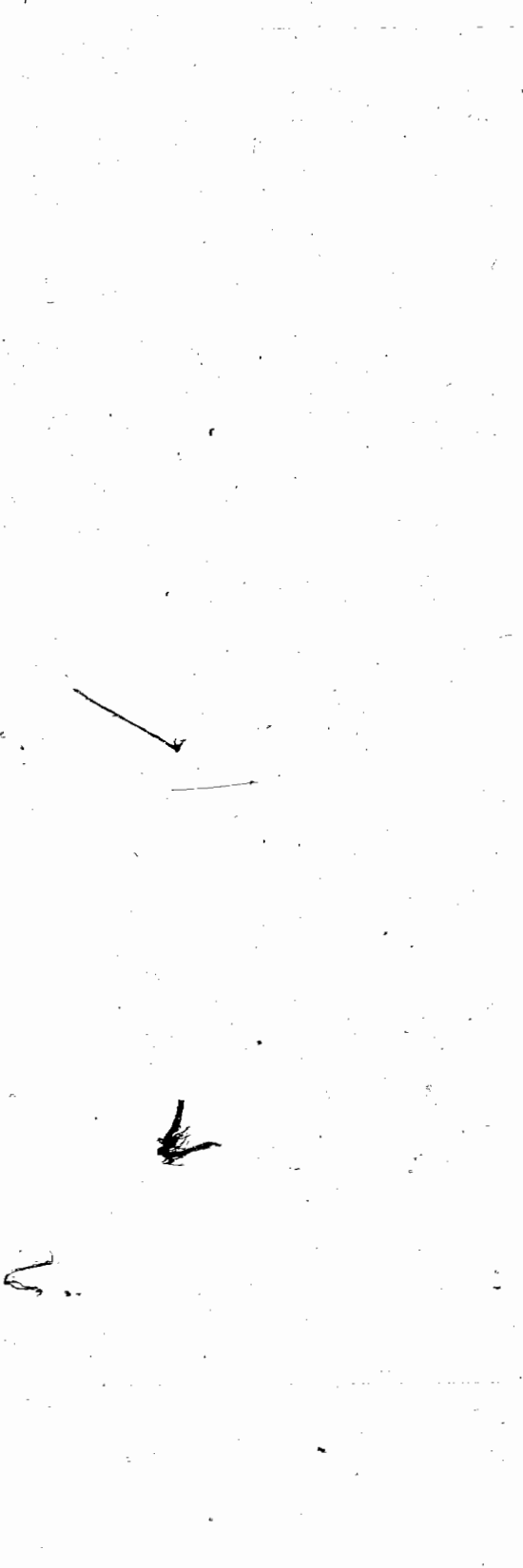$\nu\,(\text{cm}^{-1})$

Intensity (arbitrary scale)

30,000

10,000

162a

Fig. 31 Resonance Raman excitation profile, absorption spectrum and fluorescence spectrum calculated for $\nu_m = 500\ cm^{-1}$ assuming constant damping.
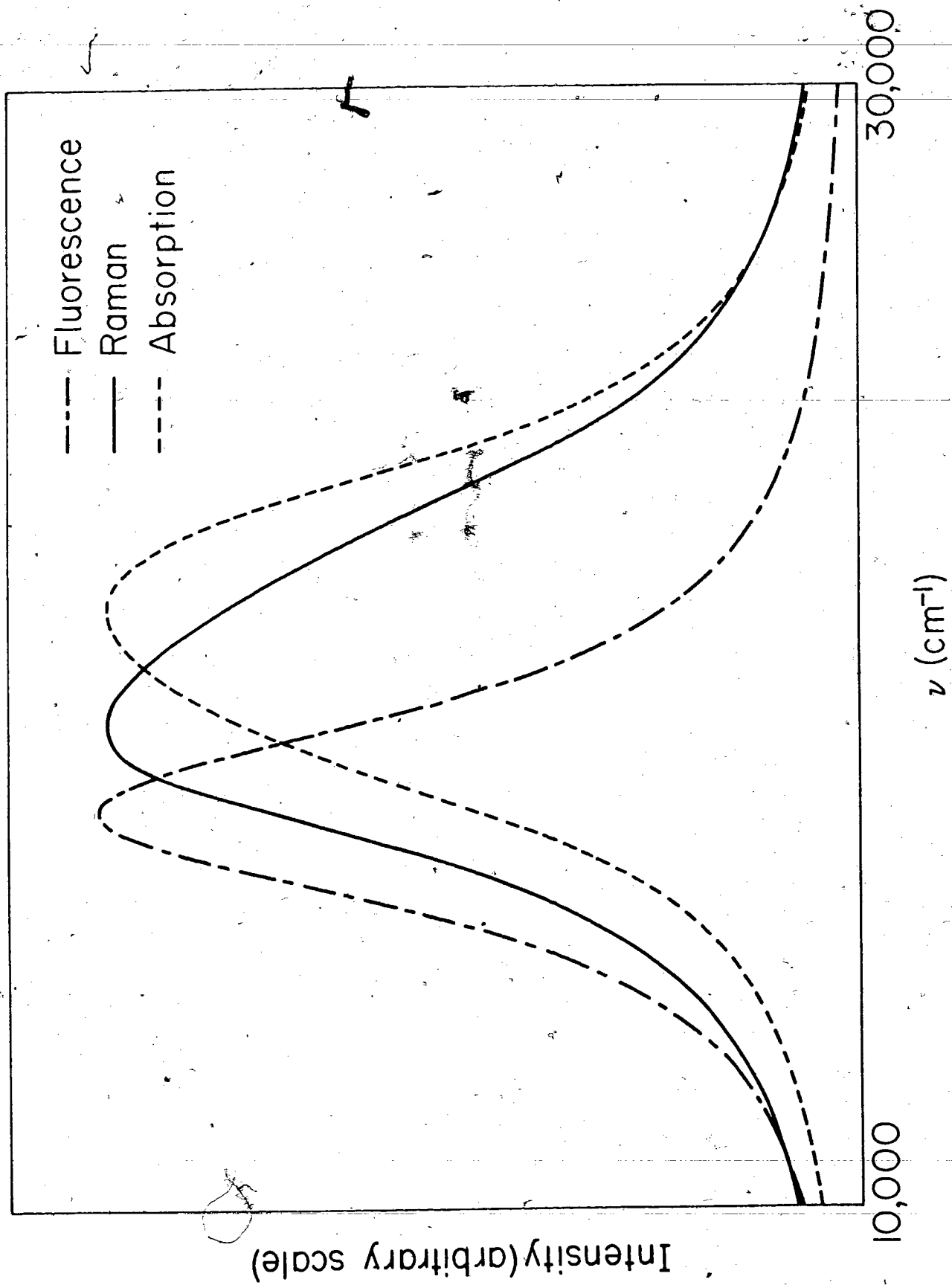
Table XXXIII. Vibrational overlap integrals for absorption and
Raman excitation profile calculations

$\nu_m (cm^{-1})$	$Q_k - Q_r (\overset{o}{A})$	v''	$<v|v''>^a$	$<v'|v''>^b$
500	.19	0	3.1486	-5.9028
		1	3.5370	-3.9408
		2	3.8567	-2.8117
		3	3.9641	-1.5950
1000	.16	0	2.8689	-5.0577
		1	4.3111	-4.8682
		2	4.8824	-2.6327
		3	4.8971	-0.3000

[a] All integrals are for v = 0.
[b] All integrals are for v' = 1.

Table XXXIV. Vibrational overlap integrals for fluorescence
profile calculations

$\nu_m (cm^{-1})$	$Q_k - Q_r (\overset{o}{A})$	v	$<v|v''>^a$
500	.19	0	3.1486
		1	-5.9168
		2	6.8227
		3	-5.1066
1000	.16	0	2.8689
		1	-5.0927
		2	6.0387
		3	-5.5127

[a] All integrals are for v" = 0.

and 31 give the results for another set of potential energy curves, which have $Q_k - Q_r = .19$ Å and $\nu_m = 500$ cm^{-1}. The characteristics of these profiles are summarised in Table XXXV.

Profiles calculated using values of $Q_k - Q_r$ as much as 15% different from those in Tables XXXIII and XXXIV are nearly the same in appearance as those in Figs. 28 to 31. The most important features of the spectra and the excitation profiles are the following:

(a) Both the RR excitation profile and the fluorescence spectrum are red shifted with respect to the absorption spectrum as calculated for each pair of potential energy curves; the shift of the fluorescence curve is greater than the shift of the RR profile in every case.

(b) The magnitude of the damping affects the size of the red shift of the RR excitation profile, while its frequency dependence influences the asymmetries of the profiles. The asymmetry of the RR excitation profile is greater than that of the absorption spectrum in every case. The absorption spectra and the RR excitation profiles are blue shifted when the damping is changed from frequency dependent to constant.

(c) The halfwidths of the RR excitation profiles tend to exceed those of the corresponding absorption bands; the difference in halfwidths is greater when the damping is constant. The fluorescence spectra are narrower than either absorption or Raman excitation spectra.

These results imply that the red shift of the RR excitation

Table XXXV. Summary of the calculated profiles[a]

ν_m(cm^{-1})		Damping (cm^{-1})[b]	ν_{max}(cm^{-1})[c]	$\Delta\nu_{\frac{1}{2}}$(cm^{-1})[d]	asymmetry[e]
500	Absorption	Variable	19,690	6970	1.2
		2000	20,710	6630	0.8
	Raman	Variable	18,240	6120	1.8
		2000	18,670	7050	1.6
	Fluorescence	Variable	17,140	3740	1.0
		2000	17,050	4250	1.1
1000	Absorption	Variable	20,280	6540	1.1
		2000	20,880	6200	0.8
	Raman	Variable	19,010	5860	1.2
		2000	19,350	6030	1.0
	Fluorescence	Variable	16,030	4590	1.1
		2000	16,030	5100	1.1

[a] Q_k - Q_r values for the respective ν_m are the same as in Tables XXXIII and XXXIV.

[b] For variable damping, $\delta_{r,v''}$ = 1756, 2000, 2250 and 2500 cm^{-1} for v'' = 0, 1, 2 and 3 respectively.

[c] Intensity maximum of the profile; uncertainty is $\pm$ 100 cm^{-1} or less.

[d] Halfwidth of the profile; uncertainty is $\pm$ 200 cm^{-1} or less.

[e] Asymmetry is the ratio $(\nu_h - \nu_{max})/(\nu_{max} - \nu_{\ell})$ where ν_h and ν_{ℓ} are the frequencies at half the maximum intensity for the high and for the low frequency side respectively.

profile with respect to the absorption spectrum has the same origin as the red shift of the fluorescence spectrum, namely the difference in potential minima $Q_k - Q_r$. Since the Raman scattering tensor contains overlap integrals corresponding to absorption and to emission, it is logical that the shift of the RR excitation profile with respect to the absorption spectrum is in the same direction, but not as great as, the shift of the fluorescence spectrum. Thus, a discrepancy between the maximum of the RR excitation profile and that of the absorption spectrum for a particular system need not require the participation of higher intermediate states, as has been proposed by some authors[5,6].

When $Q_k = Q_r$, according to equation (C.6) the Raman intensity vanishes, since for each v" one of the overlap integrals equals zero. This is essentially the conclusion reached with regard to the first term of the vibronic expansion of the scattering tensor {see equation (2.7)}[7]: this term can contribute to the RR intensity only if the potential energy surfaces of the ground and excited electronic states are not equal. The results presented here show that the difference must be in the internuclear separation, rather than in the shapes of the curves.

REFERENCES

1. J. Prochorow, Bull. Acad. Polon. Sci., Ser. Sci. Math. Astr. Phys. 15, 37 (1967).

2. J. Prochorow, Bull. Acad. Polon. Sci., Ser. Sci. Math. Astr. Phys. 22, 1283 (1974).

3. R.W. Nicholls, in Physical Chemistry, An Advanced Treatise, Vol. 3, D. Henderson, ed. (Academic Press, New York, 1969).

4. W. Heitler, The Quantum Theory of Radiation, (The Clarendon Press, Oxford, 1954).

5. S. Matsuzaki and S. Maeda, Chem. Phys. Lett. 28, 27 (1974).

6. J. Friedman and R.M. Hochstrasser, Chem. Phys. Lett. 32, 414 (1975).

7. J.A. Koningstein, Introduction to the Theory of the Raman Effect, (D. Reidel, Dordrecht, Holland, 1972).

APPENDIX D

PHOTOCONDUCTIVITY IN ELECTRON DONOR/ACCEPTOR COMPLEXES

TETRACYANOETHYLENE

In Sec. 5.2.3, experimental results which suggest the non-radiative damping of the excited states of TCNE EDA complexes by dissociation of the complexes into ions are described. Ionic dissociation of EDA complexes in the first excited CT state has already been studied in detail for tetracyanobenzene (TCNB) complexes[1-4], and has been reported in a briefer investigation of TCNE EDA complexes[4]. The experiments described in this appendix were performed to check for the presence of ions in solutions of electronically excited TCNE complexes, so that the existence of this nonradiative damping mechanism could be established. They also provide a check on the previously published data for TCNE complexes. Since the donor and the acceptor ions which are generated if ionic dissociation occurs can act as charge carriers, photoconductivity measurements such as those described here can be used to test for the creation of ions in solution.

The photoconductivity cell used has two 1 cm^2 platinum electrodes, with a spacing of 2 mm so that a laser beam can be directed between them. The cell is filled with the solution to be examined, and a potential difference (up to 200 volts) is applied to the electrodes. The laser beam is modulated at a frequency of 625 Hz with a mechanical chopper and passed between the electrodes; if ions are produced in the solution, the resulting photocurrent is detected with a lock-in amplifier by measuring, at the modulation frequency, the potential drop across a load resistor

(between 10^4 and 10^6 ohms) connected in series with the conductivity cell. The apparatus gave an S/N ratio of approximately 1 for a current of about 10^{-11} amp. Where photoconductivity was observed, currents were of the order of 10^{-10} amp or more for complex concentrations of about 10^{-4} M.

The results of the photoconductivity experiments are summarised in Table XXXVI. The CH_2Cl_2 solutions of each TCNE complex investigated showed measurable conductivity upon excitation in their CT absorption bands. For o-dimethoxybenzene/TCNE, this occurs both for excitation into the first and into the second CT absorption band. Since the two CT absorption bands of m-dimethoxybenzene/TCNE both absorb the Argon laser light used to excite the photoconductivity, Table XXXVI indicates that photoconductivity occurs for excitation in both CT bands of this complex.

The important role of the solvent in the dissociation process is also illustrated in Table XXXVI. For cyclohexane, a solvent of low dielectric constant $(\varepsilon = 2.015)$, the data indicate that any ionic dissociation must be more than an order of magnitude weaker than the ionic dissociation in CH_2Cl_2 $(\varepsilon = 8.93)$. These results are consistent with those cited earlier; the excited TCNB complexes were found to dissociate into ions in polar media and to give up their excitation energy in other ways in nonpolar solvents[1-4]. The data in Table XXXVI are consistent with the results of the flash photolysis of benzene/TCNE and HMB/TCNE in CH_2Cl_2 solutions, where the TCNE$^-$ ion was identified by means of its absorption spectrum[4]. The photoconductivity signals

Table XXXVI. Photoconductivity data for EDA complexes of TCNE

Donor	CT bands (nm)[a]	Solvent	Observed	Photoconductivity Results Excitation[b]	
				1st CT band	2nd CT band
mesitylene	466	mesitylene	no		
		cyclohexane	no		
		CCl$_4$	no		
		CH$_2$Cl$_2$	yes	x	
hexamethylbenzene	541	CH$_2$Cl$_2$	yes	x	
o-dimethoxybenzene	429, 592	cyclohexane	no		
		o-dimethoxybenzene	yes[c]	x	
		CH$_2$Cl$_2$	yes[c]	x	x
m-dimethoxybenzene	441, 559	m-dimethoxybenzene	yes	x	x
		CH$_2$Cl$_2$	yes[c]	x	x
p-dimethoxybenzene	380, 637	cyclohexane	no		
		CH$_2$Cl$_2$	yes	x	

[a] CT absorption maxima for CH$_2$Cl$_2$ solutions. For complexes with multiple CT bands, the 1st CT band is the lower energy one.

[b] Excitation sources were the Argon laser and the dye laser.

[c] The CH$_2$Cl$_2$ solutions gave photocurrents which were stronger by at least a factor 10 than those for the respective dimethoxybenzene solutions for the same concentration of complex.

observed for the o-dimethoxybenzene/TCNE and m-dimethoxy-

benzene/TCNE complexes when the respective liquid electron donors

were used were an order of magnitude weaker than when CH_2Cl_2 was

the solvent.

The mesitylene/TCNE and o-dimethoxybenzene/TCNE complexes

were selected from among those listed in Table XXXVI for further

investigation. The CH_2Cl_2 solutions of these complexes gave

photocurrents with these characteristics: (a) within experimental

uncertainty, the magnitude of the photocurrent is proportional to

the laser power; (b) the current is proportional to the potential

difference across the electrodes; (c) any excitation wavelength

dependence of the photocurrent is too small to be detected, i.e.

the current does not vary by more than about 15% over the wave-

length range accessible with the Argon laser.' This also applies

when excitation wavelengths near 600 nm (from the dye laser) are

used. Therefore, the frequency dependence of the damping

mechanism proposed for the TCNE complexes (Sec. 5.2.3) was not

confirmed by these data. It should be stated that the experimental

conditions preclude any deductions from this negative result,

because at the concentrations required to obtain reasonable

photocurrents any wavelength dependence would be masked by

differential absorption effects.

So far no attempt has been made to quantify these results with

regard to rates of ion production and lifetimes of ions in solution,

since this would require extensive systematic work beyond the

scope of this particular investigation, the purpose of which was

limited to the establishment of the ionic dissociation of the

excited complexes. Since the magnitude of the photocurrent depends on a number of parameters, most of which are either unknown or not subject to control in the rather simple experimental arrangement used here, the experiment was restricted essentially to the question of the occurrence of the photoconductivity. Hence the interaction between the electronically excited complex and the solvent molecules which is suggested in Sec. 5.2.3 as the source of the nonradiative damping does indeed lead to ionic dissociation in some solvents.

REFERENCES

1. H. Masuhara, M. Shimada, N. Tsujino and N. Mataga, Bull. Chem. Soc. Japan 44, 3310 (1971).

2. M. Shimada, H. Masuhara and N. Mataga, Chem. Phys. Lett 15, 364 (1972).

3. M. Shimada, H. Masuhara and N. Mataga, Bull. Chem. Soc. Japan 46, 1903 (1973).

4. Y. Achiba, S. Katsumata and K. Kimura, Bull. Chem. Soc. Japan 45, 1272 (1972).